THE UNIVERSITY OF MANITOBA

CORROSION OF TYPE 316L STAINLESS STEEL ORTHOPEDIC IMPLANTS.

by

Wayne W. Tennese

A THESIS

SUBMITTED TO THE FACULTY OF GRADUATE STUDIES

IN PARTIAL FULFILMENT OF THE

REQUIREMENTS FOR THE DEGREE OF

MASTER OF SCIENCE

DEPARTMENT OF MECHANICAL ENGINEERING.

WINNIPEG, MANITOBA

May 1972.

THE UNIVERSITY OF MANITOBA
ELIZABETH DAFOE LIBRARY

ABSTRACT

The effect of cold-work, pCO_2 and pO_2 on the aqueous corrosion of Type 316L stainless steel is investigated. The intent of this study is to draw conclusions which could be applied to the problem of crevice corrosion commonly found in surgical implant applications. The stainless steel was tested in two conditions; annealed (200 DPH) and heavily cold-worked (400 DPH). The basic test solution was Ringers physiological solution of pH 7.20 - 7.40. The electrochemical techniques utilized were corrosion potential vs. time measurements, potentiostatic and galvanostatic polarization.

The results showed that corrosion potentials are lower (more active) for cold worked material. Cold-work also resulted in a decrease in the breakdown potentials (for pitting) of 50-100 mV for all concentrations of O_2 and CO_2. The general effect of a high pCO_2 (110 mm Hg) was to equilibriate annealed and cold-worked material at a common corrosion potential. Passive current densities (corrosion currents) for all concentrations of O_2 and CO_2 were approximately one order of magnitude smaller for annealed specimen (200 DPH) than for cold-worked specimens (400 DPH). Carbon dioxide concentration (through formation of a $CO_3^{=}$ containing layer) has a much more marked effect on increasing breakdown potentials and lowering passive current densities than pO_2 (through an oxide passive layer) with annealed and cold-worked steel. A crevice corrosion mechanism operating on the differing passive currents for annealed and cold-worked material required to heal damaged passive layers is also proposed.

ACKNOWLEDGEMENT

The financial support of the Medical Research Council of Canada in the form of an operating grant (MA 3607) and student assistantship is gratefully acknowledged. I am also indebted to Dr. J.R. Cahoon under whose guidance this thesis was prepared and to Dr. R.H. Betts, Dept. of Chemistry, Dr. A. Naimark, Dept. of Physiology, and Dr. F.R. Tucker, Dept. of Orthopedic Surgery, for helpful discussion.

TABLE OF CONTENTS

Page

LIST OF TABLES

LIST OF FIGURES

Page

Page

Page

Page

Chapter I

INTRODUCTION

1.1 Background

Today, as a result of manufacturers, metallurgists and surgeons working together, the repair of many anatomical systems in the body with metallic devices has become commonplace. Metallic devices are especially suited for applications concerning skeletal repair and replacement where strength and rigidity are required. This area of orthopaedic surgery is a major user of metallic implants.

Most of the early understanding of metal behaviour in the human body originates from the efforts of orthopaedic surgeons. The chronological development of ferrous implants [1, 2, 3] begins with a description by Hansmann in 1886 of bone plates and screws similar in design to those used today, but made of nickel-plated mild steel. About 1912 Dr. William O'Neill Sherman of Pittsburgh, chief surgeon to the U.S. Steel Co., had the resources to design bone plates using Vanadium steel with superior design and greater strength. Vanadium steel implants containing 0.1-0.15% V with small amounts of Cr, Mo, and other alloying elements had greater strength and surface hardness than the earlier implants and were used until 1935. It was not until the middle 1920's that of materials with adequate strength and corrosion resistance really began. Activity increased in the 1930's and in 1936 Doctors C.S. Venable and W.G. Stuck experimented with the effects of Vitallium (65% Co, 30% Cr, 5% Mo alloy), chrome steel, 18-8 stainless steel, vanadium steel, plain carbon steel and other metals in bone. Of the ferrous metals the most

suitable choice seemed to be one of the stainless steels, which were considered in the following order: first Type 302 or 18-8 (18%Cr, 8%Ni, 0.15%C max.), then Type 304 (19%Cr, 10%Ni, 0.08%C max.), and finally Type 316 (17%Cr, 12%Ni, 3%Mo, 0.08%C max.) The steel implants used until this time underwent severe general corrosion in the tissues of the body and had poor fatigue strength. Fig. 1 shows a bone plate (M58), made of 4068 steel, 0.68%C, 0.87%Mn, and 0.2%Mo. This implant had been on a man's tibia for 29 years from 1939-1968 and shows a considerable amount of corrosion. A symposium in 1939 under the auspices of the College of Surgeons on the basis of work by Venable et al. [4], and studies by Hudock [5] and Key [6] recommended the use of Types 302 and 316 stainless steels for use in the body. The onset of World War II hastened the need for a standard material for use in orthopaedic implants. The U.S. government acting through the National Research Council assigned Murray and Fink [7] on a top priority project to find the most acceptable metal or alloy available for bone fixation and to determine its chemical and mechanical properties.They recommended the use of Type 302 to the medical branches of the Army and Navy in 1943. These studies were continued by Fink and Smatko [8] in various simulated physiological solutions with Vitallium, AISI Type 316 and Type 302 stainless steels. Their conclusion was that "Type 302 stainless made the best performance, but the margin is very slight".* The differences in weight losses between the material were negligible, however, the mechanical property tests showed the austenitic stainless steels to have superior ductile properties in bending over the cast Vitallium of that time. In 1945 on the basis of work by Blunt et al. [9] and a report of a subcommittee on bone plates and screws, the superior chemical and mechanical properties of

* P. 277 of reference [8].

Type 316 made it more desirable for the manufacture of surgical implants than Type 302. Today the low carbon form of Type 316, Type 316L is used (having 0.03%C max. compared with 0.08%C max. for 316) in North America for the manufacture of orthopaedic devices, with Types 316 and 317 having more limited usage.

Based on estimations by manufacturers, the number of implants bought and used runs into the millions. The most common metallic surgical implant is the bone screw and about one million of these screws were manufactured in the U.S.A. in 1967 [10]. Among the larger fixation devices, hip nails and pins are manufactured in the largest quantities. This is due to the high incidence of fracture and arthritis of the hip among the elderly segment of the population.

The use of Type 316L stainless steel has eliminated the problem of general corrosion present 20 years ago as illustrated in Fig. 1. However, another corrosion problem peculiar to active-passive metals of which austenitic stainless steels are a major group has come to the forefront. This is crevice corrosion - a localized intense attack which occurs in confined areas. It is found all too commonly in implants removed from patients where corrosion was suspected of causing tissue reactions with accompanying pain and discomfort. Generally the attack is located between the screws holding the plate to the bone or in the narrow spaces of multicomponent devices. This study will deal with this phenomena in the hope of determining the factors aiding the initiation of the electrochemical reaction and the subsequent preventation measures which then could be taken to decrease the magnitude of the problem.

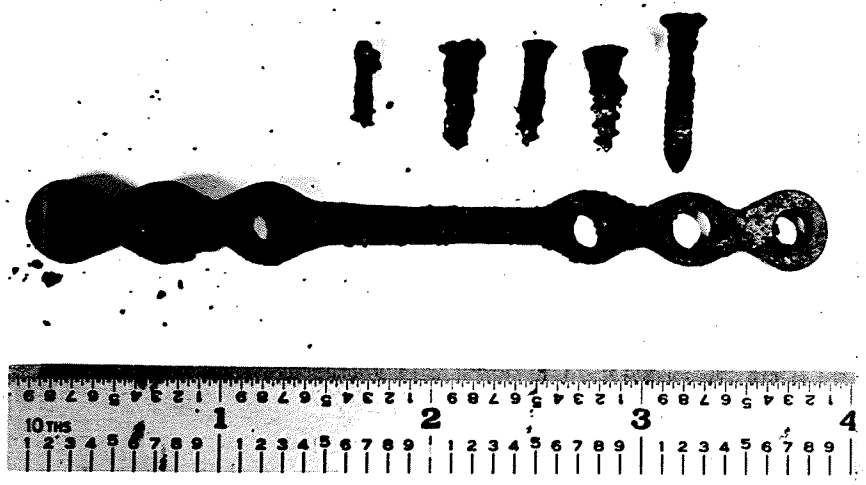

Fig. 1 General corrosion of a bone plate (M58) made of 4068 molybdenum steel implanted for 29 years.

Chapter II

PHYSIOLOGICAL ASPECTS

2.1 Ionic Composition of Extracellular Environment

There has been only scarce mention [13] of the physiological factors involved with the application of metals in human tissue by metallurgists or engineers. As corrosion is an electrochemical process it would be benefitial for the metallurgist to examine this area more clearly.

The surgical use of a metallic implant places it in a rather complex physical-chemical environment. The electrolytes of the body can be divided into two compartments - intracellular fluid and extracellular fluid. The compartment whose ionic composition is most pertinent to the study of the corrosion of ferrous implants is extracellular fluid (ECF). ECF includes blood plasma, interstitial fluid, small amounts of fluid in the joint spaces (synovial fluid), the tendon sheaths, and others [11]. The ionic concentration of ECF is roughly about one third that of sea water [12]. A further complicating aspect of human extracellular fluid, setting it apart from sea water, is the solution of oxygen and carbon dioxide. Of the ionic species found in ECF, the major cation is sodium, and the major anions are chloride, bicarbonate, and protein. The ionic composition of ECF is shown in Fig. 2 along with the ionic composition of sea water. Expression of ionic concentration in blood chemistry is in terms of equivalents, and as the concentrations encountered are very small it is convenient to use the unit milliequivalents per liter (m Eq/l)*

* $\frac{\text{wt. of substance (mg)}}{\text{atomic wt. x valence}} = \text{mEq}$

Milliequivalents are usually reported in terms of 1000 ml of solution. Milligrams are reported in terms of 100 ml of solution, therefore mg% can be converted to mEq/L by;

$$\frac{\text{mg \%}}{\text{atomic wt.}} \times 10 \times \text{valence} = \text{mEq/L}$$

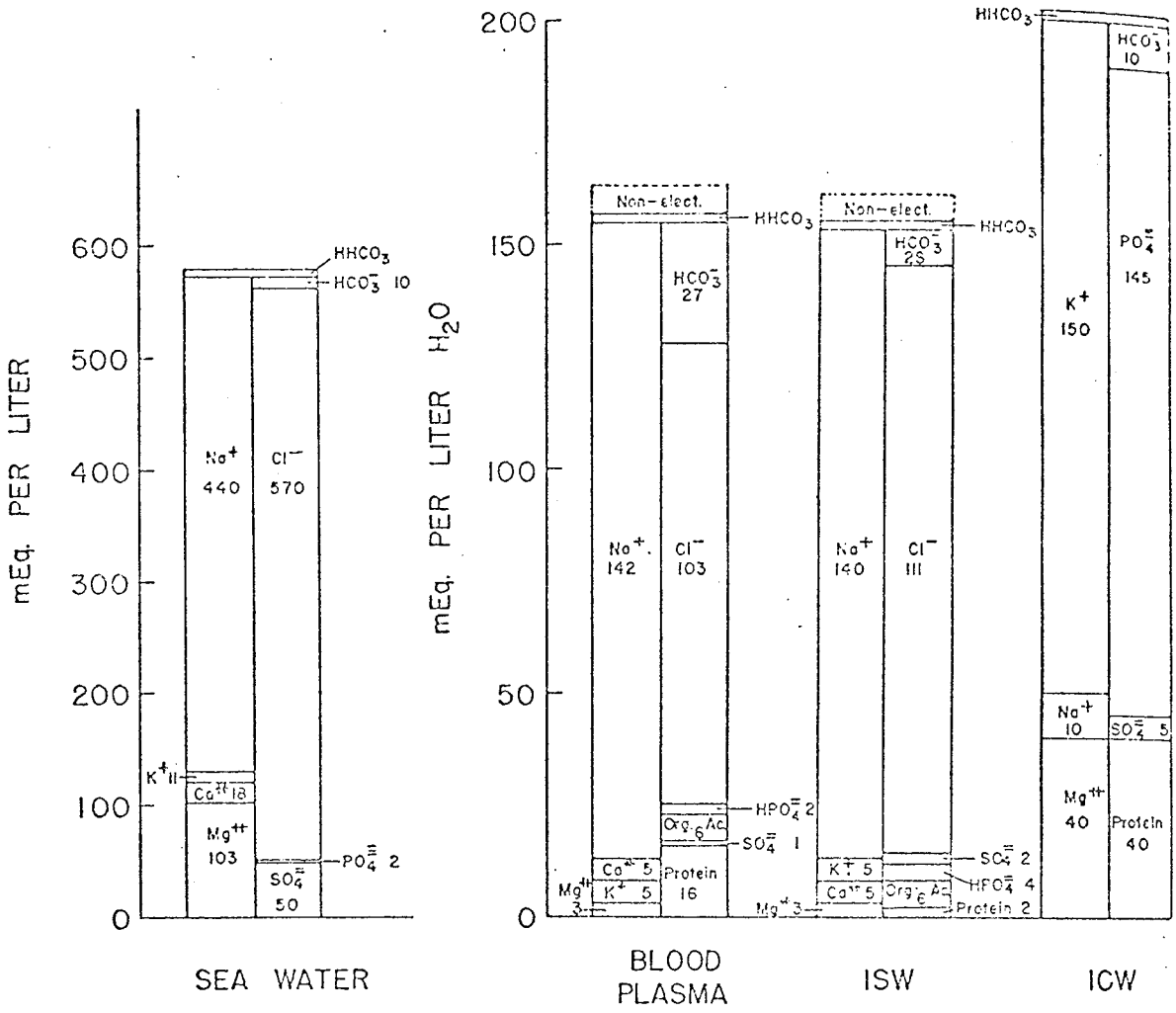

Fig. 2(a) Relation between electrolyte pattern of present-day sea water and human extracellular water. Sea water is more concentrated now than it was many millions of years ago when it first became our extracellular water. Protein is lacking in sea water, but essentially extracellular water has the same chemical composition. Compare this with the oldest biological liquid, the intracellular water. (Reproduced from J.H. Bland: Clinical Metabolism of Body Water and Electrolytes: W.B. Saunders Company.)

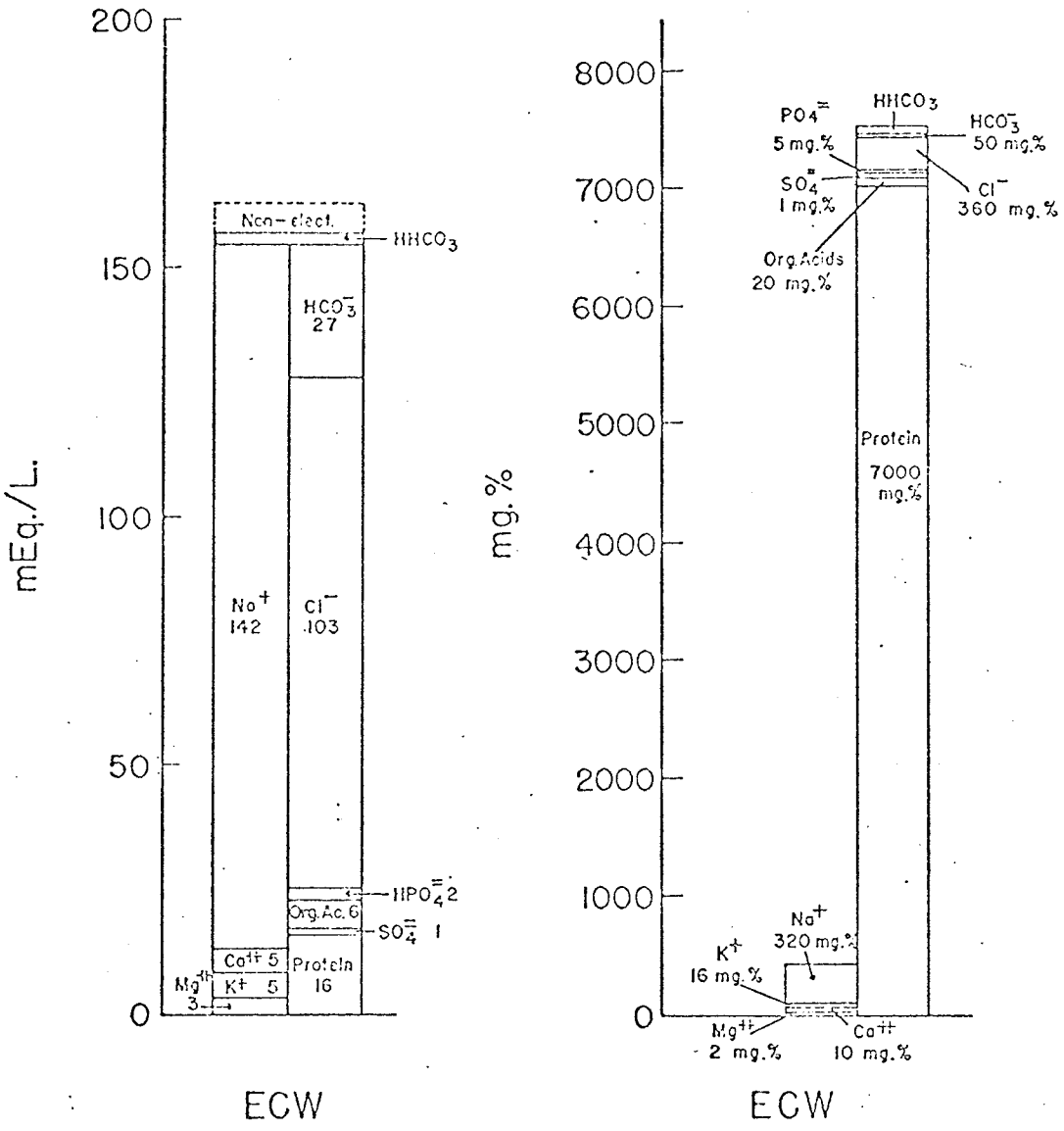

Fig. 2(b) Diagram to compare the expression of electrolytes of plasma in milligrams per cent, or weight-volume expressions. Note that protein exists as only 16 mEq. expressed as milliequivalents, but as 7000 mg. per cent when expressed in weight-volume terms. Electrolytes are not important physiologically because of their weight, but by virtue of the number of particles in solution or their combining power. (Reproduced from: J.H. Bland: Clinical Metabolism of Body Water and Electrolytes. W.B. Saunders Co.)

It should be noted that the total equivalent sum of the positively charged ions (cations) equals the equivalent sum of the negatively charged ions (anions). This balance in terms of equivalents is necessary because the solution must be electrically neutral. Balance in terms of weight per unit volume (mg%) is not achievable. The concentrations shown are not absolute. Thus ionic concentrations occupy ranges as shown in Table I.

Some of the fluids used for oral administration in the treatment of major fluid depletions in clinical medicine have been used by some workers [61,66,67]. Two of these electrolytes [11] which may have applications in the corrosion testing of implants are:

(i) Sodium chloride 0.9% (Normal saline) contains 155 mEq/L of sodium and chloride ions. This solution is isotonic with blood and is used to restore ECF volume.

(ii) Hartmann's Lacated Ringer's Solution is the solution resembling most nearly the electrolytic structure of normal blood serum. There is no excess of chloride or bicarbonate and no change in reaction of the blood is induced. The composition is given below:

Na^+ mEq/L	K^+ mEq/L	Cl^- mEq/L	HCO_3^- mEq/L	Other mEq/L
130	5	118	25	calcium - 3 magnesium - 2

Table I

Range of concentration of human plasma or serum

(from [19])

	Ionic Species	Concentration
1.	HCO_3^-	(24 - 31) mEq/L
2.	Ca^{+2}	9.8 (8.4 - 11.2) mg/100 ml.
3.	Cl^-	369 (337-400) mg/100ml.
4.	Mg^{+2}	2.1 (1.6 - 2.6) mg/100 ml.
5.	Mn^{+2}	8 μg/100 ml.
6.	PO_4^{-3}	(3.1 - 4.9) mg/100 ml.
7.	P^{+3}	11.4 (10.7 - 12.1) mg/100 ml.
8.	K^+	16.0 (13.1 - 18.9) mg/100 ml.
9.	SO_4^{-2}	3.7 (2.4 - 5.0) mg/100 ml.
		1.28 (0.94 - 1.49) mg/100 ml.
10.	Na^+	325 (312 - 338) mg/100 ml.

An examination of the electrolytic volume of blood plasma shows that protein occupies a volume out of all proportions to the few mEg/L that it represents (Fig. 2(b)). One litre of plasma* which is 6 per cent protein contains 940 ml of water in which all the ions are dissolved.** Therefore from a strict chemical point of view these concentrations can be corrected to milliequivalents/Kg of water by multiplying by 1000/940. Proteins are rather different from the usual ionic species encountered in corrosion studies. All proteins contain four essential elements: carbon, hydrogen, oxygen, and nitrogen. These four elements are bonded together to form compounds called amino acids. As an organic acid they must contain the carboxyl groups (COOH) and being an ammonia derivative they must have the amino group, NH_2. The amino group and carboxyl groups are always attached to the same carbon atom in all amino acids found in proteins. These two groups allow proteins to assume an ionic form in solution and are titratable to also allow plasma and tissue protein to act as one of the buffering acids of the blood [14]. The most striking and interesting feature of proteins are their huge physical dimensions. Proteins and nucleii acids can be spoken of as polymers because they contain a large number of similar structural units joined together by the same linkage. The term macromolecule can also be applied to proteins as they have molecular

* Blood plasma is whole blood minus the formed elements (red blood cells, white blood cells and platelets) ie. the extracellular liquid matrix of blood.

Blood serum is plasma minus fibrinogen.

** Grams and milliliters of H_2O are used interchangeably ie. 1000 ml = 1000 g. of H_2O.

$\therefore$ 1 liter of plasma contains 940 ml of H_2O (containing the dissolved ions) plus 60 g. of protein.

weights greater than 5000 due to the repetitive structural form. Most proteins are represented as ellipses of revolution [15]. Physical data on a few of the more common proteins will illustrate this point: serum albumin - MW 69,000 (150 Å major diam.), hemoglobin - MW 68,000 (54 Å major diam.), fibrinogen - MW 400,000 (700 Å major diam.) as compared to 1-2 Å for the diameters of common ions such as Na^{+}, Fe^{++}, Ni^{++}, Al^{+++}, Ca^{++} etc. Albumins are far more important than the other plasma proteins as these are several times more molecules in a given gram of albumin as in a gram of one or another of the globulins* - the large size of proteins results in new and unusual physical chemical properties. The size effect could have an influence on the mechanisms of corrosion.** No studies (to the writer's knowledge) have been done in this area.

In the previous paragraphs the ionic species found in the ECF have been described. Equally ubiquitous is carbon dioxide and oxygen. The emphasis of this work will be placed on determining the effects of oxygen and carbon concentration on the corrosion of 316L stainless steel. In the past, efforts were directed to the in vitro testing of implant materials in solutions of varying chloride concentration or chloride solutions of varying pH by means of buffering pairs. There apparently have been no attempts to measure or control the concentrations of gases in these test solutions. This point should be particularly important with a metal such as austenitic stainless steel which behaves in an active-passive fashion depending on whether the aqueous environment

* globulins (globular proteins) are more highly coiled and folded into a nearly spherical configuration and are soluble in salt solutions, acids and bases. One of the proteins found in red blood cells.

** One of the current theories on the solution of metal ions at a metallic electrode in an aqueous solution is based on the set up of a planar system of positive and negative charges relative to the metal called the Helmholtz electrical double layer [38].

will promote the formation of a passive film. In the general field of corrosion itself information of this sort is sorely lacking.

Carbon dioxide is the major acid end-product of metabolism and is continuously removed by the respiratory system. Oxygen, on the other hand, is required for cellular respiration and is continuously transported to the inner tissues by the systemmic circulation. The physical transport of these gases to the area of interest around the implant is irrelevant to this study. Of importance is the concentration and forms of these two gases in the electrolyte and tissues surrounding the implant and the measurement of these concentrations.

When a gas is brought into equilibrium with a solution, a certain number of gas molecules enter the solution increasing with the pressure of the gas above the liquid, according to Henry's Law. Then the gas can be said to be at this given pressure in the solution, whether the separate gas phase remains present or not. A partial pressure, measured in millimeters of mercury(mm Hg), then in effect, can be conveniently used as a concentration unit. The gradients of CO_2 and O_2 from the atmosphere outside of the body, through the respiratory and circulatory systems to the tissues of the human body are shown in Fig. 3. In the tissues, which require oxygen at a very low pressure [16] (which is not accurately known), the pO_2 varies from 20 - 0 mm Hg. Therefore in the case of a bone plate fastened to the long bone, the area beneath the bone and in the crevice between the screw and the hole in the plate could be very close to 0 mm Hg whereas the top of the plate could be bathed in ECF of 20 mm Hg or slightly higher. A certain pO_2 is probably required to maintain the passive layer on the stainless steel. Whereas

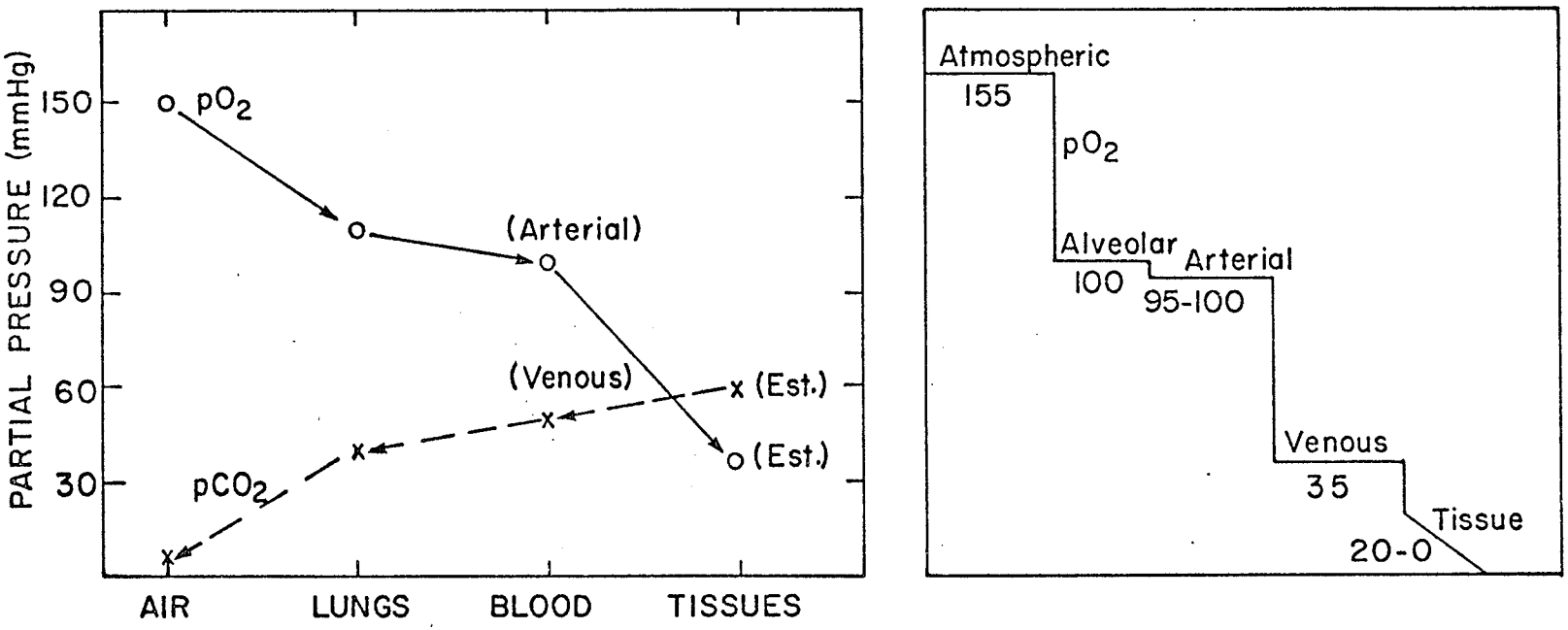

Fig.3 Summary of pO_2 and pCo_2 values in the body to show that both O_2 and CO_2 diffuse "downhill" along gradients of decreasing pressure.
(Redrawn from:(left) Ganong: Review of Medical Physiology 35:529,1969 and (right)Christensen: Body Fluids and Their Neutrality 6:87,1963)

the minimum pO_2 occurs in the tissues, the maximum pCO_2 occurs here, being about 60 mm Hg (estimated).

The range of the partial pressures have been described; however the actual physical amount of dissolved gas can be given in two ways: by the solubility factor 'a'(mM/mm Hg/L) or the Bunsen solubility coefficient α (milliliter of gas dissolved in 1 ml of solution at 1 atmosphere of the gas). The solubility of oxygen in plasma is 97.5 per cent of that in water [38] (the solubility of CO_2 in plasma is assumed to behave in a similar fashion). The solubility coefficient for oxygen is α=0.024 ml of O_2 dissolved by 1 ml of blood at pO_2=1 atm. at 38°C. Expressing in different units the amount of dissolved O_2 is 0.003 ml/100 ml blood per mmHg pO_2*, or by calculation assuming 1 millimol of O_2 occupies 22.4 ml at 0°C, 760 mm Hq, the solubility factor 'a' for oxygen is 0.00134 mM/mmHq/L. Carbon dioxide is much more soluble than O_2 and this is reflected in the solubility coefficient =0.55 and a=0.0301 mM/mm Hq/L or 0.0328 mM/mm Hq/KgH_2O (for protein appears to act as inert substance [17]) at 38°C. Both solubilities decrease with increasing temperature.

2.2 Acid-Base Status of Extracellular Fluid

Carbon dioxide exists in three forms in the body: (1) physically dissolved [CO_2(d) + H_2CO_3], (2) the bicarbonate ion, and (3) an unstable combination with hemoglobin (carbamino - CO_2) i.e. $HbNHCOO^-$. The physical dissolving of CO_2 in solution and the hydrolysis of CO_2 with water by reaction (1) accounts for only a

$$CO_2 + H_2O \underset{\text{carbonic anhydrase}}{\rightleftharpoons} H_2CO_3 \qquad (1)$$

* the concentration of a gas in a liquid is usually measured in volume per cent, ie. ml of gas/100 ml of liquid
eg. 1 mm of CO_2 occupies 22.26 ml.

∴ to convert vol. % of CO_2 to millimols/L

$$\frac{\text{vol. \% } CO_2 \text{ (0°C 760 mm. Hg)} \times 10}{22.26} = \text{mM. } CO_2/\text{L.}$$

$$H_2CO_3 \rightleftharpoons H^+ + HCO_3^- \quad \ldots\ldots\ldots\ldots\ldots (2)$$

minor fraction of the CO_2 transportation. In the body the enzyme carbonic anhydrase found in the red cells allows the reaction to proceed in either direction rapidly. Most of the transport of CO_2 occurs in the form of the bicarbonate ion. This is illustrated by the data from [16] shown in Table II.

Table II: Forms of Carbon Dioxide in Blood Plasma

Form	Arterial in mM/L	Venous in mM/L	% of Total Carried
Total Co_2	22.0	24.2	100
Physically dissolved CO_2 $[CO_2(d)+H_2CO_3]$	1.3	1.5	9
Bicarbonate ion	19.6	21.0	64
As $HbNHCOO^-$	1.1	1.7	27

The actual forms of CO_2 are closely related to the maintenance of stable physiological conditions especially regarding the hydrogen ion necessary for the metabolism of the body. The importance of the stability of the hydrogen ion concentration of this internal environment is attested to by the precision with which it is regulated. The pH in normal circumstances is maintained between 7.35 and 7.45 at 38^oC* (hydrogen ion concentrations of 4.47 and 3.53×10^{-5} mEq/L). Variations in pH can be described by acidosis whenever the pH < 7.40 and as alkalosis when the pH > 7.40. The variation of pH in the ECF compatible with life is from pH 7.00 to pH 7.70 (1×10^{-4} mEq/L and 2×10^{-5} mEq/L

* The normal plasma pH is nearer 7.6 than 7.4 at room temperature [16].

respectively) [18]. Hydrogen equilibrium is established by means of three buffering pairs:

$$\text{ie} \qquad [H^+] = K_{A1}\frac{[H_2CO_3]}{[HCO_3^-]} = K_A'\frac{[H_2PO_4^-]}{[HPO_4^-]} = K_A''\frac{[HPr]}{[Pr^-]}$$

bicarbonate phosphate protein

Buffer action is negligible at pH values more than 1.5 pH units removed from the pK of a buffer pair.* Secondary phosphate (pK = 6.8) is a moderately effective chemical buffer at the pH of extracellular fluid. However, the concentration in ECF is low (1.0 mM/L) and the role it plays is then accordingly small. The protein buffering system is beyond the scope of this work. Bicarbonate at first glance would seem to be a much less effective buffer since the pH of ECF is far removed from the pK of the bicarbonate system which is 6.1. However, the concentration is high, 28 mM/L, and the weak acid H_2CO_3 is volatile being removed as CO_2 by the lungs. Therefore the bicarbonate ion is very effective in the physiological buffering of hydrogen ions and hence is the most important buffer system in the body fluids. In order to simplify in vitro studies we will be interested only in the bicarbonate buffer pair.

The relationship between $[H^+]$ and the ratio of the constituents of the bicarbonate-carbonic acid buffer system can be expressed by Hendersons Eqn., [17,39,40]

$$[H^+] = K_{A1}\frac{[H_2CO_3]}{[HCO_3^-]} \qquad \text{.....(1)}$$

where K_{A1} = first dissociation constant for carbonic acid

* The most effective buffering occurs within limits of ±1.0 pH units to either side of pK_{acid} or pK_{base}.

Rewriting in logarithmic form transforms (1) into the Henderson-Hasselbalch equation.

$$pH = pK + \log \frac{[HCO_3^-]}{[H_2CO_3]}$$

The weak acid H_2CO_3, is in equilibrium with the dissolved CO_2 in the following relative concentrations

$$\begin{array}{ccccc} CO_2(g) & & & & \\ \uparrow\downarrow & & & & \\ CO_2(d) + H_2O & \rightleftharpoons & H_2CO_3 & \rightleftharpoons & H^+ + HCO_3^- \\ [800] & & [1] & & [0.03][0.03] \end{array}$$

The concentration of the most predominant form of H_2CO_3 to the product of its least predominant form is

$$\frac{[CO_2(d)]}{[H^+][HCO_3^-]} = \frac{[800]}{[0.03][0.03]} \approx 800{,}000/1$$

From this we see that H_2CO_3 is a very weak acid as the equilibrium of the hydrolysis reaction is very far in the direction of $CO_2(d)$. Although the weak acid form of the bicarbonate buffer system is by definition H_2CO_3, the effective concentration of weak acid in this system is most appropriately represented as $[CO_2(d) + H_2CO_3]$. The Henderson-Hasselbalch becomes

$$pH = pK + \log \frac{[HCO_3^-]}{[CO_2(d) + H_2CO_3]}$$

The concentration of the effective weak acid is proportional to the partial pressure of CO_2 in the gas phase.

ie. $PCO_2 \propto [CO_2(d) + H_2CO_3]$

or,

$$aPCO_2 = [CO_2(d) + H_2CO_3] \qquad \text{where } a = 0.03 \text{ mM/mm Hg/L}$$

and substituting pK'* for pK, the Henderson-Hasselbalch equation for the becarbonate buffer system becomes,

$$pH = pK' + \log \frac{HCO_3^-}{aPCO_2} \qquad \text{.....(3)}$$

Note; pK remains fairly constant with temperature from [19];

at 37.5°C and pH 7.4 for man, pK' = 6.10

at 49°C and pH 7.4, for man, pK' = 6.00

Clinically HCO_3^- cannot be measured directly so (3) can be simplified to,

$$pH = 6.10 + \log \frac{\text{total } CO_2 - aPCO_2}{aPCO_2} \qquad \text{.....(4)}$$

where: total CO_2 = mM/l

PCO_2 = mm Hg

a = 0.03 mM/mm Hg/L

To maintain a pH of 7.4 at 38°C only the ratio $\frac{[HCO_3^-]}{aPCO_2} = 20$ need remain constant. The individual terms themselves may vary.

The operation of the buffering system is then with the addition of a strong acid or base;

(1) Addition of H^+:

$$H^+ + HCO_3^- \rightarrow H_2CO_3 \rightarrow H_2O + CO_2(d) \rightarrow CO_2(g)$$

(2) Addition of OH^-:

* The pK changes with ionic strength, and the pK applying at a certain ionic strength (plasma) is designated pK'.

$$OH^- + H_2CO_3 \rightleftharpoons HCO_3^- + H_2O$$
$$\Updownarrow$$
$$CO_2(d)$$

The action of the bicarbonate buffering system influences the concentration of chloride ions. Fig. 4 illustrates this. There is a tendency of the serum chloride to be elevated when the bicarbonate ion concentration is depressed. This is a consequence of the fact that the m Eq'L of anions and cations must balance. Hypothetically if the bicarbonate concentration were halved, the chloride concentration would increase by an equal number of milliequivalents, and if $[CO_2(d) + H_2CO_3]$ remained constant (which is the case in the human body as $CO_2(d)$ must be in equilibrium with $CO_2(g)$), then the pH would fall from 7.40 to 7.10. A fall in pH (due to metabollic acidosis) is coupled with an increase in chloride concentration). Later the effect of pH and chloride concentration will be described on the corrosion of austenitic stainless steel.

More Detailed Study of the Chemistry of CO_2 in Aqueous Solution

The details outlined so far on the aqueous solution of CO_2 have dealt with its various forms as usually encountered in physiological measurements. The concentration of one final form of carbon dioxide - the carbonate ion, $CO_3^=$ will be determined for completeness of the electrochemical effects of CO_2 on the corrosion of type 316L stainless steel. To determine the amount of $CO_3^=$, a more exact treatment of ionization equilibria will be followed than was previously described.

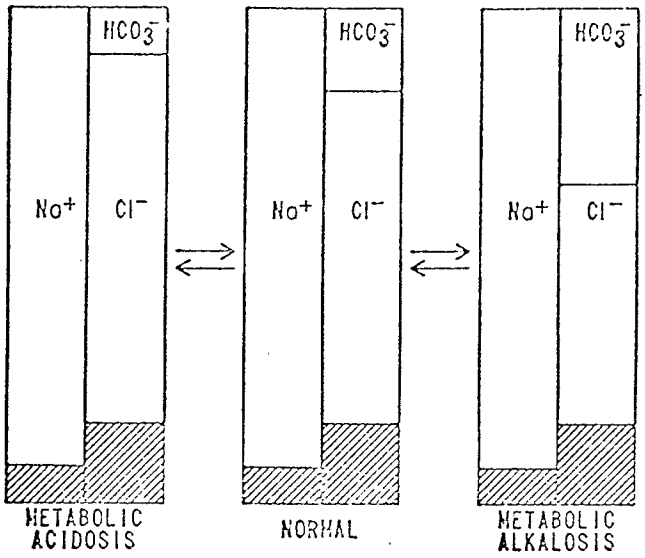

Fig.4 Change in electrolyte framework after compensation of HCl or NaOH injection. In the former case chloride ion has taken the place of the destroyed HCO_3^-; in the second case the HCO_3^- generated from $OH^- + CO_2 \rightarrow HCO_3^-$ has been added to the column, along with the injected Na^+.
(Reproduced from Christensen: Body Fluids and Their Neutrality 8:119,1963)

A solution of carbonic acid is really a mixture of two acids: H_2CO_3 and HCO_3^- with ionization constants for these acids given by:

$$H_2CO_3 + H_2O \rightleftharpoons H_3O^+ + HCO_3^-; \quad K_{A1} = \frac{[H_3O^+][HCO_3^-]}{[CO_2(d)+H_2CO_3]} = 1 \times 10^6 \text{ at } 49^oC \qquad (1a)$$

From [49]

$$HCO_3^- + H_2O \rightleftharpoons H_3O^+ + CO_3^=; \quad K_{A2} = \frac{[H_3O^+][CO_3^=]}{[HCO_3^-]} = 4.8 \times 10^{-11} \qquad (1b)$$

From [68]

$$\text{and} \quad \frac{[H_3O^+]^2[CO_3^=]}{[CO_2(d) + H_2CO_3]} = K_{A1}K_{A2} \qquad (1c)$$

Using a method of multistage equilibrium [68] for solutions prepared by mixing comparable amounts of H_2CO_3 ($CO_2(d) + H_2CO_3$) and $NaHCO_3$, an expression for $[H_3O^+]$ will be set up to be followed by a calculation for $[CO_3^=]$. The charge balance equation for a $H_2CO_3/NaHCO_3$ solution is

$$[H_3O^+] + [Na^+] = [HCO_3^-] + 2[CO_3^=] + [OH^-] \qquad (4a)$$

Choosing to express $[H_3O^+]$ in terms of $[CO_2(d) + H_2CO_3]$ by substituting from the ionization equilibria for carbonic acid and the ion product constant for water; Eq. (4a) becomes

$$[H_3O^+] + [Na^+] = \frac{[CO_2(d) + H_2CO_3]}{[H_3O^+]} K_{A1} + 2\frac{[CO_2(d) + H_2CO_3]}{[H_3O^+]^2} K_{A1}K_{A2} + \frac{K_W}{[H_3O^+]} \qquad (4b)$$

Several simplifications will be made namely: (i) on the l.h.s., $[Na^+] >> [H_3O^+]$ if appreciable $NaHCO_3$ is used to make up the solution and (ii) the last 2 terms will be small if $K_{A2} << K_{A1}$ and if $[H_3O^+] \approx 10^{-7}M$ (ie $K_W/[H_3O^+] \leq 10^{-7}M$).

From Eq. (4b) is obtained

$$[Na^+] = \frac{[CO_2(d) + H_2CO_3]}{[H_3O^+]} K_{A1}$$

$$[H_3O^+] = \frac{[CO_2(d) + H_2CO_3]}{[Na^+]} K_{A1} \qquad (4c)$$

which is the same if the mixture of H_2CO_3 and $NaHCO_3$ were treated as a simple buffer ($[Na^+] = [HCO_3^-]$), neglecting the amount of H_3O^+ ionized from HCO_3^-. The expression from Eq. (4c) when substituted into (1c) results in a determination for $[CO_3^=]$

$$[CO_3^=] = \frac{[CO_2(d) + H_2CO_3]}{[H_3O^+]^2} K_{A1}K_{A2} \qquad (4d)$$

For the high pCO_2 solutions

$$[CO_2(d) + H_2CO_3] = aPCO_2$$
$$= (0.03)(110)$$
$$= 3.3mM/L$$

$[Na^+]$ = 54mE q/L (27 mEg contributed by NaOH reacting with $H_2CO_3 \rightarrow HCO_3^-$ plus 27 mE contributed by original $NaHCO_3$).

Then from Eq. (4c),

$$[H_3O^+] = \frac{(3.3)(1x10^{-6})}{(54)}$$

$= 6.1 \times 10^{-8}$ mEq/L corresponding to a pH 7.22 and being very close to the measured pH of about 7.30, justifying the validity of the assumptions made.

Then using $H_3O^+ = 5.0 \times 10^{-8}$ mEq/L corresponding to the measured pH of 7.30 in Eq. (4d)

$$[CO_3^=] = \frac{(3.3)}{(5.0x10^{-8})^2} (1x10^{-6})(4.8x10^{-11})$$

$= 6.33 \times 10^{-2}$ mEq/L

2.3 Ionic Components of Bone Tissue

A brief summary of the salts found in bone tissue is an aid in attempts to determine the physiological conditions responsible for the initiation and continuence of corrosions through the analysis of corrosion products using the Debye X-ray diffraction technique. The amounts of corrosion products obtainable from implants submitted for metallurgical analysis by orthopaedic surgeons are usually meager at the best of times and probably contain bone salts mixed in, which would also produce lines on the diffraction film. To come to a truly conclusive identification of a corrosion products all lines produced should be accounted for. Individual ferrous corrosion products are usually formed within certain limiting physical chemical conditions, and so in a round about way, the physiological conditions having a bearing in the corrosion reaction could be determined.

Bone tissue consists of organic and inorganic material,and the properties of these two fractions vary from one part of the skeleton to another. Water free bone contains two-thirds inorganic and one-third organic material. One half of the organic fraction consists of collagen* or a substance close to collagen. The inorganic fraction of bone is called apatite. Bourne [20] states that in bone, the apatite component gives a high-angle pattern with many lines and collagen gives a wide-angle pattern in addition to a low-angle pattern with several orders of a fundamental repeating period of about 660Å. Bone also gives a low-angle diffuse pattern of a "gas-type" appearance. The overall chemical composition of bone has been known for a long time but efforts

* collagen is a fibrous protein

to determine the chemical structure of bone salts have been fruitless. Many efforts have resulted in monstrous formulas which are still inadequate in describing all facets of the complete behavior of bone salt. The chief constituents are:

$$Ca^{+2},\ PO_4^{-3},\ CO_3^{-2},\ HCO_3^{-},\ H_2PO_4^{-},\ HPO_4^{-2}$$

Other elements in bone are:

$$Na^{+},\ F^{-},\ Mg^{+2}$$

Attempts to formulate calcification theories in terms of the solubility products of calcium phosphate and calcium carbonate have been unsuccessful and it is doubtful that bone salt deposition is a simple precipitation process. There seems to be little possibility that changes in pH required for precipitation of bone salts in the healing of fractures in terms of solubility products would have an effect on the corrosion of ferrous implants. In fact from [20] in vitro studies show that a reduction or elevation of pH beyond the normal for plasma reduces calcium deposition.

Bone salts in fact can be included in the corrosion products as evidenced by the analysis of the corrosion deposits obtained from M69 which showed the salt calcium carbonate ($CaCO_3$) to be present, originating presumably from the bone tissue.

2.4 Physiological Changes Occurrding at a Fracture

Some medical researchers have noted a changing environment with the healing of a fracture. One of the earlier works dealing with the mechanisms of the healing of fractures was done by Murray [21]. He noted that tissue necrosis when present, under all circumstances "creates a pH to the acid side (often markedly so) in the hematoma and tissue fluids about the site of the fracture". A pH on the acid side, he claimed in the local tissues at the site of the fracture in the early days following the fracture was required to act as a local source of

available calcium for ossification of the healing tissue and a change of pH then to the alkaline side would allow the deposition of calcium in the new tissue to form bone". In a slightly later paper [22], but still rather dated, he reported a pH 5.5 or less follows fracture as due to products of tissue death and hemorrhage. Laing [23] notes that immediately upon insertion, a metallic implant is exposed to fresh blood. He says "fresh blood has a high oxygen tension* and a pH of about 7.4 for a short while. At once a clot forms and oxygen is lost and carbon dioxide accumulated, leading to a fall in the pH which may reach 5. These changes are accentuated if clotting does not take place or is succeeded by liquifaction in the absence of organization. Usually this stage soon ends and the pH slowly returns to normal over the course of a few days. Infection of the wound may prolong the period of the acid tide or, in the case of some bacteria, may produce an alkaline tide which will only pass off with the end of the infection." It has been noted by some investigators that demineralization of bone will occur if the pH falls below 6.8 but as mentioned previously, the changes in pH required by a simple precipitation process, and said to be brought about by necrotic tissue at the fracture site have since been shown not to hold. Much later papers also mention lower pH values at the site of a fracture, perhaps as a result of these earlier works. Crimmins [13] mentions that the normal pH of body fluids drops to 5.3 and 5.6 locally

* arterial blood has a normal oxygen tension of 100 mm Hg.

upon injury to the tissue. The return to normal pH locally usually requires approximately 10 days. Weisman [1] in listing the conditions under which an implant material ought to be tested, suggests "lowering the pH if infection is present".

Through personal communications with Dr. F.R. Tucker and Dr. R.M. Letts more recent literature in this field was reviewed. The changes in pH, pO_2 and pCO_2 concentrations as a result of fracture have been recently measured by Lauren and Kelly [24]. Measurements were made at a fractured tibia, internally fixed with a four-hole Vitallium plate in 30 adult mongrel dogs. The sampling of the venous blood was done at intervals up to 14 days, and in weekly intervals up to 12 weeks. They found no significant differences in oxygen content, partial pressures of oxygen and carbon dioxide, pH, or calcium concentrations between the fractured and control sides in contradiction to the earlier work of Murray. Union of the fracture was delayed in 2 of the dogs because of failure of the screws to maintain stable internal fixation and after 12 weeks, the pH, pCO_2, pO_2, and oxygen content were not significantly different on the fractured and control sides; the pO_2 and oxygen content in the nutrient vein was increased. In all animals blood flow was found to have increased, to a maximum of about 6 times mean normal at approximately 2 weeks. They expected increased oxygen utilization and increased carbon dioxide production, perhaps with accompanying changes in pH because of the products of rapidly metabolizing tissue in the fracture area. As blood flow was seen to increase without significant changes in pO_2,

pCO_2, and pH between the fracture and control sides their conclusion was that increased blood flow was the prime homeostatic* mechanism for increasing the oxygen supply to the fracture cite and removing the subsequent increased amounts of CO_2 from the tissues.

The low pH values found by Murray may have been due only to decomposition of the blood in the hematoma. Similar pH changes have been noted in stored samples of blood by Siggard-Anderson [25]. Wray [26] obtained fluid from 30 of 64 human fracture hematomas. The fluid was analyzed for pH, CO_2, Na, K, Cl, Mg, Ca, and P and compared with venous blood drawn at the same time. Two of these determinations in the hematoma were found to differ significantly from the blood stream. One was pH, with that of the hematoma being lower,attributed to red cell metabolism within the hematoma.

It would appear that a necessary prerequisite for engineers and metallurgists venturing into this area of medicine is to undertake a thorough study of the medical physiology involved, to gain the fullest comprehension of the problem before them and in this way bridge the gap between the medical and engineering professions before attempting to apply engineering principles of their particular discipline to this interesting field.

* homeostasis describes the various physiological arrangements which serve to restore the normal state, once it has been disturbed.

Chapter III
CORROSION PROBLEMS OCCURRING IN IMPLANTS.

3.1 Metallurgical Analysis of Failed* Orthopaedic Implants.

The problem of metal loss through corrosion as found in orthopaedic surgery has no comparison with the usual problems of corrosion which are encountered in the petro-chemical industries or food processing industries where vast quantities of stainless steel are used. The main difference is that the amount of corrosion products which can be tolerated in the body is one or two orders of magnitude less than that acceptable in industrial applications. Corrosion analyses of medical implants calls for a judicious application of ingenuity and refinement of present day corrosion study techniques.

Through cooperation with orthopaedic surgeons in the Winnipeg area a variety of devices removed because of suspected corrosion were analyzed with the intention of; firstly, determining the probable cause of the corrosion, and secondly, setting out the metallurgical variables upon which an experimental corrosion testing program of 316L stainless steel could be planned and carried out.

The 9 analyses which are presented in the following pages are indictive of the present corrosion problem in orthopaedic surgery, and the types of corrosion prevalent in austenitic stainless steel. The analyses were preformed on implants removed during the last 2 years (1969 and 1970, plus one in 1968).

Implants-M69, M70 and M74. All three are Osborne-Ball osteotomy plates of English manufacture and advertised to be fabricated of B.S. EN58J** stainless steel. These plates illustrate intergranular

* 'Failed' is used to describe those implants which have failed to remain chemically inert in the body and have been removed.

** Corresponding to AISI Type 316 stainless steel.

corrosion initiated for two different reasons. They were probably manufactured at different times from different heats of material as the plates were of 2 slightly different configurations. This particular manufacturer appeared to be having a heat treating problem in the manufacturing process during the time previous to the period 1969-1970.

Implant-M69. Manufacturer's identification: "Down J". Regarding the previously mentioned composition, a carbon analysis reported 0.072%C, within the specifications of a maximum carbon content of 0.08%C set by the ASTM specification for stainless steel. Medical History: The plate was removed November 25, 1969 after being implanted for six and a half months from an elderly lady being treated for osteoarthritis of the right hip.

PATHOLOGY:

A tissue sample (3 x 2 x 1 cm) was taken from the area of Fig. 5 of the right hip where a metal/tissue reaction was suspected. Microscopic observations of the tissue revealed granulation tissue containing very large numbers of hemosiderin laden macrophages. Fragments of crystalline extracellular Prussion blue staining iron material were also seen, clear evidence that iron had been transferred from the implant into the surrounding tissue.

METALLURGICAL ANALYSIS:

Macroscopic examination showed a large amount of corrosion product on the under side of the implant surrounding the upper screw hole, shown in Fig. 6.

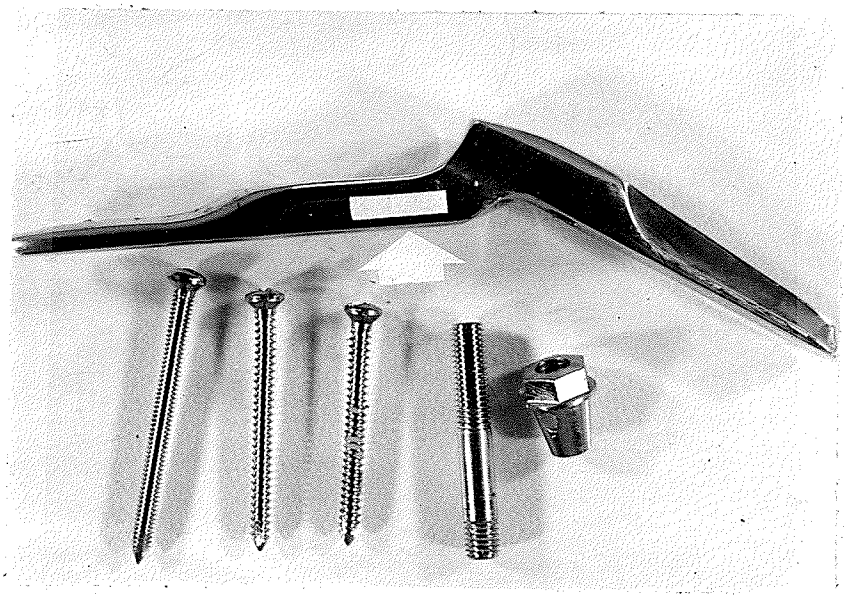

Fig. 5 Complete Osborne-Ball fixation prosthesis is shown with the location of the corrosion.

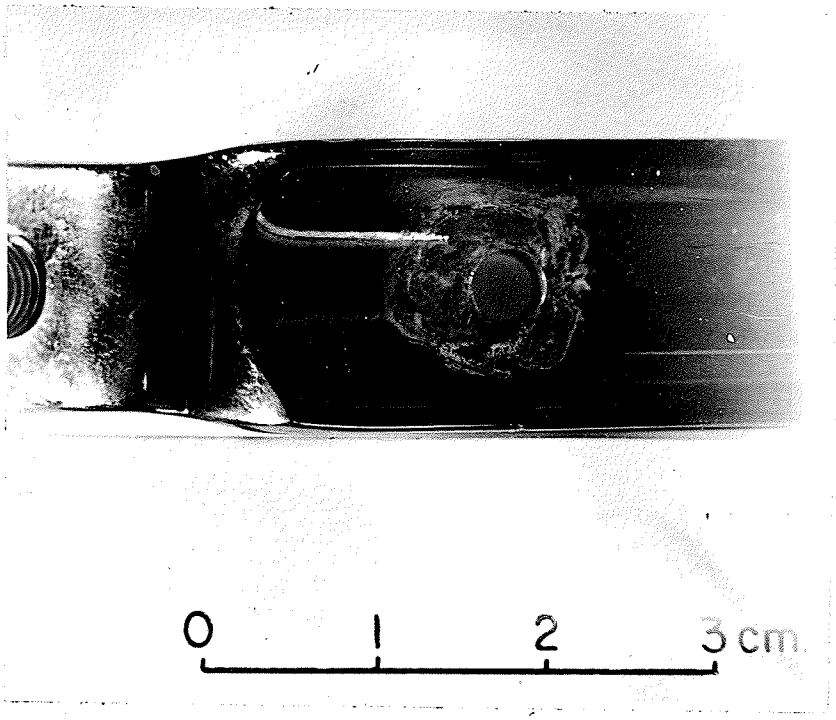

Fig. 6 Corrosion products on underside of plate.

Dull grey, corroded areas were seen in the counter-sunk portion on the upper side of the plate of the same hole and beneath the head of the screw that had been positioned in this hole. No evidence of corrosion was seen at any of the other holes in the plate or on the remaining screws.

A mounted polished section from the plate at the corroded hole showed a clearly visible "pock-marked" area centered around the hole at the center of the plate as seen in Fig. 7. The specimen(s) were etched electrolytically in 10% oxalic acid electrolyte. The structure was brought out very clearly indicating that the material was sensitized. Also,large numbers of grains were seen to have dropped out from the "pock-marked" central region during the polishing and etching processes. This feature is seen in Fig. 8. Intergranular corrosion had proceeded along the grains immediately adjacent to the grain boundaries where the chromium in the material was locally depleted, weakening the material in this immediate area to allow grains to drop out. A major portion of the cross-section had been weakened and had the corrosion been allowed to proceed further, a fracture of the plate at this section would have been emminent as the corroded material had no strength whatsoever.

Two samples were prepared from a section taken from the last hole in the plate. One sample was de-sensitized by annealing for one hour at 1000^{o}C. The two specimens were then etched following the ASTM oxalic acid electrolytic etching test. The heat treated specimen could not be clearly etched. The difficulty in etching shows that the stainless steel has regained its corrosion resistence, particularly in the

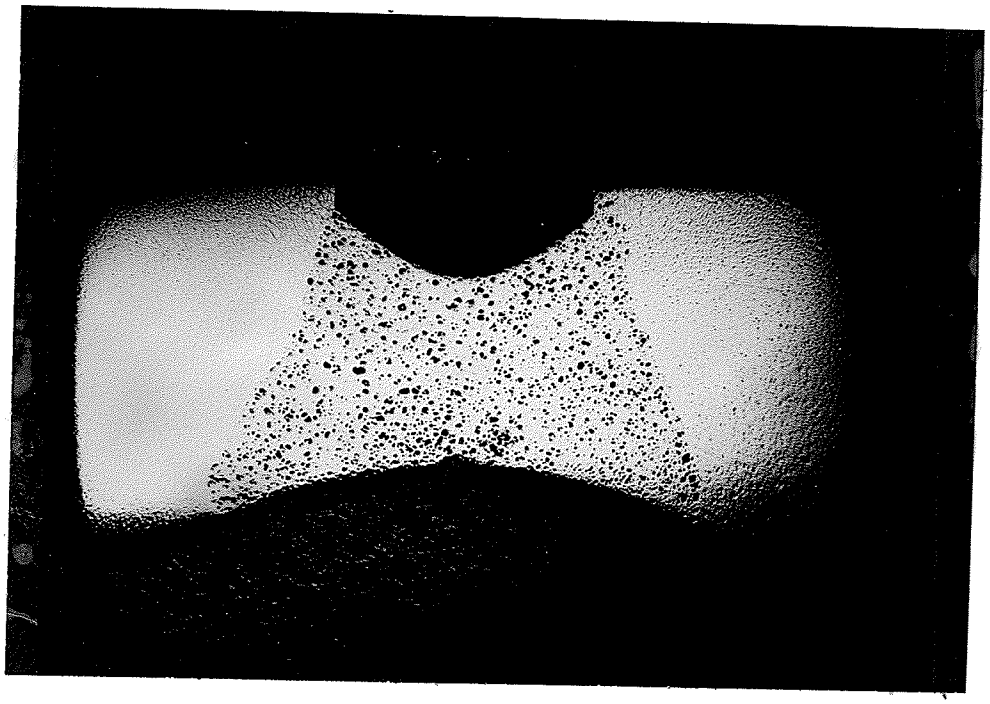

Fig. 7 Polished, unetched cross-section showing "pock-marked" area centered about countersunk portion of the hole. (x6).

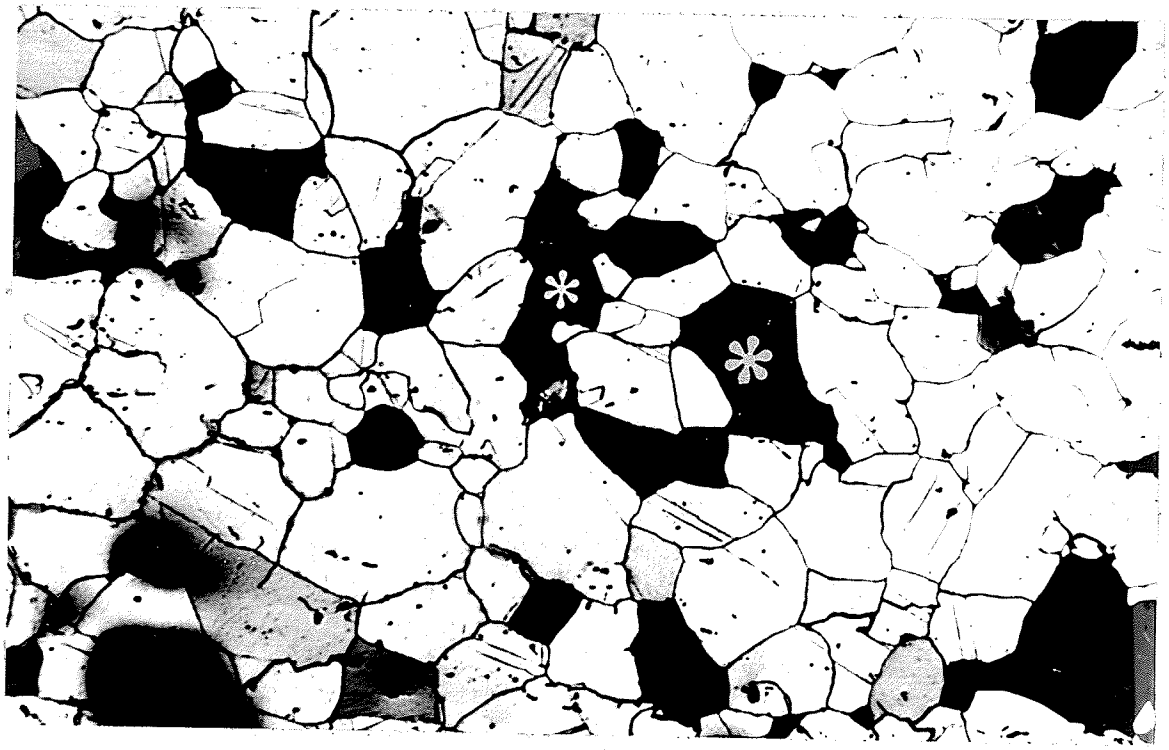

Fig. 8 Microstructure showing "grain-dropping" from "pock-marked" area. 'X' marks a dropped out grain (s). (x150)

grain boundary areas. This specimen was finally etched using 70% HCl and 30% H_2O_2 and is seen in Fig. 9(a). The sensitized structure is shown in Fig. 9(b) for comparison .

A large variation in grain size across the plate was noted. Very large grains were seen on the top outside of the plate, particularly centered around the upper countersunk portion of the hole. These grains of ASTM grain size 2-3 exceeded the allowable ASTM grain size of 5 or finer [27]. See Fig. 10(a). The inside portion of the plate showed an ASTM grain size of 7-8 as seen in Fig. 10(b). This large variation in grain size is undesirable and probably is an indication that the hot forging of the plate possibly was responsible for the whole sensitized structure.

Copius amounts of corrosion product were available to allow preparation of a powder sample for chemical identification using X-ray diffraction by the Debye-Scherrer method. Two of the compounds identified were calcium carbonate ($CaCO_3$) and α-iron oxide hydrate ($\frac{1}{2}Fe_2O_3 \cdot H_2O$) [28], a common corrosion product encountered for steel. The $CaCO_3$ originated from the bone as perhaps the result of bone absorption around the foreign screw or beneath the plate in the same immediate area. A third compound was identified, sodium iron hydroxide sulphate hydrate [29] ($Na_2Fe(SO_4)_2\,(OH) \cdot 3H_2O$), a seemingly most unlikely corrosion product but the diffraction pattern of this compound also fit the sample exactly. This product would not be expected because the concentration of the trace ion $SO_4^=$ in extracellular fluid is very small being 1 mEq/L. The source of sulphur or sulphate is unknown.

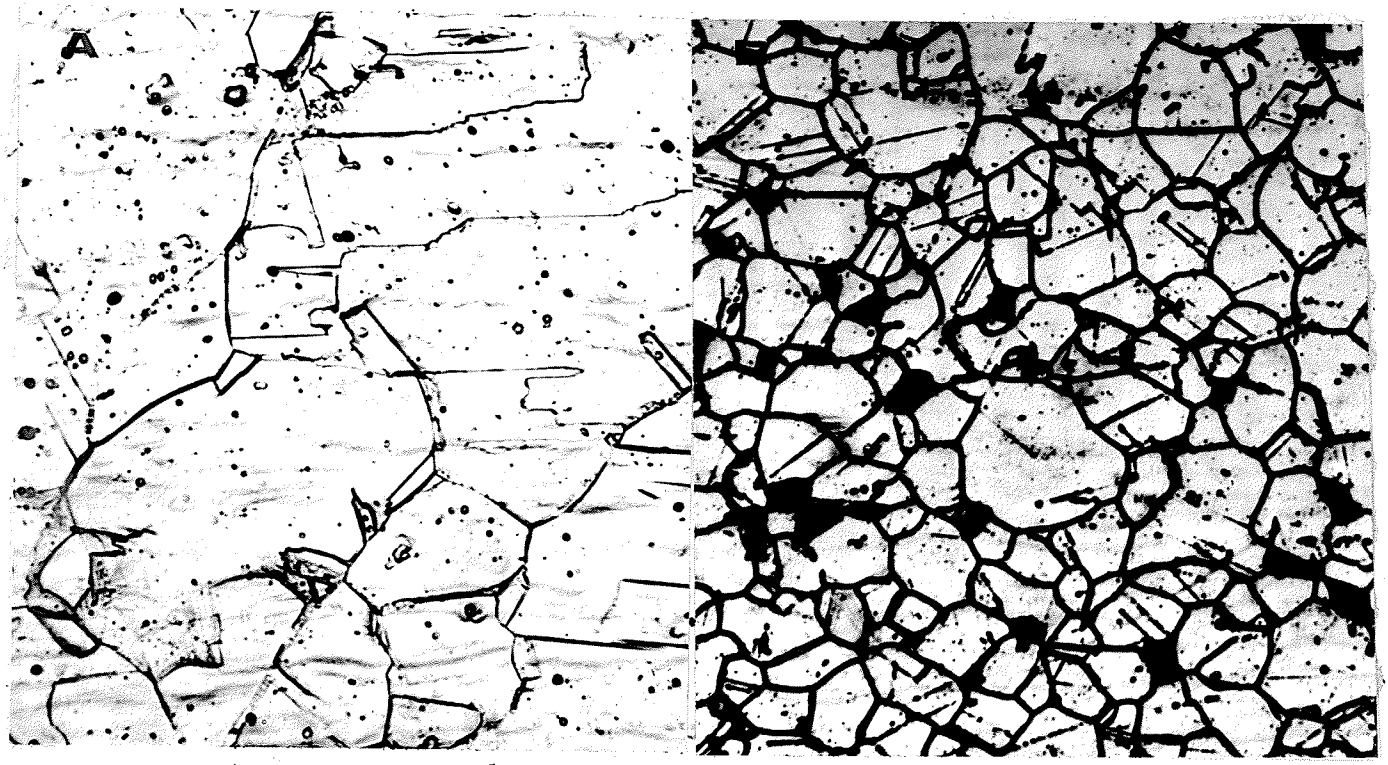

Fig. 9 Microstructures as a result of the oxalic acid electrolytic etching test: (a) De-sensitized specimen (grain boundaries just visible; the wavey lines are strain lines) (x150); (b) Sensitized specimen showing heavily etched grain boundaries (x150).

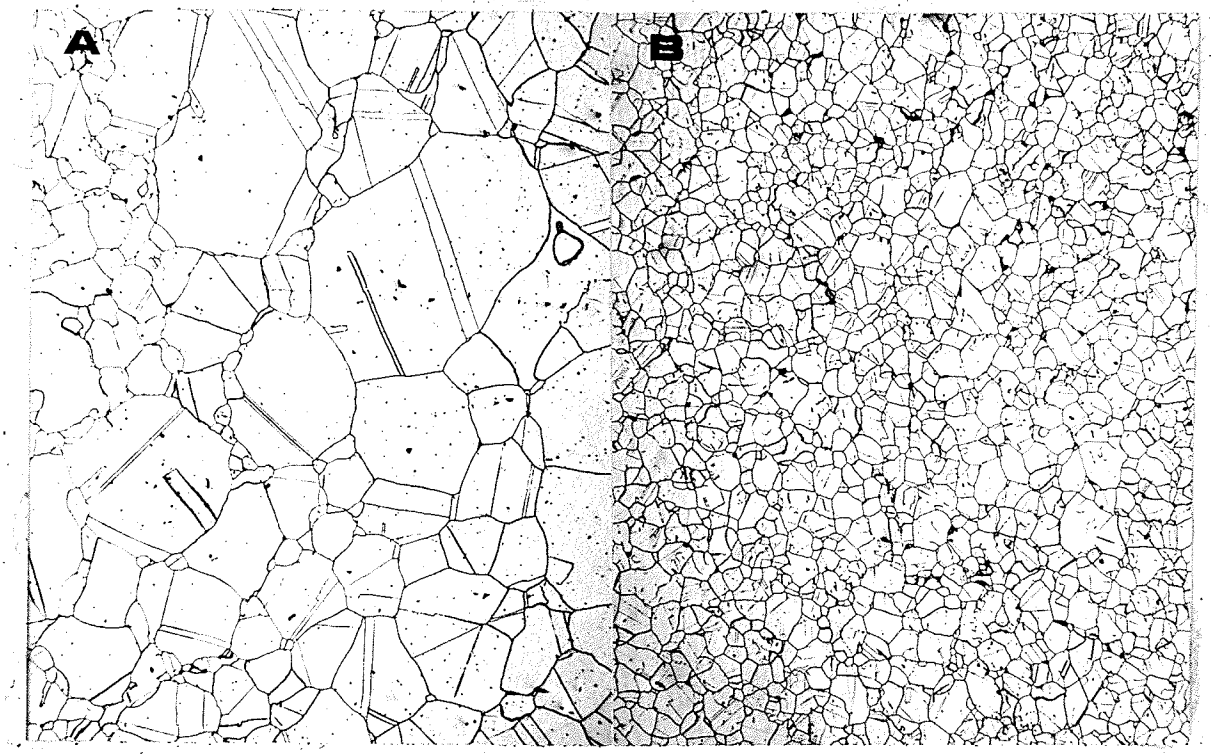

Fig. 10 Variation in grain size in microstructure of plate; (a) Large grains ASTM grain size 2-3 at top of plate by countersinking (x100); (b) Grains of ASTM size 7-8 at lower portion of the hole (x100).

CAUSE OF FAILURE:

This implant had undergone a very serious amount of intergranular corrosion in a very short time due to sensitization.

Implant-M70): Manufacturer's identifaction :"L Down J".

A chemical analysis of the material revealed the following composition: 17.38% Cr, 11.39% Ni, and about 2%Mo. There was no niobium or titanium present. Medical History: The Osborne-Ball osteotomy plate was inserted for the internal fixation of a McMurray osteotomy of the right hip for treatment of degenerative arthritis. The post-operative period was complicated by wound separation and hematoma with the patient being re-sutured. A further complication was a persistently draining sinus and the patient was treated with antibiotics. This fixation device was removed after a duration of eleven months in the hip.

METALLURGICAL ANALYSIS:

Visual observation showed marked corrosion of the slotted holes of the plate, of the hole at the end of the plate, and of the corresponding screws that had been in these holes. The specific corroded areas can be seen in Fig. 11. There was no corrosion of the gluteal post or of the plate in this area.

Optical microscopy showed that the microstructure, etched electrolytically with 10% oxalic acid was brought out very clearly in the grain boundary areas. Sensitization of the material was immediately suspected and proven to be true by the ASTM oxalic acid etching. Sensitized and de-sensitized microstructures (after 1 hour at 1000^{o}C) were produced being identical in appearance with those of M69.

A cross-section of the plate across one of the corroded

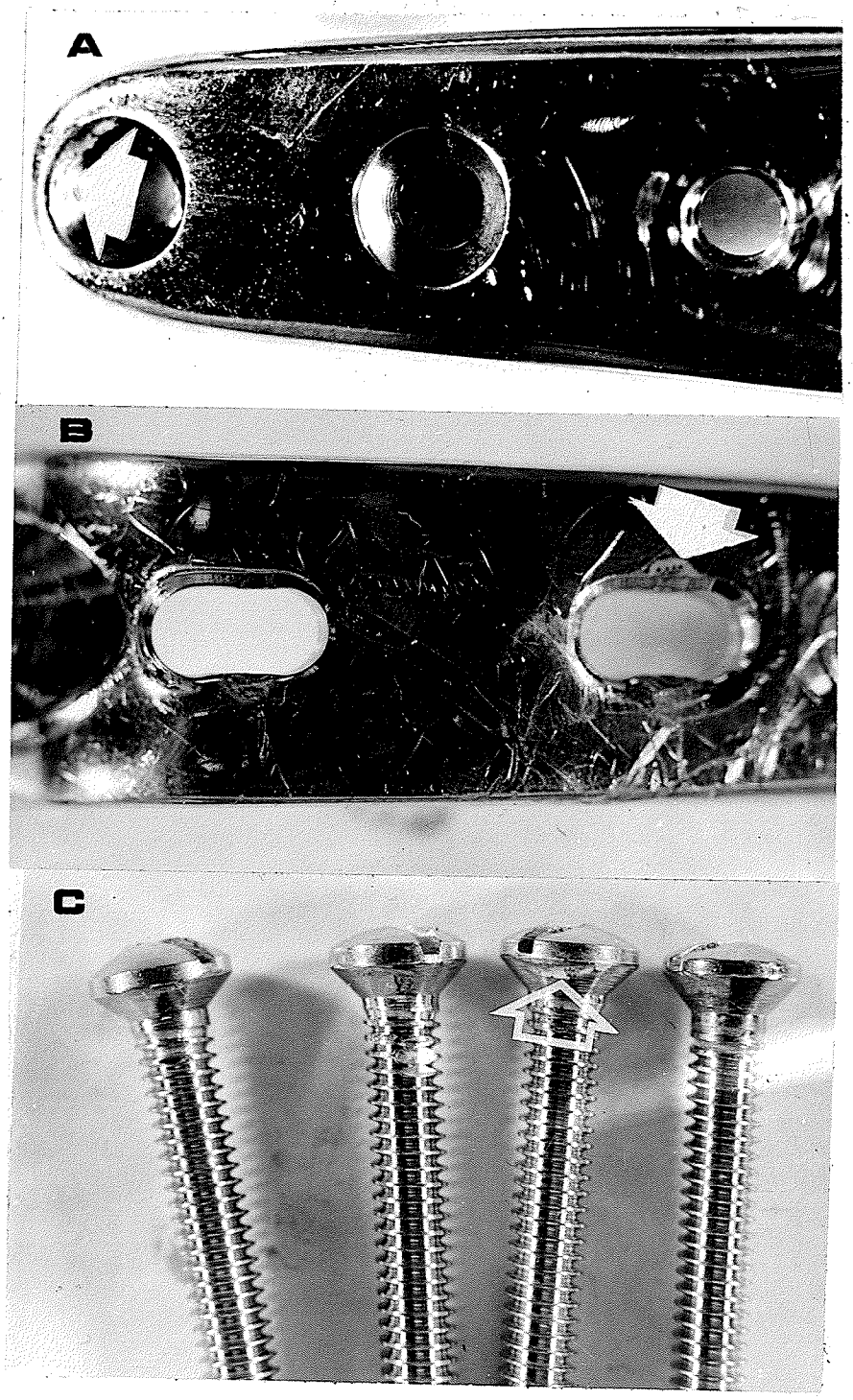

Figure 11. Location of corrosion in implant: (a) counter-sunk portion of hole at end of the plate; (b) corrosion at slotted holes; (c) four screws showing corrosion just under the head, (all 2x)

holes also showed a large variation in grain size as in M69. This peculiarity was seen in several cross-sections taken from the plate and can be considered to occur along the entire length of the plate. In all locations a very large grain size (ASTM 2-3) was noted at the top of the plate decreasing to ASTM grain size 7-8.. The large grain size is probably result of strains put in during the rolling of the plate coupled with the hot forming and/or heat-treating techniques. A small amount of strain (1-2%) accompanied with an annealing temperature critical to each material will result in a large grain condition of the material.

The medical history showed several complications and the resulting variations in the electrolyte of the body would have made it difficult for an implant to maintain its corrosion resistance under these circumstances. However a surgical device manufactured of a sensitized austenitic stainless steel would have a negligible chance of remaining completely compatible with the body tissues in these circumstances.

CAUSE OF FAILURE:

The severe corrosion of this surgical device was enhanced by the material being sensitized, severely lowering its corrosion resistance.

Implant-M74: Manufacturer's identification: "Down J".

Medical History: This plate was removed 30 months after insertion from a patient who was complaining of pain in the affected hip. At the time of removal of the implant, November 1969, large amounts of dark staining of the tissues was observed.

METALLURGICAL ANALYSIS:

Upon close examination of the complete implant as received, a large corroded area (dull satin grey in appearance) was seen on the gluteal post immediately above the threads (Fig. 12). The threads themselves were seen to be a dull charcoal colour with tiny perceivable pits. On the back of the plate at the hole where the gluteal post had been screwed was afixed a piece of dark brown tissue. When it was dislodged from the hole in the plate, a large amount of corrosion product was seen. The corrosion product was green in colour, close to the patina formed on oxidized copper.

The plate was sectioned across the hole for the gluteal post and the section was mounted and polished. Fig. 13 shows "pock-marked" areas in the immediate vicinity of the threads. This appearance was in part caused by grains dropping out during the polishing process due to weakening of the material at the grain boundaries as a result of corrosion reactions. The corrosion reaction itself dissolved large portions of the grains as seen in Fig. 14 (a and b). After etching the general microstructure was seen to have striations of a precipitate running through it bearing close resemblance to MnS inclusions (Fig. 15). The orientation of the precipitate phase was determined by the plastic flow of the material during forming. It should be noted that the aligning of the majority of these striations was coincident with the grain boundaries, indicating a grain boundary precipitate. Some of the precipitate was found growing into the grains, likely due to a stress-relieving anneal after hot forging of the plate, resulting in recrystallized material with a fine grain structure (ASTM grain size 5-6). However, the anneal did not dissolve the precipitate phase.

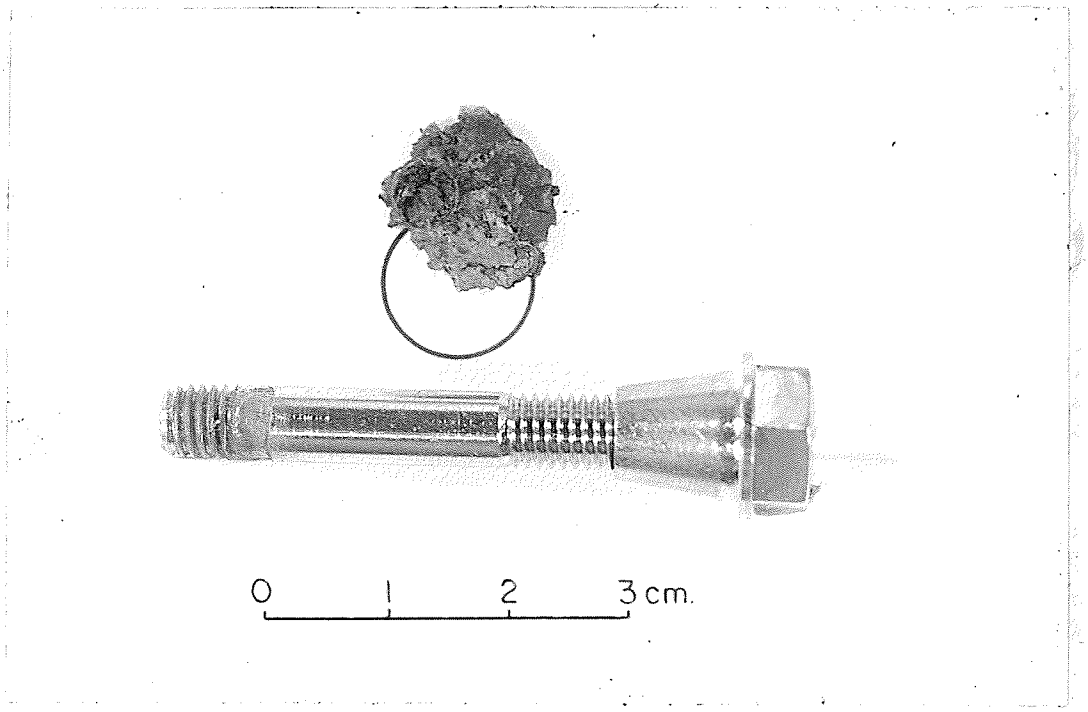

Fig. 12 Gluteal post and dry tissue removed from beneath plate at the hole of the gluteal post. Corrosion product, light green in colour, lies within the circle. Note: the corrosion in threads of gluteal post and also on the shank immediately above the threads.

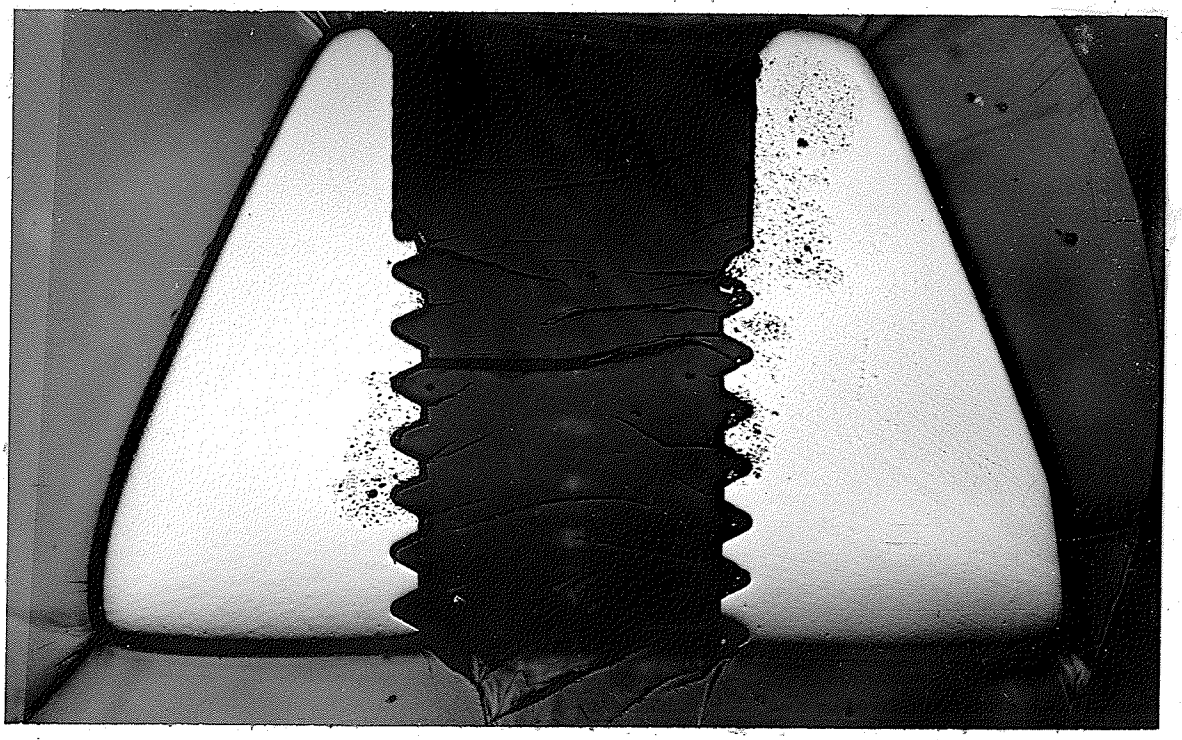

Fig. 13 Cross-section across the hole for the gluteal post shows extent of the intergranular corrosion here. "Pock-marked" appearance is the result of grain boundaries and grains being attacked by corrosion reaction, allowing grains to drop out during the polishing process (9x).

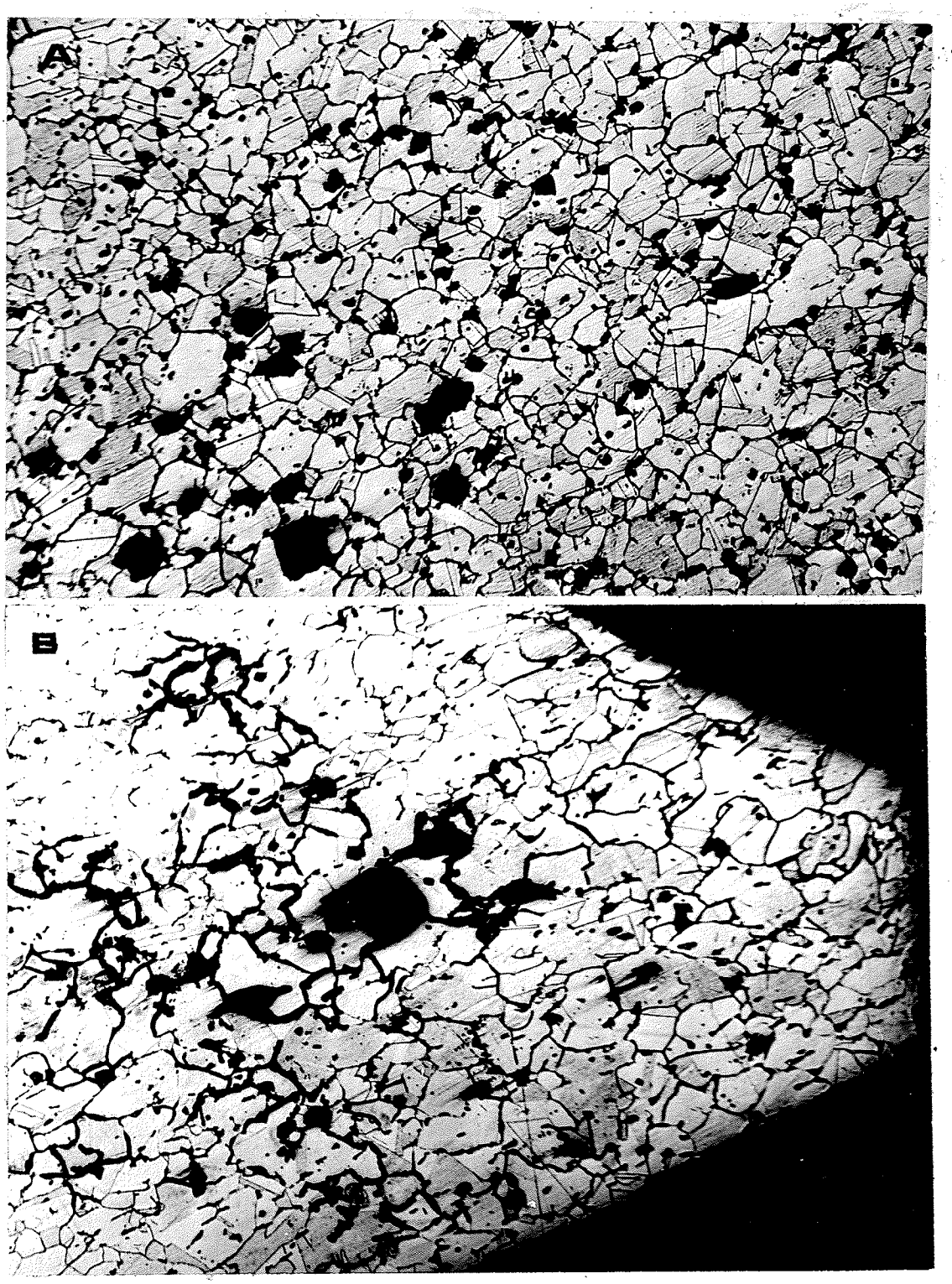

Fig. 14 Photomicrographs showing the 2 types of corrosion attack: (a) Here portions of the grains adjacent to the grain boundary have been corroded with the reaction seemingly to proceed into the grain rather than following along the grain. At the very top of the photo can be seen the very severe intergranular attack; (b) The very intense type of intergranular attack seen in the threads of the tapped hole in the plate for the gluteal post. Note how the attack seems isolated from outside portions of the plate. (both 120x).

The plate was in an almost full soft condition having a DPH of 216.

Initially the specimens were electrolytically etched in 10% oxalic acid and although the grain boundaries etched very readily as in the case of a sensitized stainless steel, the morphology of the precipitate observed in this implant indicates that it is something other than a massive form of the carbide $(Fe, Cr)_{23}C_6$ generally encountered in sensitized austenitic stainless steels. This unknown phase bore a likeness to sigma phase (FeCr) usually found in austenitic stainless steels subjected to prolonged heating at temperatures in the range 600^{o}-900^{o}. Following the technique of Gilman et al. [30] to distinguish sigma phase from carbide particles failed to positively identify the unknown phase as sigma phase. The microstructure of Fig. 16 was achieved by a light oxalic acid etch and appeared to be about the same as that obtained using the Murakami etch.

Debye-Scherrer films prepared from an electrolytically extracted sample using copper K_{α} radiation and chromium K_{α} radiation had insufficient lines to identify the unknown phase.

One sample was heat-treated for one hour at $1000^{o}C$, the usual treatment for de-sensitizing an austenitic stainless steel containing precipitated $(Fe, Cr)_{23}C_6$. The temperature of $1000^{o}C$ is sufficient to bring about dissolution of $(Fe, Cr)_{23}C_6$, restoring the chromium to the depleted austenite matrix. The resulting microstructure (Fig. 17 (a and b) showed that the heat-treatment had encouraged the phase to grow, although the grain boundaries etch less heavily as a result of the heat-treatment. A powder sample was electrolytically extracted from the heat-treated specimen. The now more bountiful precipitated phase was a chromium,

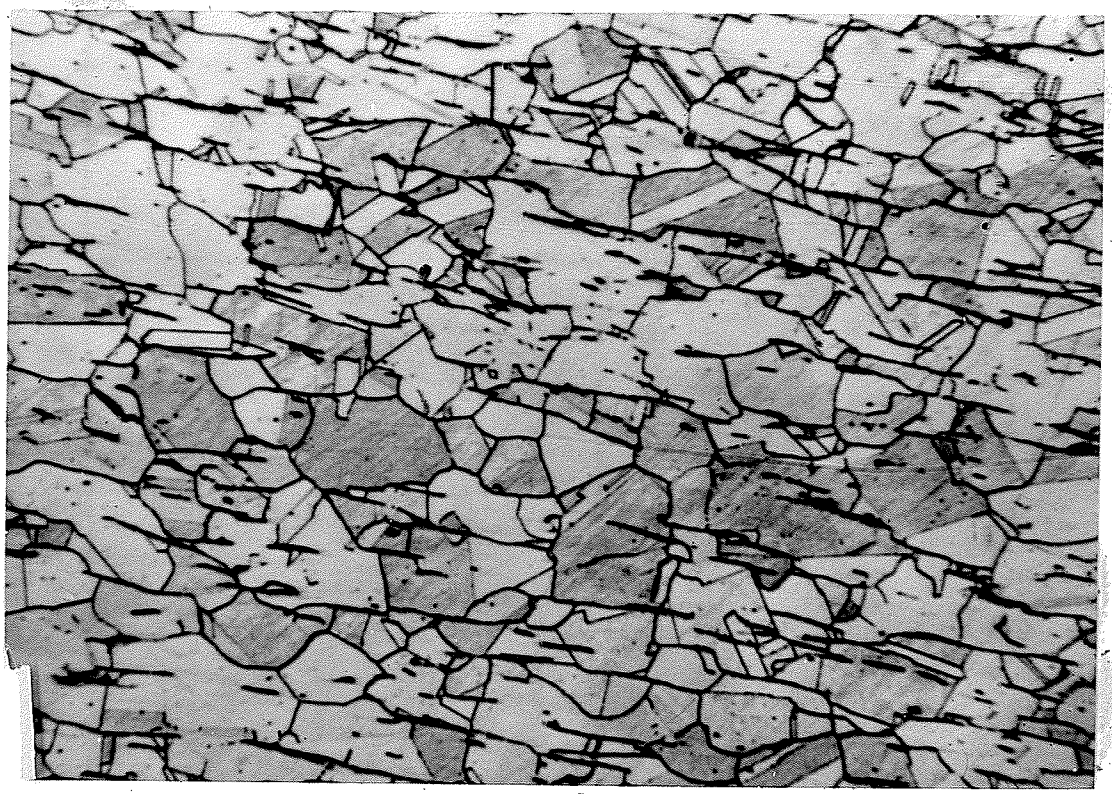

Fig. 15 Appearance of aligned precipitation phase bears resemblance to inclusions. Precipitate was formed during forging before final stress-relief anneal as they can be seen to extend into the recrystallized grains. Etched electrolytically in 10% oxalic acid (180x)

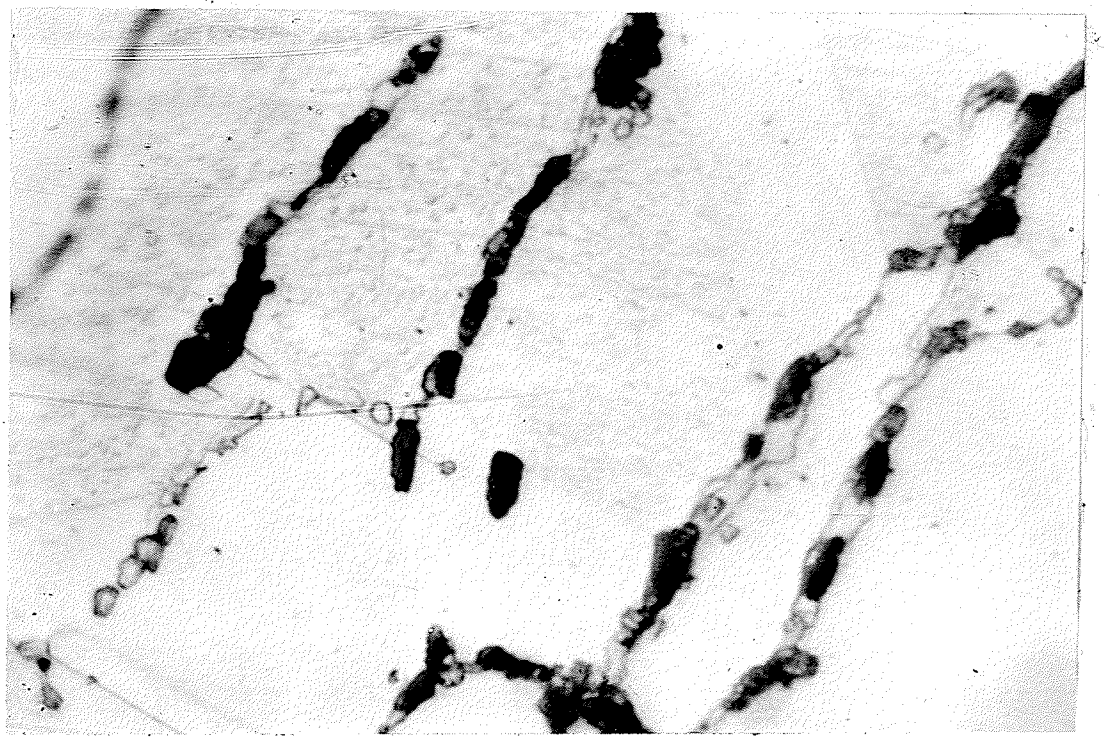

Fig. 16 The aligned particles can be seen at much higher magnification. The dark areas adjacent to the precipitated phase are corroded areas (oil emmersion, 2700x).

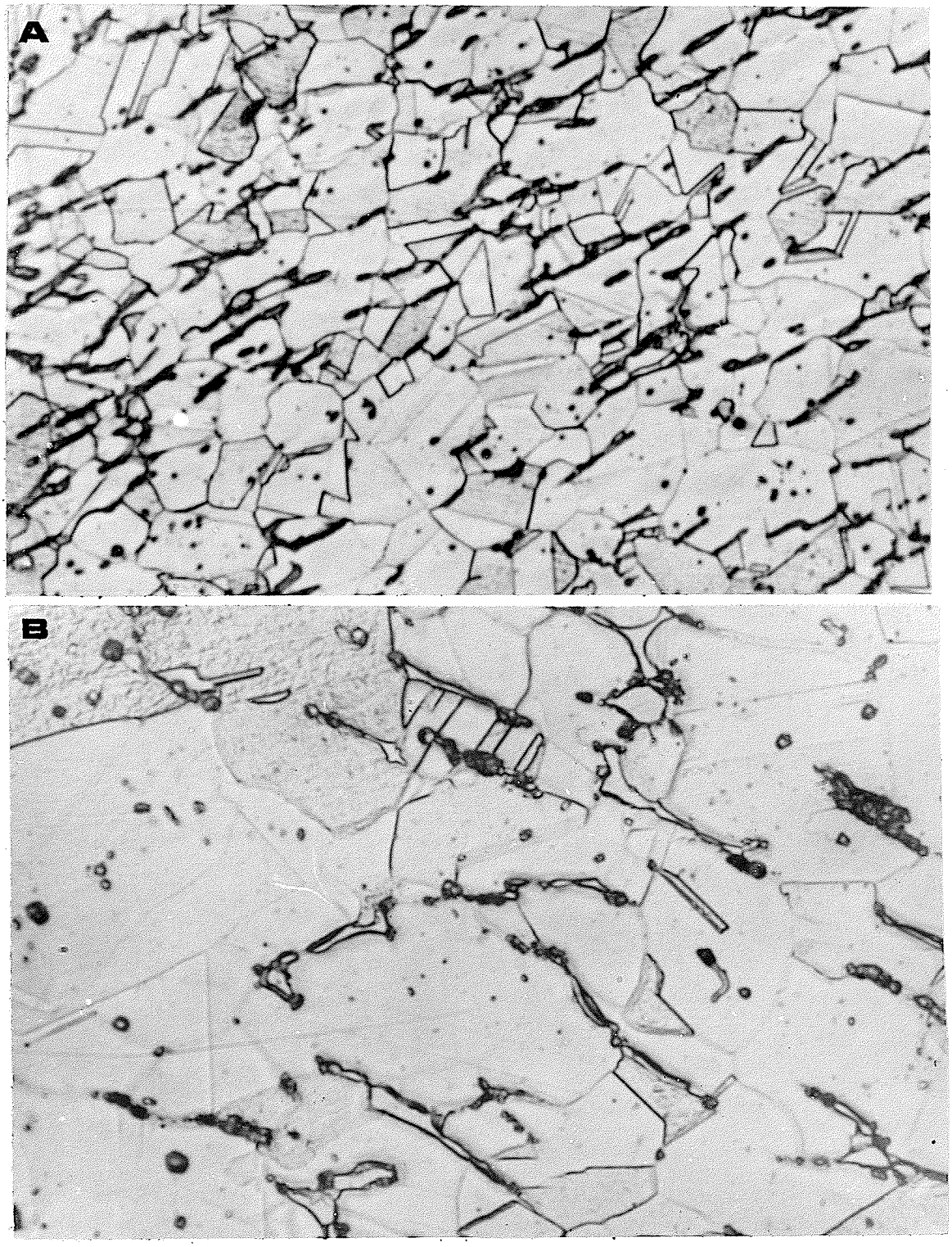

Fig. 17 Microstructure of "de-sensitized" specimen (1 hour at 1000°C): (a) Precipitate phase is seen to have grown and the grain boundaries etch quite clearly (250x); (b) Precipitate phase is seen in more detail and bears even more resemblance to sigma phase (1120x).

iron carbide ($(Cr, Fe)_7C_3$) and was definitely not $(Fe,Cr)_{23}C_6$ or sigma FeCr.

The identification and observation of this unknown phase deserves further mention. Recently Ellis and Pollard [31] observed precipitates metallographically similar to σ-phase (σFeCrMo) but developed after much shorter ageing times than had been previously reported, in a 20Cr-10Ni-3Mo steel. The phase was precipitated in appreciable quantities (upto 20 vol.%) after ageing time of only 15 minutes at 750°C and 5 minutes at 950°C.

The plate was observed to have corroded intergranularly with corrosion being centered around the hole for the gluteal post and having proceeded for at least 2 cm laterally from the hole. The intergranular corrosion did not occur uniformly across the cross-section but had occurred at several separate locations apparently where the density of $(Cr, Fe)_7C_3$ phase was greatest. The microstructure of Fig. 14(b) shows this very intense type of intergranular attack. Note the great width of the attacked grain boundary areas.

Localized corrosion (apart from the intergranular corrosion) also seems to have occurred in grains in dense areas of precipitates. It appears that the whole matrix in the near proximity of a precipitate particle is anodic, with the whole grain rather than just the chromium-depleted grain boundary areas disintegrating, as would be the case in the intergranular type of an $(Fe,Cr)_{23}C_6$ sensitized stainless steel. (see Fig. 14(a)).

The dead soft gluteal post (DPH 179) also appears to have been anodic relative to $(Cr,Fe)_7C_3$. General uniform corrosion occurred on the shank of the gluteal post and a pitting attack occurred in the threads probably complicated by the fact that small amounts of electrolyte

trapped in the threads enabled crevice corrosion to occur. The screws suffered no corrosion.

CAUSE OF FAILURE:

Corrosion was the result of the presence of $(Cr,Fe)_7C_3$ carbide precipitation. The condition which caused the formation of the carbide are not known.

A note in conclusion;

The manufacturer of these 3 Osborne-Ball osteotomy plates, Down Bros. and Meyer & Phelps Limited of Surrey, England were notified as to the corrosion problems being encountered in the use of these implants. The company is now following proper heat treatment proceedures and the problem of intergranular corrosion should no longer exist.

Implant-M59. Description: Mueller plate and 7 screws. Material: 316L stainless steel (composition, in wt-%, 16.50%Cr, 10.64%Ni, 2.40%Mo, approx. 65%Fe). Medical History: This bone plate was removed August 15, 1968 from a patient who suffered severe allergic reaction to the metal.

METALLURGICAL ANALYSIS:

Macroscopic examination showed areas of crevice corrosion in the end screw holes of the plate and of the corresponding 2 screws.

The microstructure was seen to have a small amount of inclusions and the grain size was ASTM grain size 5-6, within the recommended limits. The ASTM oxalic acid etching test was negative.

CAUSE OF FAILURE:

There was no metallurgical evidence to cause the crevice corrosion and resulting allergic reaction

Implant M-68. Description: Sliding Hip Nail and Plate with 4 screws. Material: 316L Stainless steel. Medical History: This multicomponent device was removed September 1969 after 5 months in the hip of an elderly lady who was complaining of pain in this area.

METALLURGICAL ANALYSIS:

Macroscopic examination of the 3 component device (Fig. 18) (plus 4 screws) showed a large corroded area (satining grey in colour) on the end of and on the middle of the nail which was within the slotted cylinder. The inside of this cylinder had been only roughly reamed with ridges easily seen. There were blue and purple oxide films inside this cylinder and on the shaft of the nail near the corroded area. The corroded areas of the nail are shown in Fig. 19(a and b). Fig. 19(c) shows the last three holes in the plate which were also corroded with the end hole showing the greatest amount of corrosion. The 3 corresponding screws were also severly corroded just under the head. All the components (including the screws) showed heavily worked microstructures. The ASTM oxalic acid test showed no sensitization of any of the components.

CAUSE OF FAILURE:

There was no direct metallurgical reason for the widespread crevice corrosion observed at almost every interface of this device. Because it was a multicomponent device there were a great many crevices to act as potential sites for corrosion perhaps outweighing the advantages in inserting such a multicomponent device.

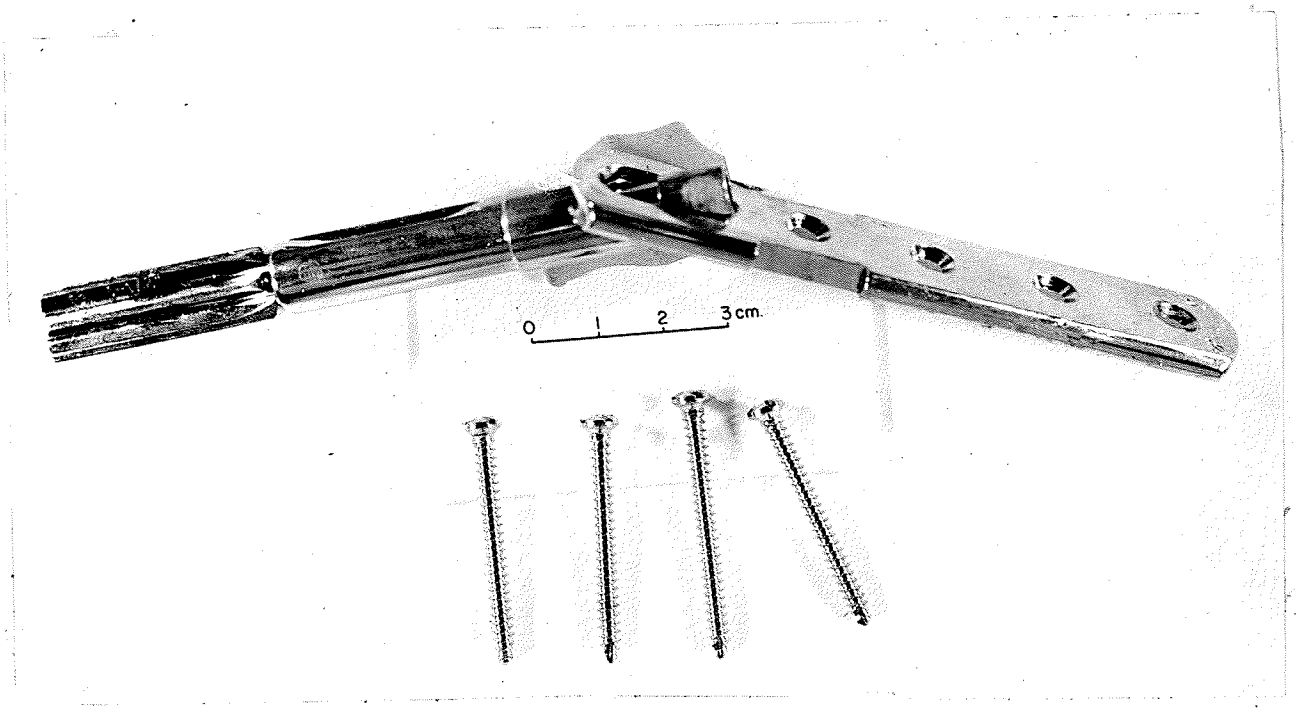

Fig. 18 M68 is shown assembled as received. Area of corrosion can be seen on the nail.

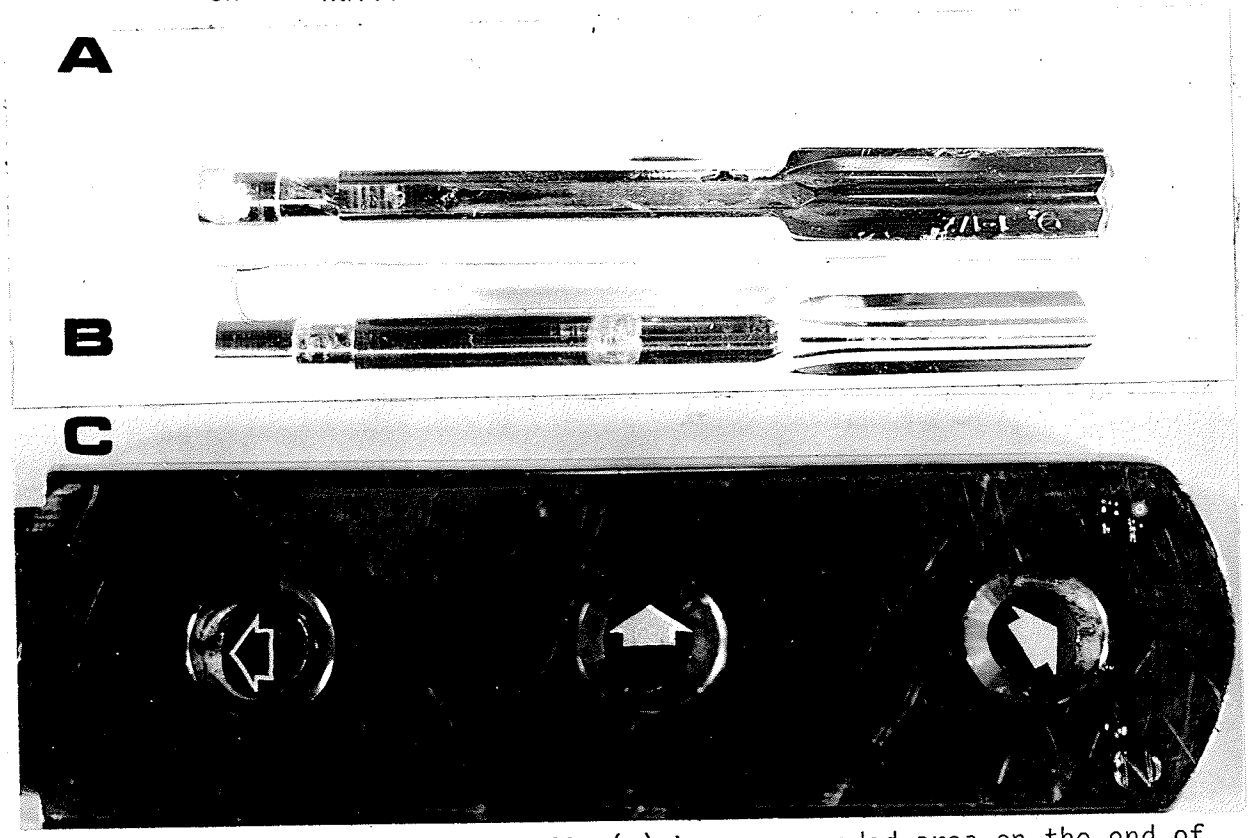

Fig. 19 Corrosion sites in M68: (a) Large corroded area on the end of the nail; (b) Corrosion on middle portion of the shaft; (c) Corrosion in the plate at the last 3 holes.

Implant-M71. Description: Zimmer bone plate (7 cm. long). Material: 316L stainless steel. Medical History: A fracture of the left radius was plated and in January, 1970, after 1 year, the plate was removed because of the pain being experienced in the arm over the plate. There was no unusual soft tissue reaction noted at the time of removal.

METALLURGICAL ANALYSIS:

Macroscopic examination showed a possible small amount of crevice corrosion in the end holes in the plate. The screws showed no corrosion.

The microstructure of the plate showed a partially annealed fine grained structure of ASTM grain size 6-7 and the screws a typical cold worked structure. The ASTM oxalic acid etching test was negative.

CAUSE OF FAILURE:

Metallurgically there is nothing to give a hint as to the reason for the suspected corrosion and the subsequent pain experienced by the patient.

Implant M-72: Description: Smith-Peterson Nail and plate with 5 screws. Material: 316L stainless steel. Medical History: 3 months following insertion pain recurred suggesting either a loosening of the implant or reaction of the tissues to the metal. One year later, in January 1970, the patient was readmitted for local skin pain over the region of the plant and the apparatus was subsequently removed.

METALLURGICAL ANALYSIS:

Macroscopic examination showed crevice corrosion at 4 holes in the plate (Fig. 20), with holes #1 and #4 showing the severest corrosion, (Fig. 21). Four of the screws showed easily detectable corroded areas immediately under head. The other components of the device - the nail,

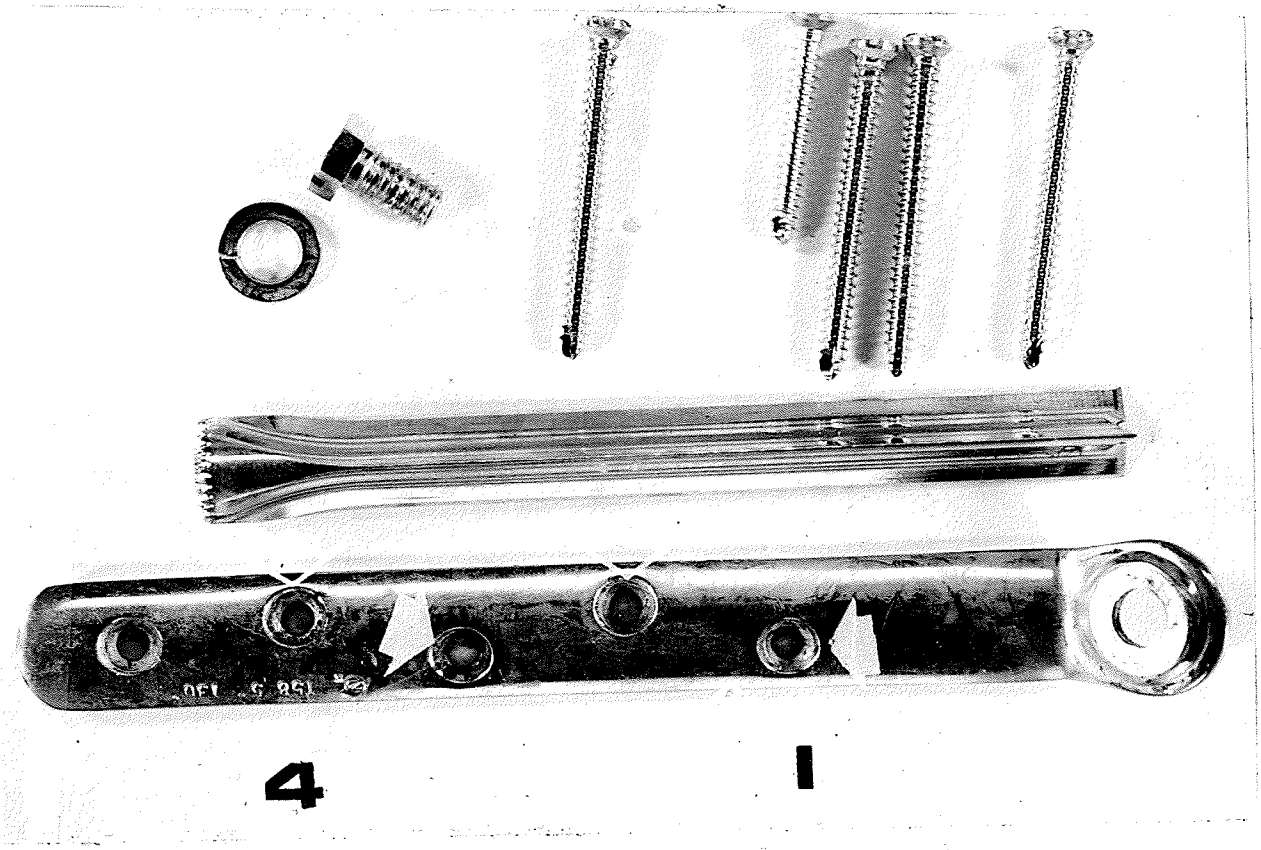

Fig. 20 All components of the Smith-Petersen Nail are shown with the sites of corrosion in the plate shown.

Fig. 21 Crevice corrosion of plate was most severe at holes #1 and #4.

the slotted bolt, and washer showed no corrosion.

Microscopically all components showed cold-worked ,fine-grained structures.

The history of this particular implant brings up the question whether movement between the screws and the plate which was suspected after 3 months causes mechanical abrasion of any protective film and leads to crevice corrosion - or does crevice corrosion once initiated cause reactions in the neighbouring bone tissue and subsequent loosening of the screw. Holes #1 and #2 were studied closely with this question in mind, and it appears that the latter would hold, ie. crevice corrosion could lead to a loosening of the screws. If there was a great deal of movement, the large irregular corroded area present at holes #1 and #4 would not be present, but should be slightly polished and certainly would not have corrosion deposits adhering to it. Such was not the case. The ASTM oxalic acid etching test was negative for all specimens.

CAUSE OF FAILURE:

There was no metallurgical reason for the observed crevice corrosion.

Implant M-73: Description: Zimmer Compression plate inserted with 8 screws plus one separate screw for a butterfly fragment. Material: 316L stainless steel. Medical History: The injury was a closed fracture of the tibial shaft and the post-operative period was uncomplicated with no evidence of infection. The plate was removed February 27, 1970 after the patient fell down some steps 2 weeks previous and later experienced

pain in her leg. X-rays showed no evidence of a new fracture. A brownish fluid was found around the plate and brown and black fragments (which appeared to be metal) in the surrounding tissues.

METALLURGICAL ANALYSIS:

Macroscopic examination showed severe amounts of crevice corrosion at the 4 central holes of the plate and was especially severe at one particle hole shown in Fig. 22(b). This amount of crevice corrosion occurs, fortunately, very rarely. On the back of the plate at this particular hole there was a large concentration of brown coloured corrosion product which had been between the plate and the tibia. Here crevice corrosion had been taking place with the corrosion products being separated from the other body tissues by the shiny membrane which covers implants, as described by [1,32,33]. This membrane encapsulates the implant very tightly; allowing no apparent tissue fluid space, and usually makes the removal of an implant quite difficult. The fall perhaps, damaged this sheath and allowed these accumulated corrosion products to come in contact with the soft tissues in the vicinity. Hence the pain in the leg and the brown coloured fluid found at the time of removal. It is not likely that this amount of corrosion could have occurred in 2 weeks, initiated in some way by the fall. The microstructure of the plate was fine-grained, and slightly annealed. The screws possessed a cold worked structure. The ASTM oxalic acid etchings test showed that there was no sensitization of the implant.

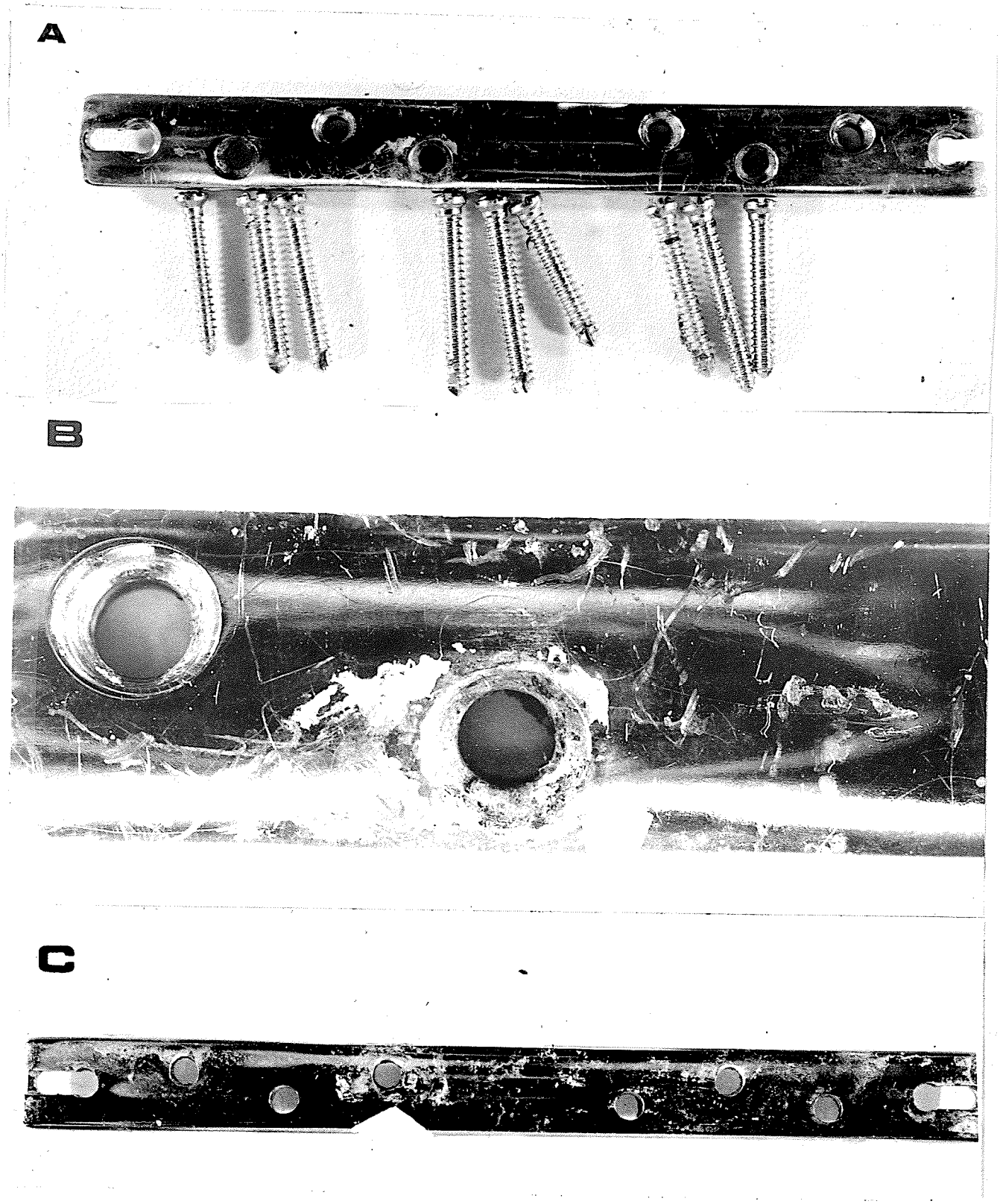

Fig. 22 Crevice corrosion which occurred at 4 centrally located holes of Zimmer compression plate: (a & b) Show the front of the plate with gross crevice corrosion in (b); (c) Reverse side of plate at the same hole shows extent of large corrosion deposit.

CAUSE OF FAILURE:

No metallurgical reason could be seen for the wide-spread crevice corrosion.

3.2 Summary of the Analyses of Crevice Corrosion

From this limited survey it can be seen that crevice corrosion is occurring in implants which appear by present thinking to be metallurgically compatible with the body environment. The incidence of corrosion, mostly of the crevice type, has been compiled by two workers for a number of excise implants. Colongelo and Green [34] in 53 devices examined found 45% to be corroded and only 8% to have been removed due to fracture. Similar corrosion figures have been compiled by Scales [35]. Colongelo and Greene also found that the incidence of corrosion in 30 single component devices was 10% while out of 23 multicomponent devices a staggering 91% was found to be corroded. Because of the much larger incidence of corrosion in multi-component devices efforts have been made to reduce the number of crevices to a minimum by careful design and to avoid the mixed use of steels of slightly varying composition. Today crevice corrosion is still occurring, though somewhat reduced, in multicomponent implants of seemingly homogeneous materials.

One avenue which has not been investigated is the range of hardness encountered between the components of implants, especially between the screws and plates. The hardness values of all the implants analyzed above have been compiled in Table 3. Examination of Table 3 shows that there is some correlation between corrosion and/or tissue reactions and a hardness gradient between the screw and the plate.

Table III

HARDNESS SURVEY OF EXCISED ORTHOPAEDIC IMPLANTS

Implant	Description	Component	Hardness Value-DPH (average of 5 readings)	Extent of Corrosion	Tissue Reduction
M-69	Osborne-Ball osteotomy plate	plate	166	gross	yes
		screw	385		
M-70	Osborne-Ball osteotomy plate	plate	184	gross	no mention
		screw	408		
		gluteal post	194		
M-74	Osborne-Ball osteotomy plate	plate	216	gross	pain
		gluteal post	179		
		screw	376		
M-59	Mueller Plate	plate	341	slight	allergic reaction
		screw	291		
M-68	Sliding Nail	plate	335	gross	pain
		screw	349		
		nail	328		
		cylinder	322		
M-71	Zimmer Bone Plate (7cm)	plate	291	minimal	pain
		screw	383		
M-72	Smith-Peterson Nail and Plate	plate	354	severe	pain
		screw	378		
		bolt	422		
		washer	353		
		nail	347		
M-73	Zimmer Compression Plate	plate	276	gross	pain
		screw	335		

Implants M-59, M-71, M-72, and M-73 have plate and screw hardnesses of 341 : 291, 291 : 383, 354:378, and 347:276 respectively. Laing [36] also pointed out that for optimum corrosion resistance, all components of the same device should be of the same hardness or else they will behave as different metals. It appears to be simply a matter of convenience on the part of manufacturers to make a nail out of a three-quarter hardness material and the rest of the implant out of a dead-soft alloy. The reason of convenience also seems to apply to the fact that screws are manufactured of AISI 316 (0.08%C max.) stainless steel, as Schmeisser showed [37] in a survey of 4 manufacturers, while the plates or other larger parts are fabricated of 316L or 316L VM (0.03%C max). From [23] Laing indicates a hardness for implants made of AISI 316 stainless steel of 30-35 on the Rockwell C Scale (DPH 300-345) would be preferred. According to Hochmann and Taussig, "most implant devices are produced in the work-hardened condition to provide the maximum strength, and if implanted under adverse conditions such as nonunion, they will provide the best possible service like from a mechanical standpoint."* Only a few implants are essentially in the annealed state.

3.3 Statement of the Problem

Screws being limited in cross-section by the dimensions of the bone into which they are driven, by necessity must have the greatest strength. Therefore they should be in the cold-worked condition. On the other hand the corrosion resistance of stainless steel is optimum when it is essentially in the annealed state. The option is open, for other

* P. 429 of Reference [3].

parts of the device such as the plate, larger bolts, nuts, and larger nails not requiring the highest strength to be manufactured in the essentially annealed state. However, by itself an annealed stainless steel may have the best corrosion resistance but its performance may be affected adversely when it is coupled with a cold-worked material (the screw). Therefore the essence of the problem is:

(i) To determine whether a cold-worked material (the screw) should be coupled with an equally hard or with an essentially annealed material and (ii) to investigate the performance of cold-worked and essentially annealed 316L stainless steel in physiological solutions of varying pO_2 and pCO_2.

Chapter IV

ELECTROCHEMISTRY OF CORROSION

4.1 Thermodynamic Basis of Corrosion

Corrosion is the reaction of a metal with its surroundings. The products of the reaction with which we are concerned are solids in the form of hydrated oxides or carbonates. In orthopedic surgery it is the products of the corrosion reaction and damage to surrounding tissue which are important rather than the damage itself sustained by the device corroding (as the corrosion is seldom allowed to proceed to a castrophic stage).

Metallic corrosion is the net result of 2 partial chemical reactions; (i) an oxidation reaction and (ii) a reduction reaction. The direct consequences of corrosion is the oxidation reaction in which the metal loses electrons and goes to a higher valency state by combination with an atomic or molecular group. The oxidation of iron to ferrous ions is:

$$Fe \rightleftharpoons Fe^{++} + 2e$$

The reaction is balanced by a reduction reaction involving the gain of electrons. Theoretically, it can be any reaction which is more positive than the equilibrium potential of the metal-dissolution reaction. In aqueous electrolytes, the electron-acceptor species present are H_3O^+ ions and dissolved oxygen. Possible cathodic reactions are:

$$2H_3O^+ + 2e \rightarrow 2H_2O + H_2(g) \qquad \text{[acid solutions]}$$

and

$$O_2 + 4H^+ + e \rightarrow 2H_2O \qquad \text{[acid solutions]}$$

In neutral or alkaline solutions (such as ECF); hydrogen ions will be available only in limited quantity, and the cathodic reaction is the reduction of dissolved oxygen;

$$O_2 + 2H_2O + 4e \longrightarrow 4OH^- \qquad [\text{alkaline or neutral solutions}]$$

Notice that the overall effect of these reactions is the same in increasing pH. If several cathodic reactions are possible, i.e. their equilibrium potentials are positive with respect to the metal - dissolution equilibrium potential, the one adopted will be the one yielding the highest corrosion current. An example illustrating this point is used by Bockris and Reddy [41]; the corrosion rate of iron in oxygenated solution is greatly increased in comparison with that in a deoxygenated solution. The rate in the former is determined by the cathodic reaction

$2H_3O^+ + 2e \longrightarrow 2H_2O + H_2$ while in the latter by oxygen reduction. Since the solubility of oxygen in the electrolyte is proportional to pressure, the higher the partial pressure of oxygen in the gas phase the greater is the corrosion rate.

A pure metal immersed in a solution establishes a characteristic potential which reflects a equilibrium with its ions. This metal/electrolyte interface constitutes a half-cell which can be denoted as M/M^{++}. A half-cell potential cannot be measured in absolute terms, but the potential between M/M^{++} and another half-cell can be measured. Therefore a table of Standard Electrode Potentials at 25^oC relative to the standard hydrogen electrode (SHE) has been established. This hydrogen reference electrode has by convention been assigned a reversible

potential value (E^o) of zero. Then experimentally, a measured emf is equal in sign and magnitude to the experimental half-cell if the SHE is on the left (by convention this electrode becomes oxidized) and the electrode in question is on the right [15].

For example, using a short hand notation to denote the two half-cells with the SHE shown on the left and the verticle double line representing the boundary between the two different solutions of the half-cells

$$Pt\left|H_2\ (1\ atm)\ H^+\ \ (a \pm = 1)\right\|M^{++}\left|M\right.$$

then, the emf is:

$$E_{cell} = E_{right} - E_{left} \qquad (5)$$

$$= E_{M/M^{++}} - E^o_{H_2/H^+} = E_{M/M^{++}}$$

Experimental work is usually conducted using the saturated calomel electrode (SCE) as a reference potential. The SCE is more robust and easier to use under experimental conditions and has a potential of +0.2420V at 25°C on the hydrogen scale. When a potential of a metal has been found using the SCE as a reference electrode, then the corresponding point on the hydrogen scale can be found by adding 0.2420V to the observed potential. This conversion will have to frequently be performed as corrosion potentials in the literature are measured relative to both the SHE and the SCE.

As absolute potentials have not been measured the sign conventions of the electromotive series are arbitrary. The metals below hydrogen which have negative potentials are the base metals, and form ions more readily than the noble metals having positive potentials

above hydrogen. It is generally assumed that base metal potentials are negative as a result of electrons remaining in the metal [42].

Previously it was mentioned that a cathodic reaction must have a equilibrium potential which is positive to the metal-dissolution reaction. Equation (5) can be written as:

$$E_{corr} = E_{cath} - E_{anode}$$

to describe the corrosion process. This is a result of thermodynamic considerations. The reversible emf is a measure of the free energy of the cell reaction by

$$\Delta G = -|z| FE_o$$

where E_o = reversible potential, ie no net accumulation of product.

z = number of electrons involved in the reaction

F = the Faraday equivalent (96,497 coulombs/equiv.)

This would allow the total free-energy for the corrosion process to be negative, E_o being positive, and the reaction will proceed spontaneously - from a thermodynamic viewpoint; from a kinetic viewpoint the rate may prove to be negligible. Kinetics take into account the effect of anodic and cathodic electrode areas, the exchange-current densities for hydrogen evolution and oxygen reduction, and the effect of film formation on the metal being examined.

The relationship between the value of equilibrium potentials of metals in contact with electrolytes where metal cation activity is different from unity and the standard electrode potentials (where

cation activity* is equal to one) is given by the classical Nernst equation,

$$E_{metal} = E_o + \frac{RT}{ZF} \ln a_{Mz+} \qquad (6)$$

where E_o = standard electrode potential of the metal at temperature T

T = the absolute temperature (^oK)

a_{Mz+} = in gram-ions/L

R = gas constant (1.99 joules/mole^oK)

Z = valency.

It should be stressed that this equation only describes an equilibrium situation where the rates $M \rightarrow M^+ + e$ and $M^+ + e \rightarrow M$ become equal. As a result there is no net product - hardly the situation in a corrosion process. The exchange current i_o flows in both directions and a net zero current exists. This equation explicitely describes the potential difference across a metal/solution interface if the activity ratio of electron donor atoms is altered. If the ratio is altered the equilibrium potential changes.

This equation has in the past had extensive use in electrochemical and corrosion studies, perhaps an overuse which has impeded progression this field.

* Oppositely charged ions in an electrolyte exert attraction effects which alter the behavior of the electrolyte from the measured concentration. This attraction effect, which increases with concentration, can be corrected with the use of an activity coefficient γ used in conjunction with a molal concentration (gram-ions of solute/1000g of solvent) to express activity.

i.e. $a = \gamma m$
when $m \rightarrow 0; \gamma \rightarrow 1$

for dilute solutions of 10^{-3}m, concentration can be used interchangeably with activity with little error

4.2 Kinetics Aspects

Bockris and Reddy [41] in a critical review of the use of the Nernst equation and the Butler-Volmer equation to be described shortly, point out that the Nernst equation applied only to reversible electrodes (ie net current density across the metal-solution interface is zero) where the overpotential (η) is zero. They go on to say "the heyday of the uses of this equilibrium equation is over".* It has been pushed into every electrochemical situation (including nonequilibrium ones). Corrosion processes usually being non-equilibrium in nature limit the use of the Nernst equation to a rather secondary role. Again from Bockris and Reddy, in reference to use of the Nernst equation. "It should not be forced into interpreting a situation which is far from equilibrium (as electron transfer reactions often are)" **.

For corrosion to proceed there must be a net current density i across the metal (solid)/electrolyte interface and this current is related to the overpotential $\eta = E_i - E_o$ where E_i is the potential of the metal at the applied current density i and E_o is the reversible potential. This polarization may be either anodic or cathodic. The Butler-Volmer equation [41] shows how the current density across a metal-solution interface depends on the difference η between actual non-equilibrium and equilibrium potential differences. At equilibrium it becomes the Nernst equation (the proof is beyond the scope of

* P. 906 of reference [41].

** Ibid. p. 908.

this study) and near equilibrium reduces to a linear i versus η Ohm's law for interfaces. Thus the immediate kinetic theory to follow applies to a non-corroding metal electrode in which only the ions of the metal itself (M^{z+}) are involved in the anodic and cathodic partial reactions. Some confusion may arise as to why this analysis cannot be applied to a corroding system if it does involve the kinetics of metal dissolution (oxidation). In a corroding system the cathodic reaction is something other than one involving metallic ions and therefore has a different Tafel slope*. However, the equations used in determinations of actual corrosion rates are evolved from it.

The importance of this equation arises from the fact that it connects two basic aspects of charge transfer at an electrified interface; namely; (i) the equilibrium current i_0, which represents the rate of transformation of substances at the interface without the accelerating effect of overpotential and (ii) the electrical effects resulting from the application of overpotential. The chemical and electrical aspects of charge transfer are described by:

$$i = i_0 [\exp (1 - \beta) F\eta/RT - \exp (-\beta)F\eta/RT] \qquad (7)$$

which is the Butler-Volmer equation [41] where the partial currents: $\overleftarrow{i}$ (cathodic deposition current) equal to $i_0 \exp(1-\beta)F\eta/RT$ and $\overrightarrow{i}$ (the anodic dissolution current equal to $i_0 \exp(-\beta)F\eta/RT$ are represented. If η is negative (electrons are pushed into the metal from the negative pale of the external source), then the net external current =

$$i = \overleftarrow{i} - \overrightarrow{i} = i_0, \text{ is a net "cathodic"}$$

* The Tafel slopes, β_a and β_c are the slopes of the logarithmic anodic and cathodic polarization curves.

deposition current. If η is positive (ie, the metal potential is made more noble, so that electrons are withdrawn from the metal into the "electron sink" of the positive pale of the external source, and a net "anodic" dissolution current

$$i = i_a = \overleftarrow{i} - \overrightarrow{i} \quad \text{results}$$

As an aside, two experimentally measurable quantities can be identified in equation (7); these are the slopes of the anodic and cathodic polarization curves, β_a and β_c respectively

$$\beta_a = 2.3\ RT/\beta F \tag{8a}$$

and

$$\beta_c = 2.3\ RT/(1 - \beta)F \tag{8b}$$

β itself is a symmetry factor which is an intrinsic characteristic of the given charge-transfer reaction at the given interface. For simple, single electrode exchange reactions $\beta \simeq 0.5$.** A plot of i versus η of the Butler-Volmer equation with a symmetry factor of ½ yeilds a curve resembling a hyperbolic sine function. Then equation (7) becomes

$$i = i_o\ [\exp(F\eta/2RT) - \exp(-F\eta/2RT)]$$

and since

$$\frac{\exp(x) - \exp(-x)}{2} = \sinh x$$

$$i = 2i_o \sinh F\eta/2RT \tag{9}$$

Because $\beta = \frac{1}{2}$, this curve is symmetrical (Fig. 23) and equal anodic and cathodic currents produce equal overpotentials, η. The hyperbolic sine function has 2 interesting limiting cases;

(i) η very large:

$$\exp(F\eta/2RT) >> \exp(-F\eta/2RT)$$

and as exp(-Fη/2RT) tends to zero.

** The electrochemical activation energy hump presented to the ions leaving the electrode occurs at 1/2 of the distance across the Helmholtz double layer.

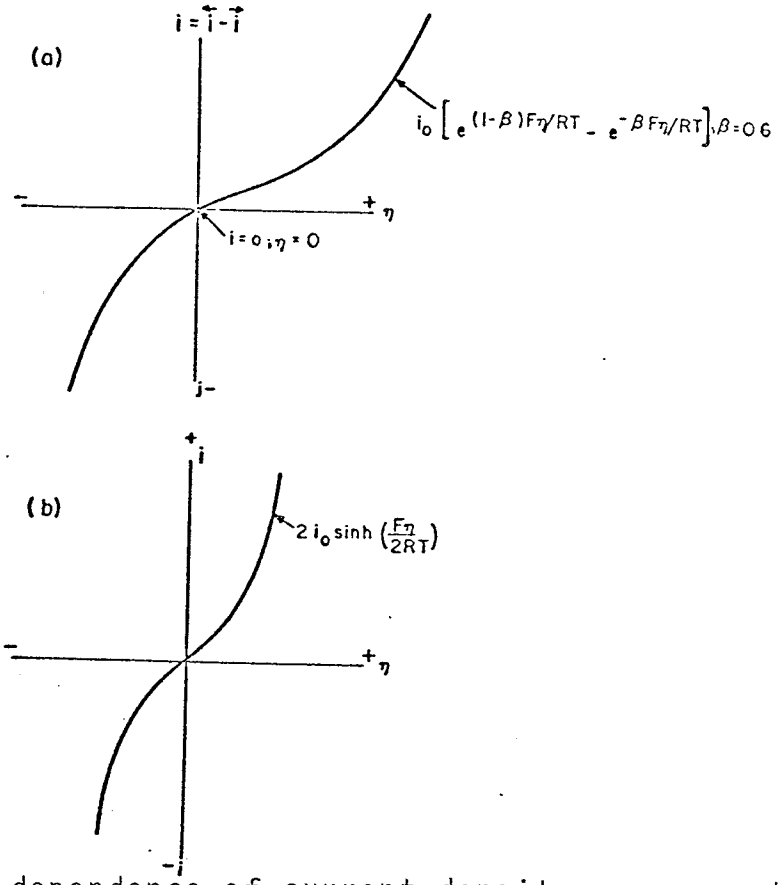

Fig.23 The dependence of current density on overpotential (a) is of the shape of a hyperbolic sine function(b). (Reproduced from Bockris and Reddy [41]).

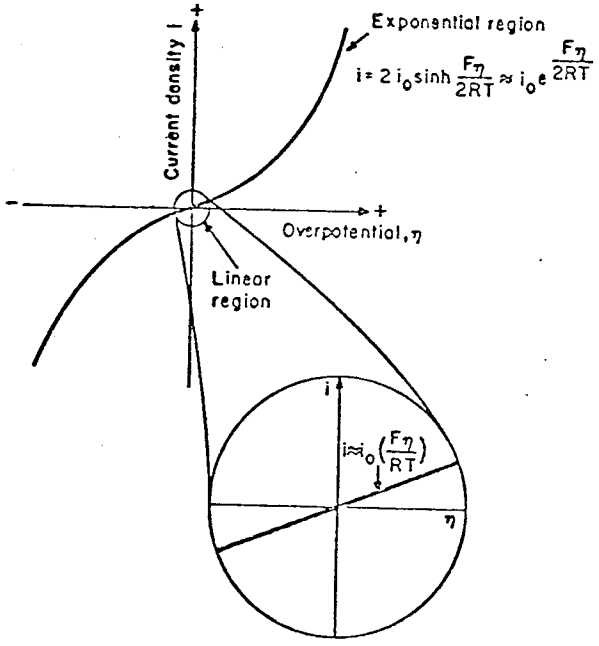

Fig.24 In the narrow region of small overpotentials, the i vs. n relationship is linear,and, at sufficiently high positive or negative overpotentials,the i vs. n realtionship becomes exponential. (Reproduced from Bockis and Reddy [41]).

$$2 \sinh F\eta/2RT \overset{\sim}{\approx} \exp(F\eta/2RT$$

$\therefore$ under high fields the Butler-Volmer equation reduces to

$$i \tilde{-} i_o \exp(F\eta/2RT)$$

(ii) η is small:

For small η, the two exponentials of (7) are expanded but only the first two terms of each exponential term are retained:

$$\begin{aligned} i &= i_o [\exp (1-\beta) F\eta/RT - \exp (-\beta)F\eta/RT] \\ &\simeq i_o \left[1 + \frac{(1 - \beta)F\eta}{RT} - 1 + \frac{\beta F\eta}{RT} \right] \\ &\simeq \frac{i_o F\eta}{RT} \end{aligned} \qquad (10)$$

The high and low field cases are shown in Fig. 24.

Further rearranging of this equation yields:

$$\frac{\eta}{i} = \frac{RT}{Fi_o} = \rho_{m/s}$$

where $\rho_{m/s}$ = reaction resistance (m/s denoted the metal and solution side of the interface). This quantity is also equal to the differential resistance $\left(\frac{\partial \eta}{\partial i}\right)_{C_A,C_D,T}$

where C_A = concentration of the electron acceptor

C_D = concentration of the electron donor

$$\text{ie} \quad \left(\frac{\partial \eta}{\partial i}\right)_{C_A,C_D,T} = \frac{RT}{Fi_o} = \rho_{m/s} \qquad (11)$$

$\rho_{m/s}$ determines the polarizability or the over-potential a particular current density requires and depends upon the exchange-current density i_o. As $i_o \to \infty$, $\rho_{m/s} = \left(\frac{\partial \eta}{\partial i}\right)_{C_A,C_D,T} \to 0$

The slope of the η versus i curve is zero, despite the fact that a current density i is flowing across the interface. Therefore the

interface remains virtually at its equilibrium potential and the electrode can be said to be nonpolarizable.

Establishing ranges of η where high field and low-field approximations can be used

(i) high fields

the high field approximation is based upon

$$\exp(F\eta/2RT) \gg \exp(-F\eta/2RT)$$

Assuming that the R.H.S. should be less than 1% of L.H.S.

ie. $F\eta/RT > 2\ln_e 10$

$$\eta > 120 \text{ mV at } 298^oK$$

Hence when the imposed potential E_i exceeds the equilibrium (rest or corrosion) potential by about (120 mV) for a one-electron transfer process this approximation will be valid.

(ii) low-field

condition for low-field approximation is $F\eta/2RT \ll 1$.

This can also be taken to be

$$\frac{F\eta}{RT} < \frac{1}{5}$$

then $\eta < 10mV$

When the overpotential η is about 10mV or less for a one-electron transfer reaction, the linear i versus η law be used with little error.

Bockris and Reddy have tabulated errors for the linear approximation of the Butler-Volmer equation and three such examples are with $\beta=0.5$, $i_o = 1mAcm^{-2}$ and $T=25^oC$ the error in the limiting law

is -0.7% for η = 10mV, only -2.5% at η = 20mV, and rises to -4.9% for η = 30mV.

4.3 Electrochemical Techniques

The theoretical background for corrosion studies investigations have been briefly covered. Now the various types of electrochemical techniques used to interpret corrosion processes will be reviewed from the viewpoint of determining what particular points would be relevant to this particular study.

(i) Potential Measurements

The measurement of corrosion potentials* and its variation with time can be employed in a general manner to interpret corrosion phenomena. This variation with time can be interpretted in terms of the condition of the protective films on the metal surface [43, 44]. Hoar and Mears [44] in a study to chose suitable medical implant materials used the variation of time of electrode potential between an isolated specimen and the test solution (0.17M NaCl at 37^{o}C) to group alloys as poorly resistant, moderately resistant, and completely resistant to that particular solution. Schematic potential-time curves are shown in Fig. 25. Curve (a) typifies an alloy undergoing film breakdown and general corrosion. Curve (b) is typical of an alloy showing an initial period of film thickening, followed by film breakdown and pitting corrosion. Curve (c) represents a film thickening which remains intact. Quoting from Hoar and Mears, "Only alloys giving curves such as (c) can be considered to be properly suitable for situations in which long term inertness is essential."** The falling

* Other terms used are rest potentials, natural potential or equilibrium potential of the metal M under the prevailing conditions.

** P. 487 of reference [44].

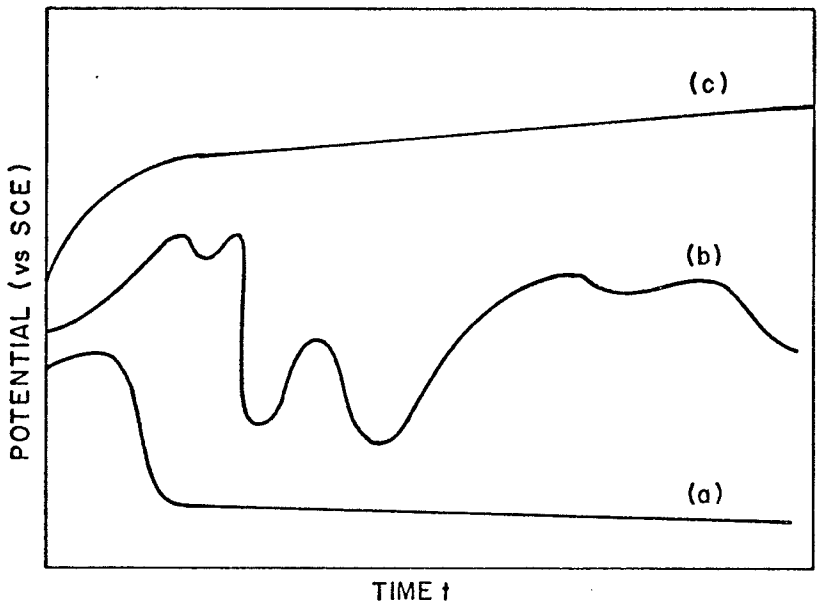

Fig.25 Schematic potential-time curves:(a) general corrosion (b) pitting corrosion;(c) film thickening. (Redrawn from Hoar and Mears [44]).

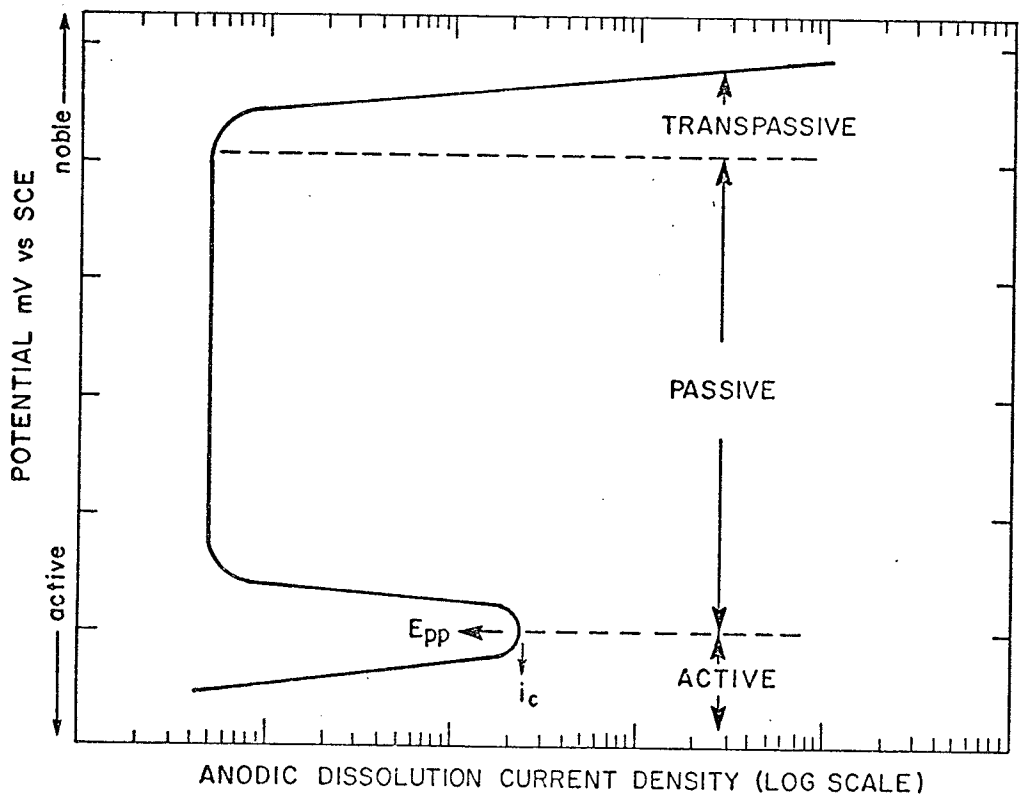

Fig.26. Schematic anodic dissolution behavior of metal demonstrating an anodic-passive transition. (Redrawn and modified from Greene. [46]).

and/or fluctuating characteristic of several stainless steels (Types 302,304, 316 and others) shows that these alloys are liable to film breakdown and consequent pitting in aerated dilute chloride solutions.

Phelps [43] says that potential measurements give an indication of whether anodic or cathodic processes, or both, are controlling the corrosion rate. For example; if E_{corr} is close to the reversible potential of the expected anodic reaction indicates cathodic control; a metal corroding under anodic control exhibits a corrosion potential that is close to the reversible potential for the expected cathodic process; and an intermediate corrosion potential indicates mixed control. Potential measurements when combined with corrosion rate measurements can be used to gain insight into the effect of changes in the environment on corrosion processes. "If a change in solution velocity, temperature, concentration, or the addition of an inhibitor or an accelator causes an increase in the corrosion rate, a corresponding change in the corrosion potential in the cathodic direction (negative) indicates depolarization of the cathodic reaction. A corresponding change in the corrosion potential in the anodic direction indicates increased depolarization of the anodic reaction. Conversely, if the environmental change causes a decrease in corrosion rate, a corresponding change in the corrosion potential in the cathodic direction indicates increased polarization of the anodic reaction. A corresponding change in the corrosion potential in the anodic direction indicates increased polarization of the cathodic direction".*

Other workers have attempted potential measurements in studies of the compatability of metals in biological fluids. Clarke and Hickman [45] found that the measurement of static potentials between

* P. 241t of reference [43].

a piece of test metal (one of those tested was Type 316 stainless steel) and a calomel electrode both placed in equine serum at 37°C produced readings which bore no relation to the known inertness of the metals concerned. Their results were also not reproducible. One reason they experienced difficulty in this measurement was because the calomel electrode was also at 37°C rather than room temperature connected by a salt bridge to test solution. Its stability as a reference electrode decrease rapidly if the temperature is much different than room temperature and if it is not kept in a saturated potassium chloride solution. Only limited interpretation can be placed in potential-time measurements with regard to protective films unless this type of measurement is combined with corrosion-rate measurements.

(ii) Potentiostatic* Polarization Curves

One of the most promising electrochemical technique applicable to metals displaying active-passive transitions are potentiostatic determined anodic dissolution curves. The constant potential measurements (see Fig. 26) utilize a logarithmic scale permitting the presentation of a wide range of current densities. As the potential of the metal is made increasingly more noble (positive) the dissolution rate of a typical active-passive metal passes through a maximum and then remains essentially independent of potential. The maximum current is designated, i_c, the critical anodic current density and the corresponding potential E_{pp}, the primary passive potential. As shown in Fig. 26 the actual behaviour of an active-passive metal can be divided into 3 different

* A potentiostat is an electronic device capable of holding a constant potential with respect to a standard reference electrode (eq. SCE) between a test electrode and a counter electrode.

regions: active, passive, and trans-passive. Greene [46] describes the curves as capable of allowing description and prediction of the corrosion behaviour of a active-passive metal. From them it is possible to determine: (i) the passive potential region. (ii) the passive corrosion rate, and (iii) the condition necessary for achieving passivity. The measurement of an anodic (or cathodic) polarization by application of an external current does not yield the actual polarization behaviour of shown in Fig. 26. This follows from the fact that the applied current is equivalent to the difference between the rate of oxidation and the rate of reduction. Figures 27, 28 and 29 show three different conditions when a cathodic reduction polarization curve is superimposed on an actual anodic polarization curve. The curve of Fig. 29 ressembles the low pO_2 curves to be shown later. Note the distortion in the vicinity of E_{corr} and the fact that the characteristic nose of the active-passive metal cannot be observed. This distortion (Greene [46]) is a result of the metal spontaneously passivating and obscuring Epp and I_c. A further distortion of the curves occurs if oxygen reduction begins at or within the transpassive region. Then the measured anodic curve does not represent metal dissolution but rather a summation of 2 anodic processes: metal dissolution and oxygen evolution. In [46] Greene states that it is usually observed that the measured anodic polarization curve closely corresponds to the actual anodic dissolution curve at potentials more noble (positive) than 50mV above the corrosion potential and below approximately 0.8 to 0.9 V versus saturated calomel.

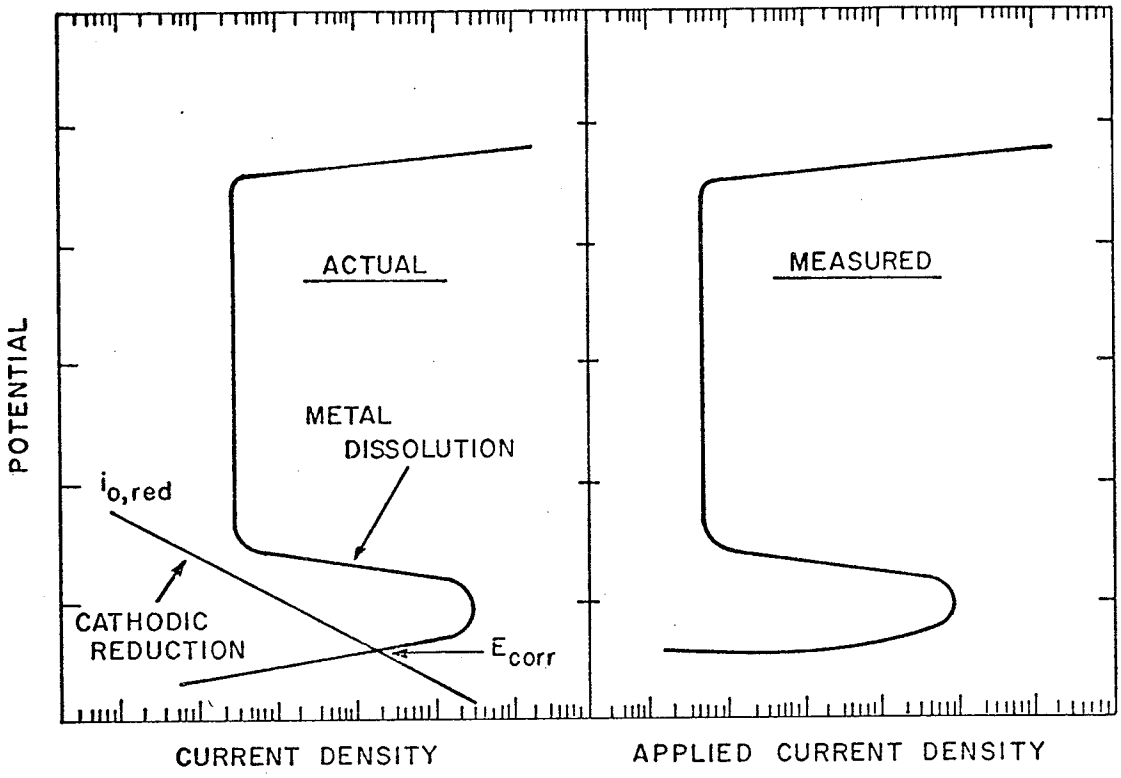

Fig.27 Actual versus measured anodic dissolution behavior of an active-passive metal.Active state stable.(Schematic) (Redrawn from Greene [46]).

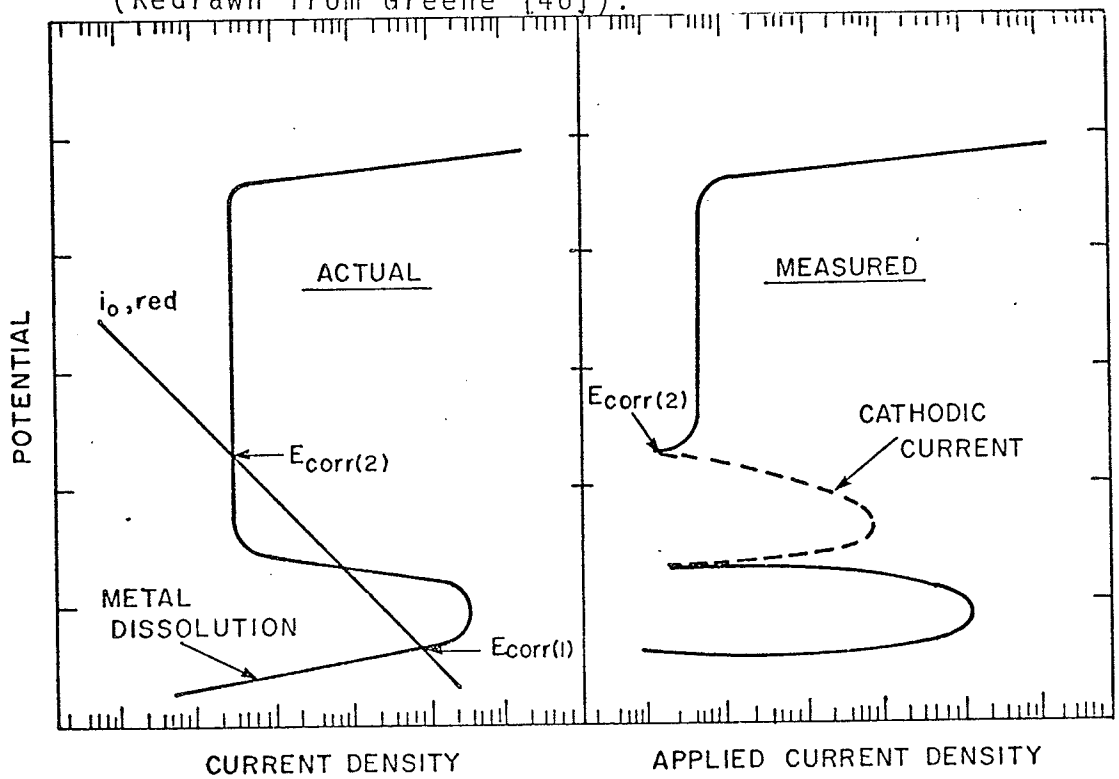

Fig.28 Actual versus measured anodic dissolution behavior of an active-passive metal.Active and passive states (schematic) (Redrawn from Greene [46]).

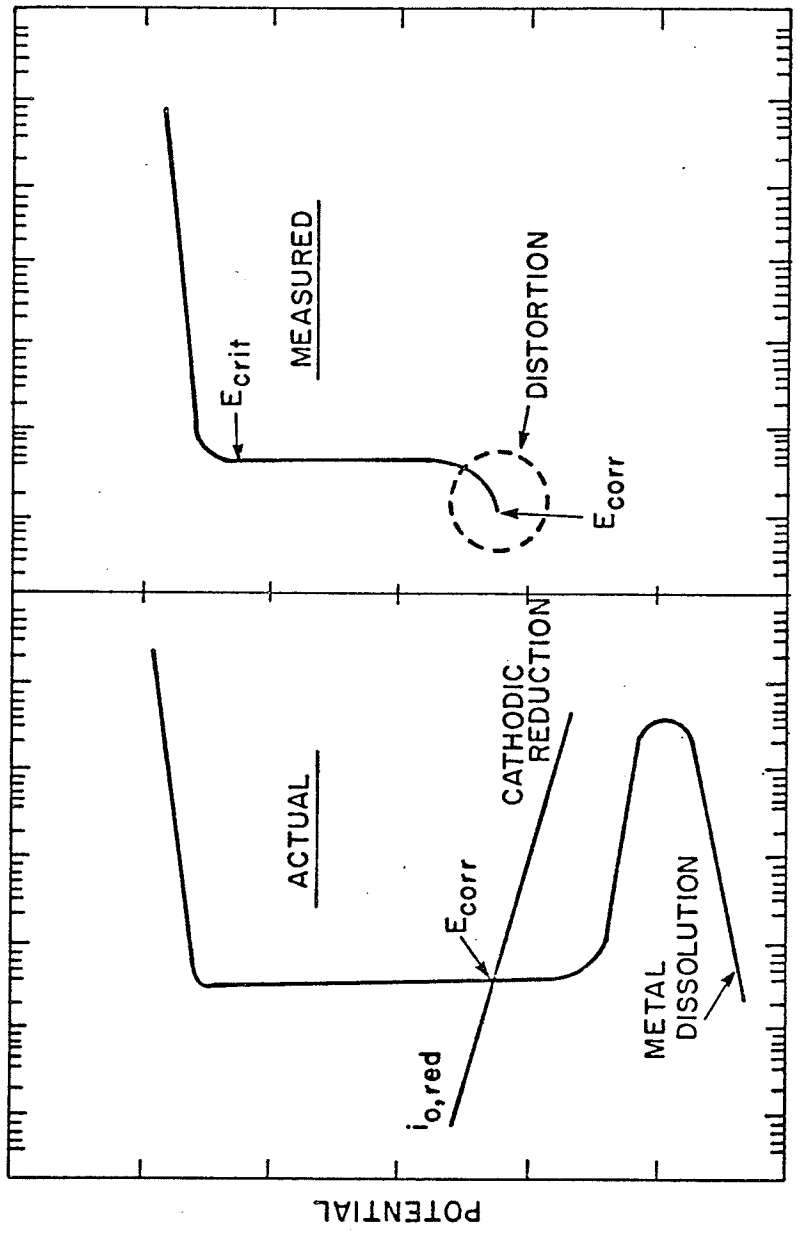

Fig.29. Actual versus measured anodic behavior of an active -passive metal. Passive stste stable (spontaneous passivation) Schematic. (Redrawn from Greene [46]).

The measured anodic polarization curve of Fig. 29 is representative of the performance of stainless steels in chloride solutions. At potentials higher than Epp the polarizing current decreases with increasing potential to reach a fairly constant value in the passive region. As the polarizing potential is increased, a "breakdown" potential* is reached. Above this breakdown potential the sharply increased anodic current indicates the breakdown of passivity and the onset of pitting corrosion. Leckie and Uhlig [47] using solution annealed (1050°C for 1 hour) 18-8 stainless steel in deaerated 0.1N NaCl solutions affirmed that this pitting would not occur in any degree below the critical potential determined from short time potentiostat tests, and was not simply delayed by time. The passive current and E_{crit}, in relation to the measured E_{corr}, were also used by Hoar and Mears [44] to classify the observed performance of corrosion resistant alloys (including 316L and Vitallium) in chloride solutions. A smaller passive current indicated more perfect passivity. Fig. 30 shows 3 types of resistant alloys. For the first type the anode breakdown potential measured potentiostatically is much lower than the highest potentials (E_{corr}) measured in potential/time measurements. In this case film breakdown would readily occur. If E_{crit} is close to E_{corr} of long term exposure tests (Fig. 30(b)), film breakdown would not occur as long as the specimen undergoes prolonged exposure. In Fig. 30(c) when E_{crit} is far higher (more noble) than the highest observed E_{corr}, then breakdown on isolated specimens during prolonged exposure is very unlikely. Finally if

* Also called the critical potential for pitting or the critical breakdown potential.

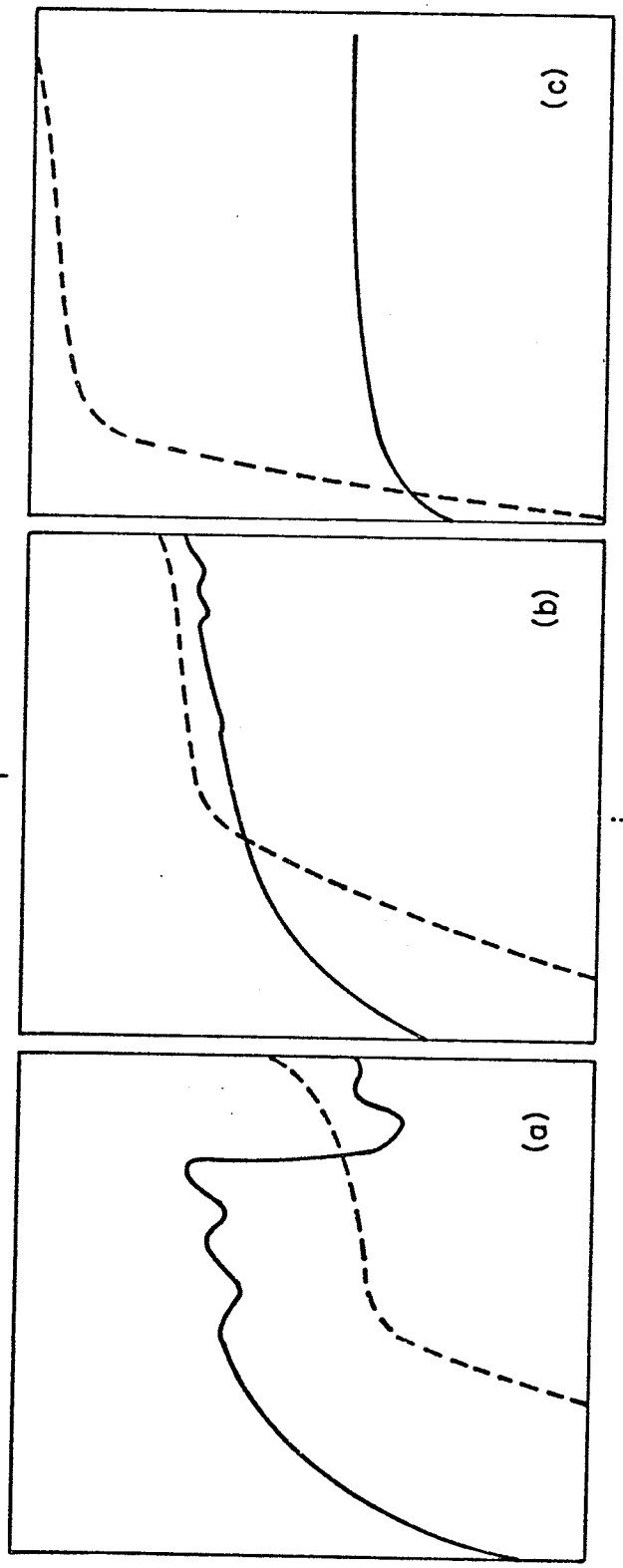

Fig.30 Characteristic relations between breakdown potentials measured by polarization curves(----) and potential/time curves(_____).
(Redrawn from Hoar and Mears [44]).

E_{crit} is higher than the highest possible potential at which oxygen reduction can occur, then breakdown on isolated specimens in aerated solutions is impossible unless mechanical breakdown of the oxide film occurs. The value of E_{crit} is so important in determining the extent of stability of stainless steel that the effect of various changes which might be encountered in the physiological environment on E_{crit} are listed below;

(1) Effect of pH on E_{crit}

The findings of several investigators was that the critical potential is not affected appreciably in the acid pH range. It moves markedly in the noble direction in the alkaline range corresponding to observed resistance to pitting in alkaline Cl^- media: Such were the conclusions of Leckie and Uhlig [47] with 18-8 stainless steel in deaerated 0.1N NaCl adjusted in the acid range by HCl additions at 25°C. These results are summarized in Fig. 31. Small shifts in the acid range were further affirmed by determining values of E_{crit} in 0.25, 0.50, and 1N HCl. Here E_{crit} shifted in the anodic direction a maximum of only 50 mV which is probably accounted for mainly by increasing Cl^- activity rather than by the change of H^+ activity. This seems to be contrary to what seemingly should occur in that "oxide films being soluble in acids ought to be thinner or more porous, hence more easily penetrated at low pH than at high pH values, yet the critical potential is not appreciably altered in 0.1 N NaCl on going from pH 7 to 1" *.

* P. 1266 of [47].

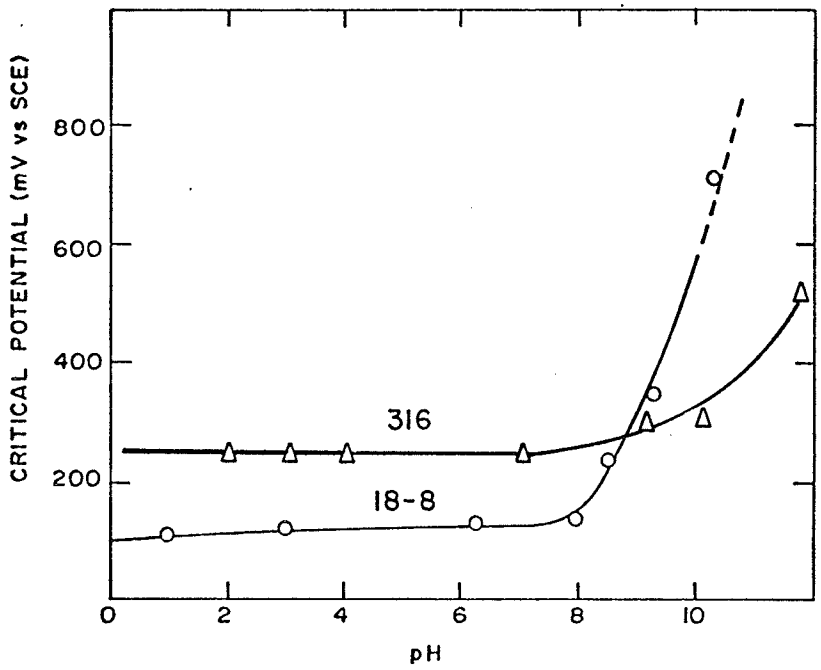

Fig.31 Effect of pH on breakdown potential for pitting: open circles-18-8 stainless steel in deaerated 0.1N NaCl, 25 °C [47]; open triangles -type 316 stainless.

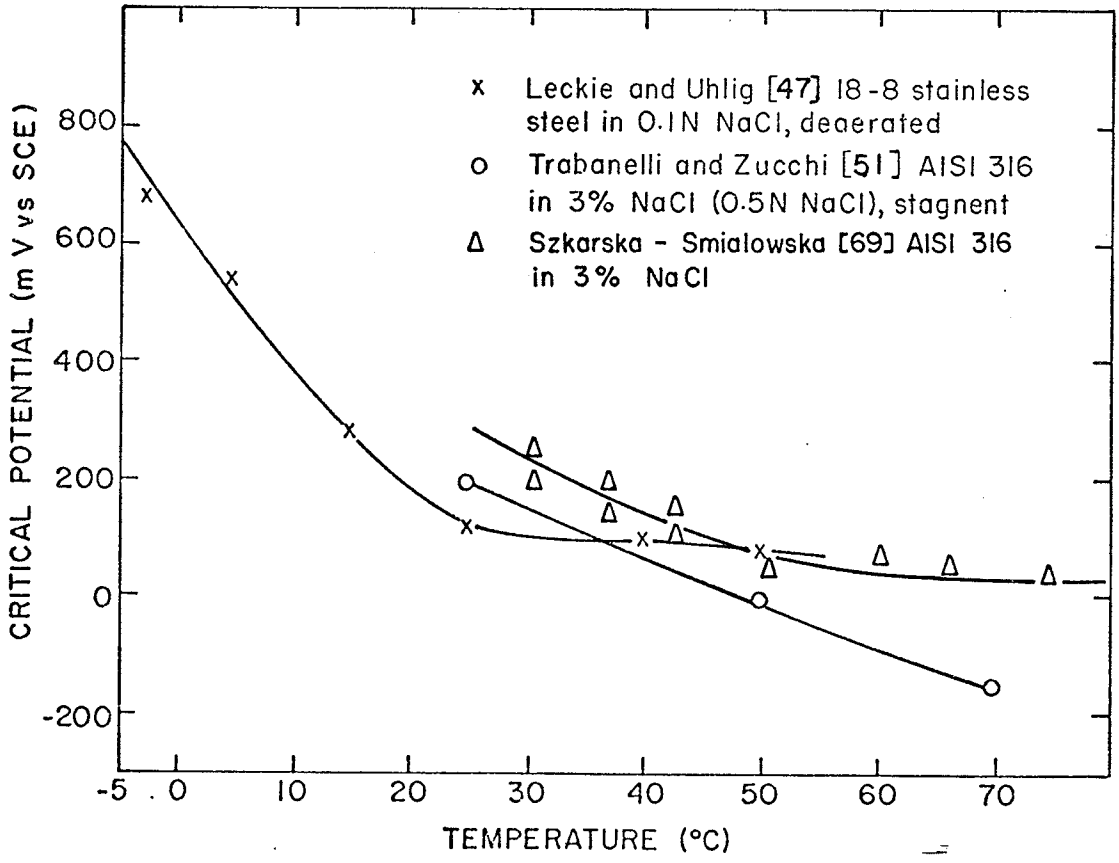

Fig.32 Variation of E_{crit} in sodium chloride solutions as a funstion of temperature.

Similar results were found in experiments conducted at higher temperatures, closer to that of the body ($37^{o}C$), and beyond this such as the testing temperature of this experimental work ($60^{o}C$). Rocha [48] presented data at $50^{o}C$ showing only a small effect of pH on critical potentials in the acid range of pH and Uhlig and Morril [48] showed that the pitting of 18-8 stainless steel in 4% NaCl at $90^{o}C$ decreases markedly as the pH is increased above 7.

(2) Effect of $[Cl^{-}]$ on E_{crit}

A shift of the critical potential to more active values (negative) on increasing the Cl^{-} was noted by Leckie and Uhlig [47]. E_{crit} was shifted 0.09 V for a 10-fold change in concentration (in moles) in the negative (active) direction. This was interpretted in terms of "competitive absorption" of Cl^{-} and other anions for sites on the alloy surface. Only at sufficiently high surface concentrations is oxygen, making up the passive film, displaced locally, and passivity thereby destroyed resulting in a pit. This is one of the reasons why crevices, if they exist, are the first to pit because they harbour higher concentrations of Cl^{-}. This factor and also perhaps nonuniform composition alloy surfaces (screw and plate of different hardness) may account for scattered values of E_{crit} reported in the literature and the occurence of crevice corrosion in implants where no apparent metallurgical reason for the corrosion can be found.

(3) Effect of O_2 on E_{crit}

Wilde and Williams [50] on the influence of dissolved gases on the critical breakdown potential in halide media using solution annealed AISI type 304 stainless steel in 1M NaCl at 25°C found a E_{crit} of +0.050V (Vs SCE) and a current in the passive range of 40-50 A with Argon bubbled through the solution. The metal was seen to be in a more active state in this solution as compared to one through which oxygen was bubbled as E_{crit} was more noble being +0.060V (Vs SCE) and the passive current of approximately 10 A was smaller.

(4) Effect of temperature on E_{crit}

Up to a temperature of 70°C the general effect on raising the temperature of the electrolytic environment on an austenitic stainless steel is to lower E_{crit} to more active potentials [47,51,69] as shown in Fig. 32. Above this in the range 70-100°C the breakdown potential of Type 316 stainless steel in 3% NaCl has a constant value of about 10-20mV vs SCE [69]. Thus breakdown potentials determined for 316L stainless steel in physiological solutions at 60°C would be roughly 80-100mV vs SCE more negative than those occurring at 37°C therefore constituting a slightly more demanding environment in which to evaluate the performance of an implant material.

(iii) Galvanostatic* polarization Measurements

These techniques are the result of the latest efforts in corrosion studies and are perhaps the most exciting and interesting as they are aimed at the heart of the corrosion problem, mainly the measurement of instaneous corrosion rates solely from electrochemical data. The successful use of such methods will allow a nearly complete assessment of the performance of metallic medical materials under labratory conditions.

One of the methods makes use of the polarization resistance (not a true ohmic resistance which is normally associated with electrical current) which is the slope of the polarization curve in the region very close to the corrosion potential. Its initial advantage is that it has a sound basis in theory which will be shown in relation to the kinetic theory developed previously for non-corroding metal electrodes. This is partially due to the fact that the potential range investigated is close to the corrosion potential and the applied currents are generally smaller than the corrosion current [52]. Thus the nature of the surface of the electrode under investigation is not significantly changed and the reactions proceeding during polarization are essentially those which actually occur during the corrosion process. Finally this method permits corrosion rate measurements of alloys under conditions in which the rates are so close

* Constant current polarization measurements the basics of which are a stable D.C. power source and a variable range of high value resistances to allow several different current values within approximately 10mV of the corrosion potential.

to being negligible to make measurement by any other means existing today impossible and, as such, are especially applicable to Type 316L stainless in various in vitro environments.

Initiation of this technique was by Skold and Larson [53] who described empirical observations existing between the polarization slope $\Delta E/\Delta I$ at low current density, and the corrosion rate measured by weight loss. This study was done after potential-time studies confirmed that a particular specimen potential was not related in any way to the corrosion rate. Their work was with mild steel in solutions containing 2.4 epm NaCl and 0.5 epm $NaHCO_3$ with the pH being maintained between 7.0 and 8.0 by continuous addition of carbon dioxide, and constant dissolved oxygen at 20-29^{o}C. They noted that the polarization potential appeared to be a straight line function of the applied anodic or cathodic currents at low current density with the slope $\Delta E/\Delta I$ being higher for specimens having a low corrosion rate. A plot of the logarithm of time averaged values of $\Delta E/\Delta I$ versus the logarithm of corrosion rate, produced a linear relationship.

Stern and Geary [54] in a discussion on the shape of polarization curves for corroding systems controlled by activation polarization showed that a linear relationship is expected in the region where the polarized potential is close to the corrosion potential. Basically using the theory reviewed by Bockris and Reddy [41], that is treating a corroding electrode like a noncorroding one they developed

an equation relating the slope of the linear region to the corrosion rate and Tafel slopes. Thus for a corroding electrode the corrosion current, i_{corr}, is analogous to the exchange current of a non-corroding electrode. Also the deviation from the corrosion potential of an electrode potential polarized by an applied current is designated ε, ie:

$$\varepsilon = E_i - E_{corr} \tag{12}$$

If an electrode is polarized cathodically (as was done with equation (7))

$$i_{app} = i_c - i_a \tag{13}$$

and using (12) then,

$$\begin{aligned} i_c &= i_{corr} \exp(-2.30\varepsilon/\beta c) \\ i_a &= i_{corr} \exp(2.30\varepsilon/\beta a) \end{aligned} \tag{14}$$

where βa and βc are the Tafel slopes for the oxidation and reduction reactions respectively of the cathodic process. Fig. 33 illustrates the linear (Tafel) relationship between ε vs log i_{app}. A deviation from a Tafel slope exists at low values of applied current. This behavior can be explained, if for illustrative purposes only, a anodic polarization is carried out.

For anodic polarization

$$i_{app} = i_a - i_c$$

Only when i_c becomes insignificant with respect to i_a will a true Tafel relation be seen. Further more, Tafel slopes cannot be obtained until applied currents reach magnitudes of several times the corrosion current. In non-corroding systems, experimental verification of

(i) ACTIVATION POLARIZATION

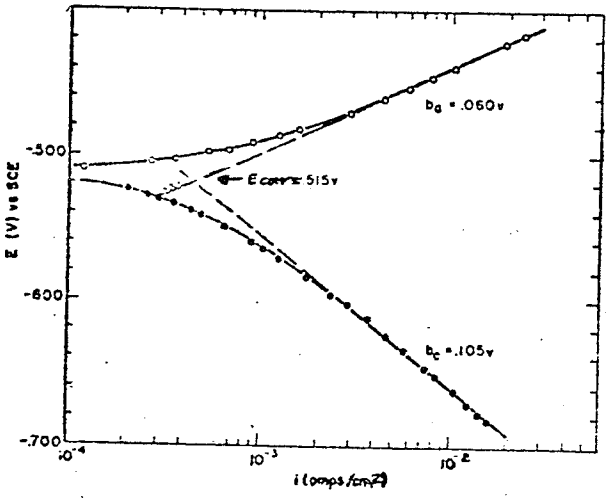

Fig.33 An example of activation polarization is the behavior of iron in 0.52N suluric acid. (Reproduced from Steigerwald [55]).

(ii) CONCENTRATION POLARIZATION

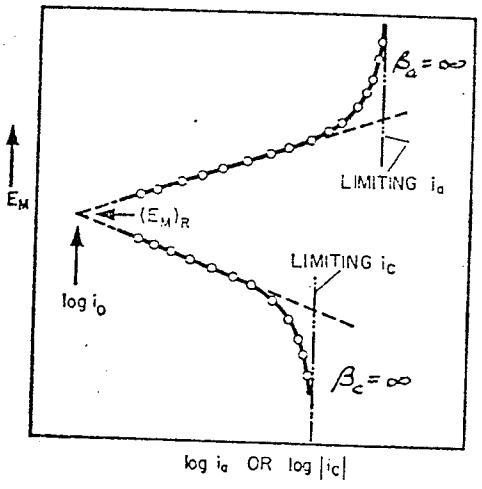

Fig.34 Schematic representation of concentration overpotential at a metal electrode showing limiting anodic and cathodic current densities. (Reproduced and modified from West [38]).

linearity between ε and i_{app} requires about 2 logarithmic cycles of current and measurements of 1000 times the exchange current, i_o*.

Substituting (14) into (13)

$$i_{app} = i_{corr}\left[\exp\left(\frac{-2.30\varepsilon}{\beta_c}\right) - \exp\left(\frac{2.30\varepsilon}{\beta_a}\right)\right] \qquad (15)$$

and expanding the exponential series around $\varepsilon=0$, neglecting the higher terms for small ε, the equation given by Stern and Geary for activation polarization is obtained

$$i_{corr} = \frac{\beta_a\beta_c}{2.30\,(\beta_a+\beta_c)\,(\varepsilon/i_{app})}$$

or

$$\frac{\Delta E}{\Delta I} = \frac{\beta_a\beta_c}{2.30\, i_{corr}\,(\beta_a+\beta_c)} \qquad (16)$$

where $\frac{\Delta E}{\Delta I}$ is the polarization resistance. Taking the logarithm of both sides of Eq. (16) yields

$$\log\frac{\Delta E}{\Delta I} = \log\frac{\beta_a\beta_c}{2.30\,(\beta_a+\beta_c)} - \log i_{corr} \qquad (17)$$

Thus, a plot of polarization resistance versus corrosion current on logarithmic scales should yield a straight line with slope of -1.

However not all corroding systems are freely corroding, that is controlled by simple ionization, as in activation polarization. In practice metal dissolution may proceed at a rate limited by diffusion. This was noted by Stern [52] who determined that corroding

* i_o is found by extrapolation of the Tafel region to the reversible potential. The corrosion current can be found in a similar fashion by extrapolation to E_{corr}. In fact this method is used in the over-voltage-intercept method to determine corrosion rates. Values of ε are much larger for this method.

systems controlled by concentration polarization also exhibited a linear section and that the slope of the linear section was also related to the corrosion rate. Concentration polarization occurs at a cathode when the reaction rate or the applied cathodic current is so large that the substance being reduced cannot reach the cathode at a sufficiently rapid rate. The solution adjacent to the electrode becomes depleted of the reacting ions, and the rate (of the cathodic partial reaction and therefore of the anodic partial reaction) then is controlled by the maximum rate at which the reacting species can diffuse to the surface. Stern accomplished this relationship in a similar fashion to that of activation polarization, by considering concentration polarization first on a non-corroding electrode and then introducing the complexity arising when the electrode corrodes. Basically a limiting diffusion current is reached so that the slope of the cathodic polarization curve, β_c, approaches infinity. Taking the limit of Eq (16) as $\beta_c \rightarrow \infty$

ie $$\lim_{\beta_c \rightarrow \infty} \frac{\beta_a \beta_c}{2.30\, i_{corr}\, (\beta_a + \beta_c)} = \frac{\beta_a}{2.30\, i_{corr}}$$

and the polarization resistance in the case of concentration polarization is:

$$\frac{\Delta E}{\Delta I} = \frac{\beta_a}{2.30\, i_{corr}} \qquad (18)$$

Polarization resistance measured cathodically or anodically should be identical as can be seen from derivations of equations (16) and (18) and has been confirmed experimentally. The only difference between these 2 methods is that the region of linearity is somewhat more limited in the anodic case. The applied currents should be such to limit ε to a 10mV or, at the greatest, 20mV deviation from the

corrosion potential, as was noted for non-corroding systems. Therefore the subsequent corrosion rate of the material will not be affected by surface changes brought about by large deviations from the corrosion potential. This is the most important advantage of this method.

Keeping in mind that β_a and β_c are the slopes of the logarithmic local anodic and cathodic polarization curves which may be determined experimentally by potentiostatic polarization, it is quickly seen that the use of Eqs. (16) and (18) depends on the values of the β constants. Fortunately the range of values which β may assume is really quite limited. This observation was made by Stern and Weisert [59] in a detailed study of the available data on activation polarization kinetics. In general β values ranged between 30 and 180mV. β values at these lower and upper limits are rather rare with the greater majority of values lying between 60 and 120mV. The effect of a change in β in Eq. (16) does not produce a corresponding change in the proportionality constant between polarization resistance and corrosion current as β appears in both the numerator and denominator of the expression.

Fig. 35 shows a variety of bands of limiting β_a and β_c values describing all systems which may be encountered. The cathodic Tafel slope varies from 60 to infinity (a limiting diffusion current) and the anodic Tafel slope from 60 to 120mV. Stern and Weisert cite an example situation controlled by activation polarization where the β values fall within the range β_c = 60mV, β_a = 60mV and β_c = 60mV, β_a = 120mV. A measurement of the polarization resistance then would produce a

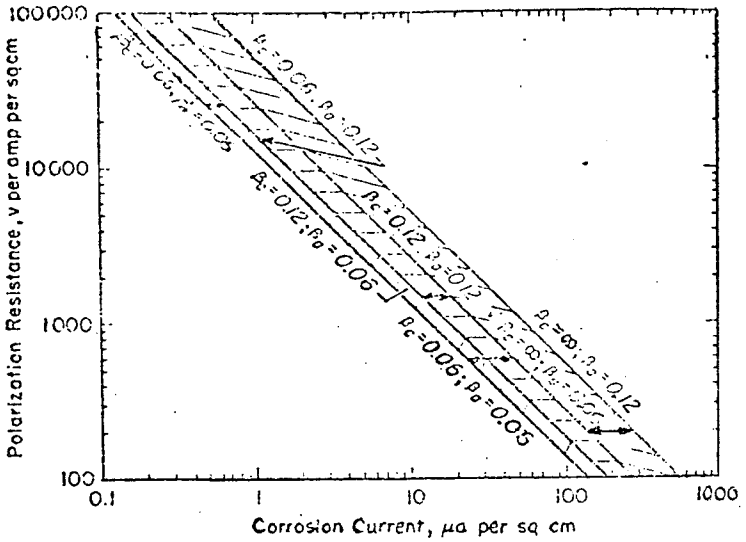

Fig. 35 Limits within which the relation between polarization resistance and corrosion current applies for most real systems. (Reproduced from Stern and Weisert (59), p. 1284).

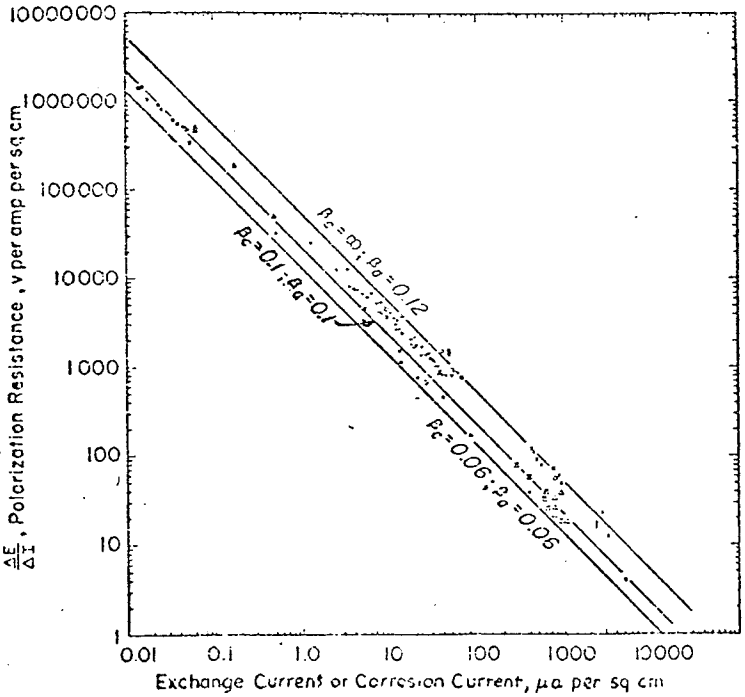

Fig. 36 Experimental observations: Open circles and triangles represent nickel in hydrochloric acid; open diamond represents iron in dilute hydrochloric acid containing sodium chloride; X's represent various steels in sulfuric acid; open squares represent steel and cast iron in high conductivity waters; crosses represent cast iron in natural and synthetic waters; solid circles and solid squares apply to ferric-ferrous exchange current on a variety of passive surfaces. (Reproduced from Stern and Weisert (59), p. 1285).

calculated corrosion current within about 20 per cent. Similarly, in the case of a system controlled by a limiting cathodic diffusion current where Eq. (18) applies, β_c equals infinity and β_a varies from 60 to 120mV. Measurement of the polarization resistance permits a corrosion rate estimate to within a factor of 35 per cent. Even without any prior information concerning values of a given corrosion system, that is lying somewhere in the limiting bonds of Fig. 35, the corrosion rate can be determined within a factor of 2. A further calibration curve covering 6 orders of magnitude is shown in Fig. 36 with experimental observations. For high corrosion rates, points would be expected to fall into positions where β_c is near infinity while for low corrosion rates the points should fall in the activation polarization range of the bond.

A more specific survey of constants used in the measurement of corrosion rates of stainless steels in chloride solutions bearing a ressemblance to the physiological environment is given in Table IV.

Table IV Tafel Slopes of Stainless Steels in Chloride Containing Solutions.

Stainless Steel	Solution and Conditions	β_a (mV)	β_c (mV)	Reference
En 58A (Type 302)	Aerated 1% NaCl (4 Polarization runs)	140	α	[57]
Type 304	Oxygen saturated, 3% NaCl thermostatted at 90°C	α (Assumed)	50 (Assumed)	[60]
Type 304	Isonotnic NaCl (0.9%) at 38.6°C (nitrogen-saturated)	α	119	[61]

Thus corrosion rate calculations based on assumed values of β_a and β_c can be justified in this situation where the emphasis is on the relative difference in corrosion rates between annealed and cold-worked material in an environment of varying pO_2 and pCO_2.

Chapter V

EXPERIMENTAL METHOD

5.1 In Vitro Test Conditions

The initial step was to synthesize a test solution ressembling from a chemical viewpoint the physiological situation into which an implant is placed and in which pO_2 and pCO_2 could be manipulated. Going even further, the concentrations of carbon dioxide and oxygen should cover a wide range and yet be such that conclusions can be applied to in vivo conditions. And finally, it should be kept in mind that any in vitro corrosion model will be, at best, only a rough approximation of actual in vivo conditions.

The basic physiological solution used in all the corrosion tests is given in Table V. It is roughly 0.11N in the chloride ion and 0.03N in the bicarbonate ion which are the major ionic species. In this respect it closely resembles Ringers solution [11]. Initially 2mM of $CaCl_2$ were also included but later removed as this salt yielded one of the ions of (Ca^{++}) of the sparingly soluble salt $CaCO_3$. This salt had a solubility dependent on pH and easily precipitated in the pH range of about 7.2 to 7.4. A second modification was to make $[H_2PO_4^-]=[HPO_4^-]$ so that these two phosphate compounds would provide some buffering action around pH 7.20 where pH = pK and give a combined phosphate ion concentration of about 1mM/L. A conversation with Dr. A. Naimark of the Dept. of Physiology and correspondence with Drs. F.R. Tucker, Dept. of Orthopedic Surgery and R.M. Letts, Resident in Orthopedic

TABLE V Basic Synthesized Extracellular Fluid

Modified from Ref. [12] and [19].

		Approximate Ion Yields in mEq/L							
	Mg/L	Na^+	HCO_3^-	Ca^{+2}	Cl^-	SO_4^{-2}	Mg^{+2}	K^+	PO_4^{-3}
$NaHCO_3$	27(94.006) = 2538.2	27	27						
$MgSO_4 \cdot 7H_2O$	0.5(246.477) = 123.2					1	1		
$MgCl_2 \cdot 6H_2O$	1.0(203.31) = 203.3				2		2		
KCl	5.0(75.55) = 377.8				5			5	
$NaH_2PO_4 \cdot H_2O$	0.5(138) = 69	} approx. 2							approx. 3
Na_2HPO_4	0.5(142) = 71								
NaCl	100(58.44) = 5844	100			100				
Total Ion Concentrations (mEq/L)		279	27		107	1	3	5	3

Surgery at the Winnipeg Children's Hospital were valuable in the selection of the final test solution.

The physiological test solution was prepared as a stock solution of five times concentration in two liter volumes to ensure uniformity of test solutions. It was desired to maintain a constant pH between 7.20 and 7.40 while the corrosion tests were being conducted. Therefore as the pCO_2 was varied, the pH of the solution would vary in response, requiring supplementary amounts of acid or base to control the pH. The base used was 0.2N NaOH and the acid 0.2N HCl so that no new chemical species were added to the basic solution. (Sodium bicarbonate proved to be too weak a base to be used as the pH modifying base).

Three corrosion environments were produced of the following descriptions:

(i) Low pCO_2, low pO_2

The preparation of 2000 ml of this solution was:
324 ml of 0.2N HCl added to 400 ml of five times strength stock solution and the remainder distilled water. The effect of the HCl addition was to add 64.8 mEq/2L of chloride ion to increase $[Cl^-]$ to approximately 139 mEq/L or 0.14N. Argon gas was bubbled into the solution through an air stone to remove dissolved O_2 and CO_2. The solution was held at $60\pm0.1^{o}C$ in a Blue M constant temperature bath. Twenty-four hours were allowed to pass to ascertain that a stable pH in the range 7.30-7.40 had been reached along with stable values of pCO_2 ($<$8mmHg) and pO_2 (10-11mm Hg). During the tests 2-5 ml additions of 0.02N HCl were required daily for the first week after which additions of more dilute HCl sufficed to maintain the pH as it tended to drift slightly in the basic direction.

(ii) High pCO_2, low pO_2

A 1800ml volume of test solution were prepared from: 360ml of 5 times strength stock solution, 240ml of 0.2N NaOH and remainder distilled water. Carbon dioxide at tank pressure of 3 psi was further regulated with a needle value and hose clamps and lead into the corrosion cells to form a two inch blanket over the test solution in the sealed beaker. Argon was bubbled through the solution to maintain the pCO_2 between 100-110mm Hg. The CO_2 by itself was soluble to the extent to exceed the scale of the pCO_2 electrode. The pressure of the CO_2 in the blanket over the solution and in equilibrium with the dissolved CO_2 in the solution was measured by a draft manometer and was between 0.05-0.10 inches of water. The pO_2 of this solution was about 5mm Hg.

(iii) High pCO_2, high pO_2

This electrolyte was identical to the high pCO_2, low pO_2 test solution. Here oxygen was bubbled through the solution to equilibriate it at an increased pO_2 of 260mm Hg while driving out part of the dissolved CO_2 and maintaining the pCO_2 at 100-110mm Hg. To maintain the pH 1-2ml of 0.02N NaOH were required daily for the first week and similar volumes of 0.002N NaOH during the remainder of the test.

The concentrations of O_2 and the various forms of CO_2 for these solutions and the slight modifications from the basic physiological solution are given in Table VI.

5.2 Measuring the Physiological Parameters: pH, pCO_2, and pO_2

A Radiometer acid-base analyzer. Type PHM71, was used to measure the parameters pH, dissolved carbon dioxide and oxygen in the physiological test solution. This unorthodox application of a clinical

TABLE VI Concentrations of O_2 and Various Forms of CO_2 in the Physiological Solutions.

Solution	Total CO_2* mM/L	$[HCO_3^-]$* mEq/L	Physically Dissolved CO_2 $CO_2(d)+H_2CO_3$ mM/L	$[H_2CO_3]$ µM/L	$[CO_3^=]$ µEq/L	Dissolved O_2 µM/L
low pCO_2, low O_2	negligible	negligible	negligible	-	-	13.4
high pCO_2, low pO_2	69.1	65.8	3.3	4.1	63.3	6.7
high pCO_2, high pO_2	69.1	65.8	3.3	4.1	63.3	348

* Using the Henderson-Hasselbalch equation, Eq. (4), and pK_{A1}=6.00 at 49°C, pH 7.4

instrument in a corrosion testing program would give measurements in units which would allow direct comparison with the literature values as given in Chapter II. The acid-base analyzer operated with a pCO_2 module, type PHA933 and a pO_2 module, type PHA930. The two gas electrodes were individually mounted in thermostatted cells connected to a Haake Model TP41 constant temperature bath and circulator controlled at 60±0.01°C. This temperature was at the upper end of the working temperature of 20-60°C for all 3 electrodes.

The Radiometer pCO_2 electrode, type E5036, was a combined glass and silver/silver chloride reference mounted in a electrode jacket and covered by a teflon membrane which trapped a weak electrode solution (0.005M $NaHCO_3$/0.02M NaCl) in contact with the electrode. The electrode functioning like a normal pH electrode related the linear change in pH of a bicarbonate solution with its pCO_2 when equilibrium had been reached by way of Eq. (3). The scale range was 8-190mm Hg.

The pO_2 electrode, type E5046, operated on the polarographic principle (Clark type) and consisted of a combined platinum and silver/silver chloride electrode mounted in an electrode jacket and covered by a 20μ thick polypropylene membrane. A phosphate buffer and potassium chloride solution was trapped inside the electrode. In operation a constant polarizing voltage of approximately 630mV was applied to the platinum electrode and a current proportional to pO_2 was generated through the reduction of oxygen diffusing towards the cathode. There were three scales: 0-100mm Hg, 0-200mm Hg and 0-1000mm Hg.

A Radiometer general purpose combination pH electrode, type

GK2321C was used to measure hydrogen ion concentration. It was of a small diameter (6.5mm) and 103mm long to fit the confines of the various corrosion test cells. The electrode was calibrated at 60°C and was brought to this temperature prior to use.

5.3 Specimen Materials and Preparation

To investigate the corrosion performance of cold-worked and essentially annealed Type 316L stainless steel, specimens having a hardness of 200 and 400 DPN appeared to represent the two extremes of cold-worked material encountered in a multi-component implant - specifically that of the plate and screws respectively. This choice was based on the hardness survey of Table III. The 200 DPH value die not represent a dead soft condition (which for 316L would be about 170 DPH [10]) but a reasonable hardness value which could be reached in manufacturing operations corresponding to a steel having received up to 12% cold work and an ultimate tensile strength of about 80,000 psi. A hardness of 400 DPH represents the near maximum strength condition for Type 316L stainless having an ultimate tensile strength of about 190,000 psi after having undergone in excess of 40% cold work [64].

The specimens of Type 316L stainless steel were cut from a sheeting having the following composition: 0.046%C, 17.25%Cr, 12.50%Ni, 2.33%Mo, 1.4%Mn, and 0.8%Si.

The material was lightly and heavily cold-rolled to these two hardness values. The hardness was measured as the average of 6-8 readings taken by a Vickers macro-hardness testing machine. The specimens were then cut to size for the particular test, and electropolished. The electrolyte for electropolishing was 95% acetic,5% perchloric acid in an ice bath

at a temperature of 15-22°C. This was followed by washing in ethanol, then acetone and air drying. Two or three coats of Varathane were sprayed on the specimens to prevent the occurence of pitting corrosion on the edges of the specimen and to limit the surface area. A further 2 coats of acrylic clear plastic were then applied. The specimens were stored in a calcium chloride dessicator prior to use.

5.4 Single Electrode Corrosion Potential - Time Measurements

The intent of this test was to measure and record the effect on the natural resting (corrosion) potentials of solutions of varying pO_2 and pCO_2 on single type 316L stainless steel specimens of 200 and 400 DPN hardness at a constant pH of 7.30 to 7.40.

Specimens ($12cm^2$) of a configuration as shown in Fig. 37 were placed in 400ml tall form beakers filled with 350ml of solution which had been brought to the desired state of pH, pCO_2, and pO_2 for a 24 hour period. The two hardness ranges of 200 and 400 DPN were represented by 3 specimens per corrosion run. Each cell was fitted with a acrylic plastic lid which had openings for two gases, the specimen and the Luggin probe which was kept a distance of about 2-3mm from the specimen. The Luggin probe (capillary) and salt bridge served to extend the reference electrode to the near vicinity of the electrode under study to permit the measurement of the potential difference between this electrode (S.C.E.) and the solution immediately adjacent to the corroding electrode. The 6 test cells for each run were supported in a acrylic plastic lid in a Blue M constant temperature bath at 60±0.1°C. A Radiometer saturated calomel electrode was immersed in a thistle tube filled with saturated KCl and having a capillary tube end of 1mm

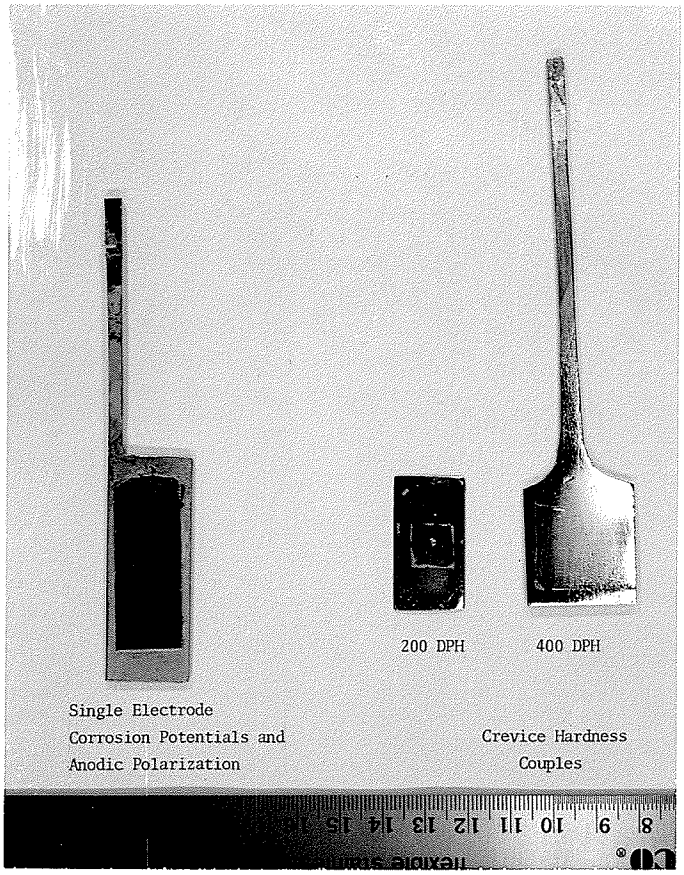

Fig. 37 Specimen configuration used in the corrosion test.

inside diameter with an agar plug, to prevent mixing of the saturated KCl and the test solution. This agar plug was made by drawing up into the capillary section of the vessel, a heated solution of 3-4g agar-agar per 100ml of test solution. The reference electrode was fitted into a manifold type of salt bridge set-up leading to each of the 6 cells. The Luggin capillary in each of the test cells was gel filled. Coaxial wire connected each of the 6 specimens to a 16 position thermocouple switch in series with a Keithley digital voltmeter. The outer sheath of all the leads were grounded together so that stray signals picked up different specimens would not result in different measured potentials. A schematic of one of the test cells connected through the digital voltmeter to the reference electrodes is given in Fig 38(a) and a overall view of the apparatus in Fig 38(b).

The number of connections and liquid junctions necessitated the use of a procedure to verify that the potential being measured was solely the corrosion potential and not influenced by systematic errors. Firstly, the half-cell potential of the S.C.E. itself was checked by measuring the potential between it and a Cu/sat. $CuSO_4$ (1.47M) half-cell. The potential of the Cu/sat. $CuSO_4$ half-cell is 318 mV vs. the N.H.E. at 25^{o}C. The potential of the Hg-$HgCl_2$, sat. KCl half-cell is 242 mV vs. N.H.E. Theoretically the potential observed between these two half cells should be therefore +76 mV at 25^{o}C. The observed measured potential was +76.2 mV after a stabilization period of 30 minutes.

Possible variations in potentials between corrosion cells due to inhomogenities in the Luggin capillaries were checked in the

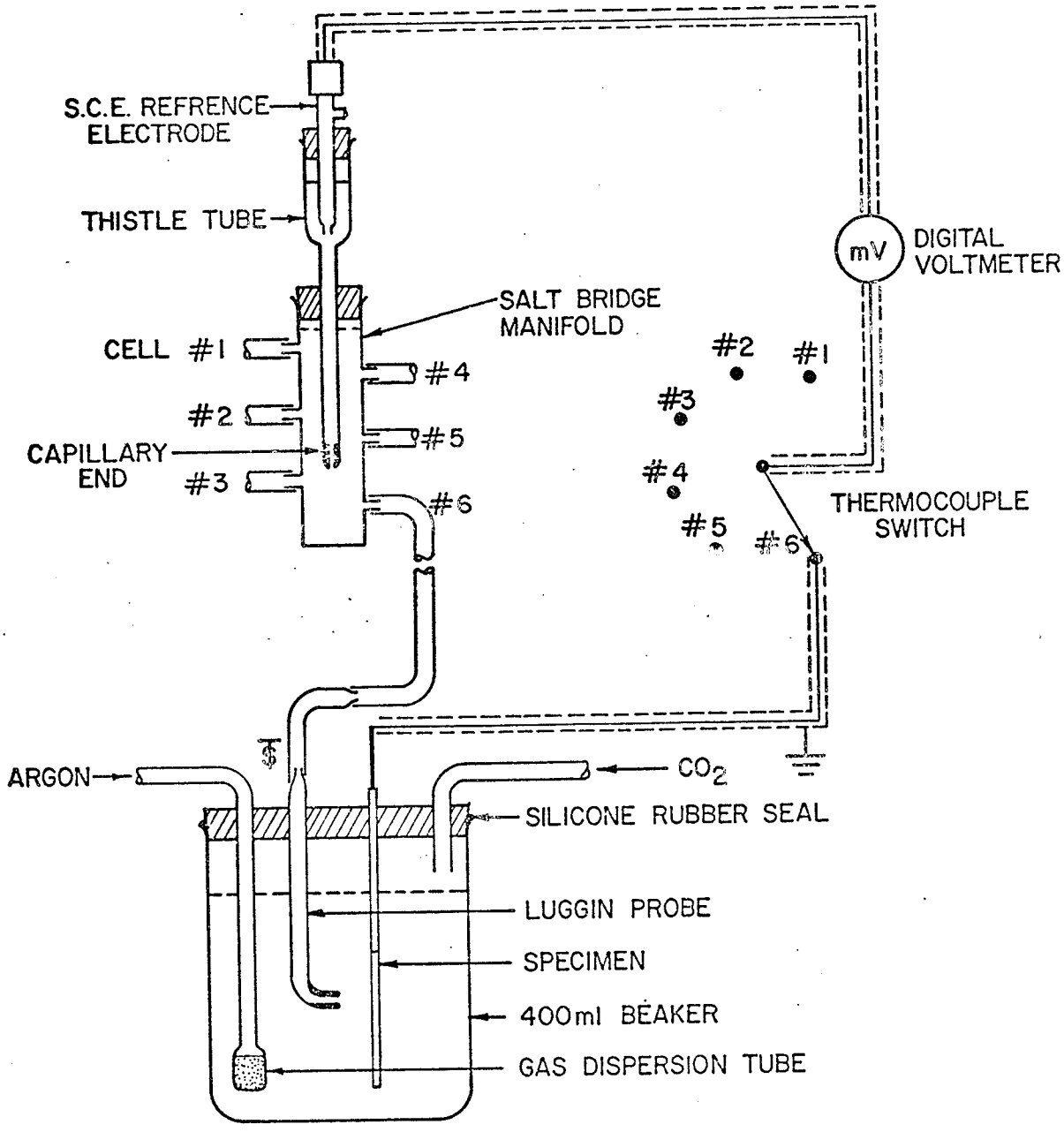

Fig.38(a) Schematic for single electrode corrosion potential-time measurement.

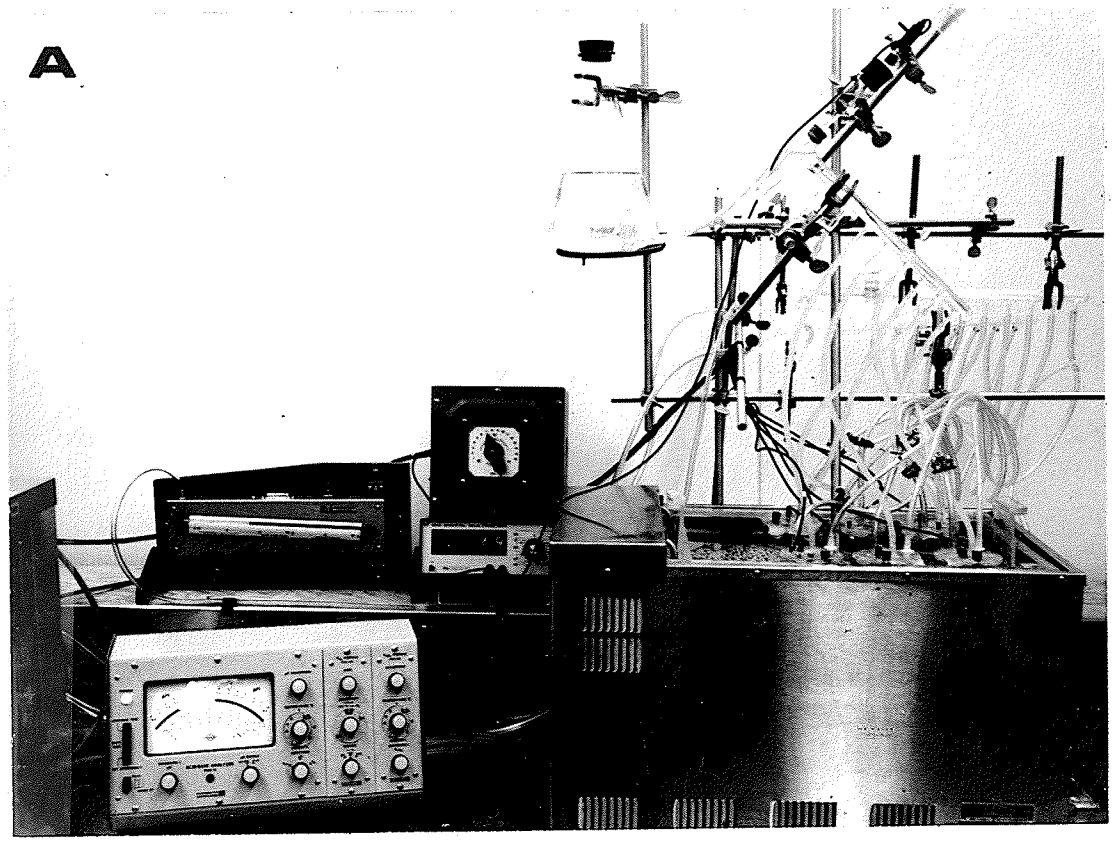

Fig.38(b) Ancillary apparatus for single electrode corrosion potential - time measurements.

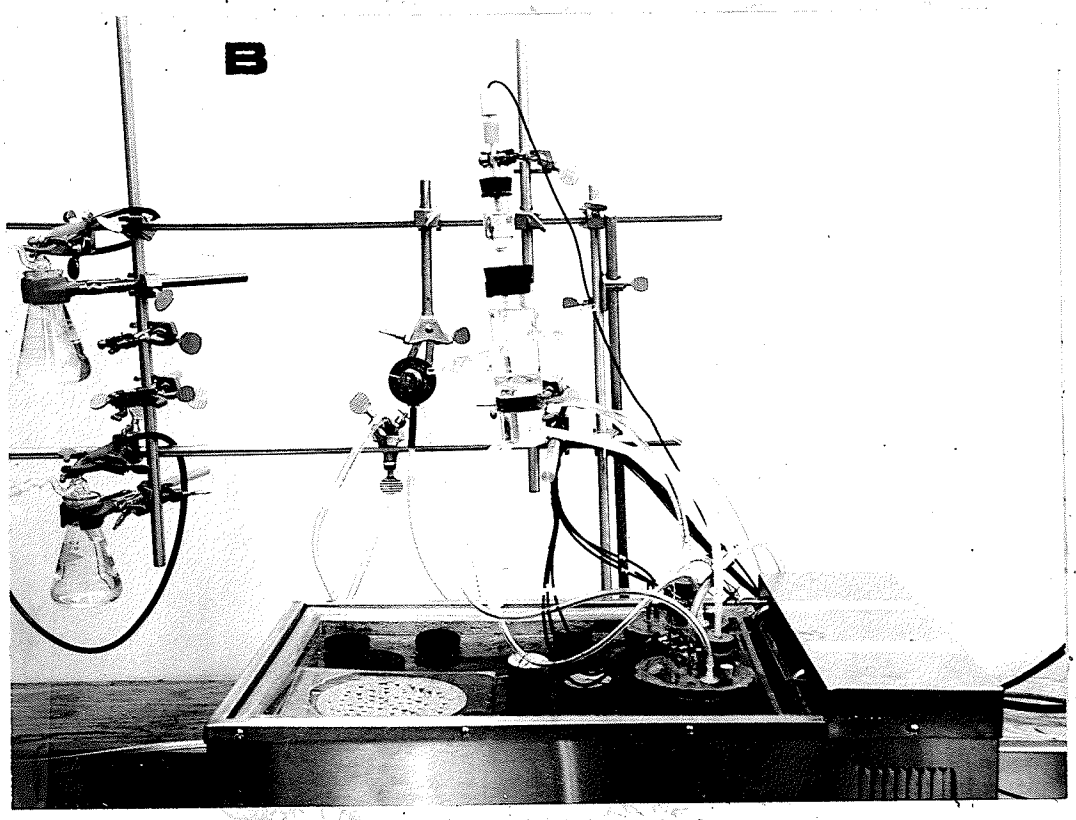

Fig.39(a) Overall experimental set-up for measurements of corrosion potentials in the crevice of hardness couples;
(con'd)

same set-up just described, except that the Luggin capillary containing agar in the physiological test solution was immersed in the saturated $CuSO_4$ solution. The potential was taken after about 1 to 1.5 minutes to avoid contamination of the capillory with Cu or $CuSO_4$, after which the capillary was then thoroughly washed with distilled water. The potentials measured using 6 different capillaries were between 66 and 70 mV. This variation of 4 mV among 6 capillaries agrees favourably with the observations of Popiel [61] that a small emf of about 5 mV can be tolerated due to liquid junction effects. Other variations of the Luggin capillaries could have been due to small air bubbles in the agar itself or if the agar itself has pulled away from the end of the capillary to form a concave interface. The agar should be perfectly flush with the end of the capillary for the formation of a stable and reproducible liquid junction. The best liquid junction is one in which the 2 different solutions meet at a sharp initial boundary [62,63].

A stabilization period of 24 hours for the potential of the specimens to adjust and reach a steady state. Then the corrosion potential measurements were taken 4 times daily over the length of the test. The average corrosion potential for the two groups of 3 specimens was then plotted. Hydrogen ion concentration, pO_2 and pCO_2 measurements were taken twice daily and adjustments made if necessary. Most tests were conducted up to a period of about 3 weeks at which time fluctuations in the corrosion potential had disappeared and either a general trend or a constant value was observed.

5.5 Corrosion Potential-Time Measurements in a Crevice

In visualizing the corrosion occurring between the screw and softer bone plate of an orthopedic prosthesis, a corrosion model

was constructed in an attempt to study this situation. The model consisted of specimens 8 cm^2 in area of 200 DPH hardness representing the portion of a bone plate surrounding a screw and a smaller specimen of 400 DPH hardness, 1 cm^2 simulating the screw. Both specimens are shown in Fig. 37. It was then possible to assess the effect of the very near proximity of the 400 DPH specimen clamped to a 200 DPH specimen by measuring the corrosion (resting) potential of the 200 DPH specimen in the crevice formed by the two clamped specimens. The potential observed is that of the 200 DPH specimen as it was this specimen that was connected to one side of the digital voltmeter. To allow this measurement, a 1.4mm diameter hole was spark machined through the 400 DPH specimen using a copper tool in a servomet spark-cutting machine permitting a tubulus from the S.C.E. to enter the confines of the crevice. Electropolishing followed the making of the hole.

Three couples were tested in each electrolytic cell, with 2 cells being used, for a total of 6 couples per test run. The test cell was a 800 ml beaker fitted with a 0.75 inch thick plastic lid to which was fastened a jig to hold the 3 couples separately in the electrolyte. About 600 ml of physiological test solution was used in the cell. There were provisions in the lid to allow entry of argon, oxygen, carbon dioxide, the combination pH electrode, and also an opening for a syringe to collect samples which were checked for pO_2 and pCO_2. The 2 types of couples were a soft/soft couple: a 200 DPH (1 cm^2) plate held against a 200 DPH (8 cm^2) specimen and a soft/hard couple: a 400 DPH (1 cm^2) plate pressed against a 200 DPH (8 cm^2) specimen.

The teflon tubulus of 0.8mm inside diameter was glued on the outside of the 1 cm^2 plate with General Electric silicon rubber sealant

and was cut flush on the inside of the crevice. The width of the crevice was 0.3 to 0.4mm due to the coating of Varathane and acrylic. The other end of the 0.7 cm long (Luggin) tubulus was connected to the S.C.E. as shown in Fig. 39(b). In this way all 6 crevice couples were connected through a thermocouple switch to a common reference electrode. Again coaxial wiring was used with the outside sheath from all the couples being grounded together. The complete electrochemical apparatus is shown in Fig. 39(a).

The physiological test solution was poured into the cell via the tubules to insure that no air bubbles would be present in this narrowest part of the salt bridge to hinder the potential measurements. The 200/200 DPH and 200/400 DPH couples were tested in the same solution under identical conditions as for the single electrode potential-time tests. The same general procedures were also followed.

5.6 Anodic Potentiostatic Polarization

The polarization cell was a 1000 ml beaker fitted with a 0.75 inch acrylic plastic lid machined to position the working electrode, Luggin probe, auxillary electrodes, and accomodate the entry into the cell of the combination pH electrode, argon, oxygen, carbon dioxide, and a sampling syringe. The cell was immersed in a Blue M constant temperature bath at 60±0.1^{o}C. A larger electrolyte volume was thought necessary to minimize the effects of corrosion products accumulating as the test progressed. The auxillary electrodes were 2 bright platinum foils (12 cm^{2} each) located 3 cm on either side of the working electrode.

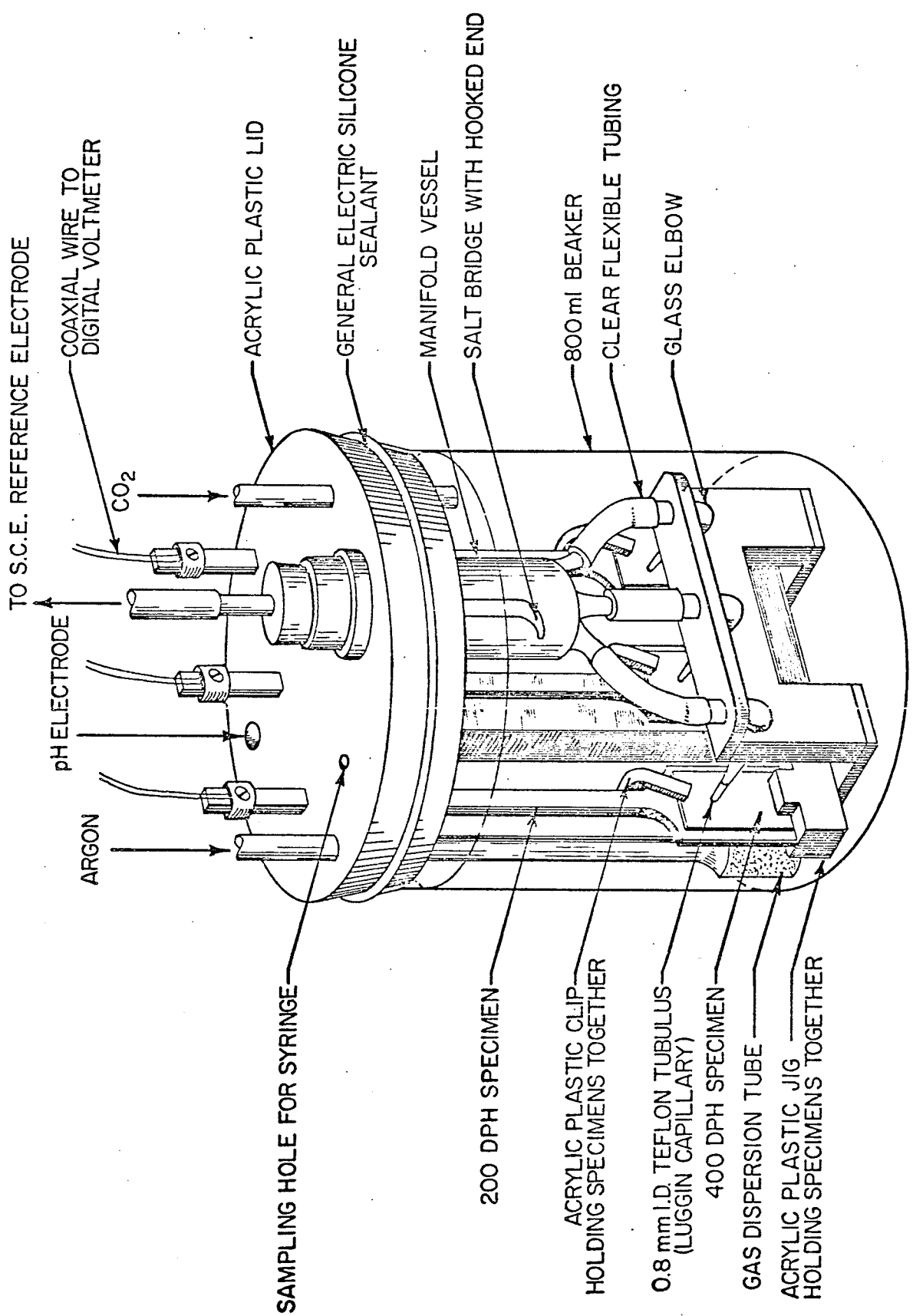

Fig. 39(b) CELL CONTAINING 3 CREVICE COUPLES

The Luggin probe measured the potential of the working electrode centrally at the top of the specimen area to prevent the probe itself from screening the working electrode. The polarization cell set-up is shown in Fig. 40 (a&B). All leads were shielded and the shield grounded to limit A.C. noise. The working electrode, S.C.E., and auxillary electrode were connected to a Wenking electronic potentiostat. The potential steps were set on the potentiostat while the corresponding current was measured by a Honeywell Electronik 194 potentiometric chart recorder. A capacitor-resistor set-up connected across the recorder terminals of the potentiostat was sometimes required to cut down on noise pick up by the recorder which occurred particularly at the lowest current densities.

Before polarization was started, the specimen was allowed to form a passive layer and reach a relatively constant rest potential over a period of about 24 hours. The potential of the working electrode was made progressively more noble (positive) in 25 mV steps. The potential step technique entailed maintaining the specimen for an interval of 10 minutes at each potential level after which time the anodic current, I_a, was measured before the potential was changed. This technique corresponds to a traverse rate of 150 mV/hr in the anodic direction. The 2 types of specimens, 200 and 400 DPH, were each tested in the physiological solutions under varying conditions of pO_2 and pCO_2 at constant pH.

5.7 Galvanostatic Linear Polarization Measurements

The polarization cell used for these tests was the same as that used for the potentiostatic polarization measurements. To apply this technique a constant current sourve was built using a 45 V battery

(a)

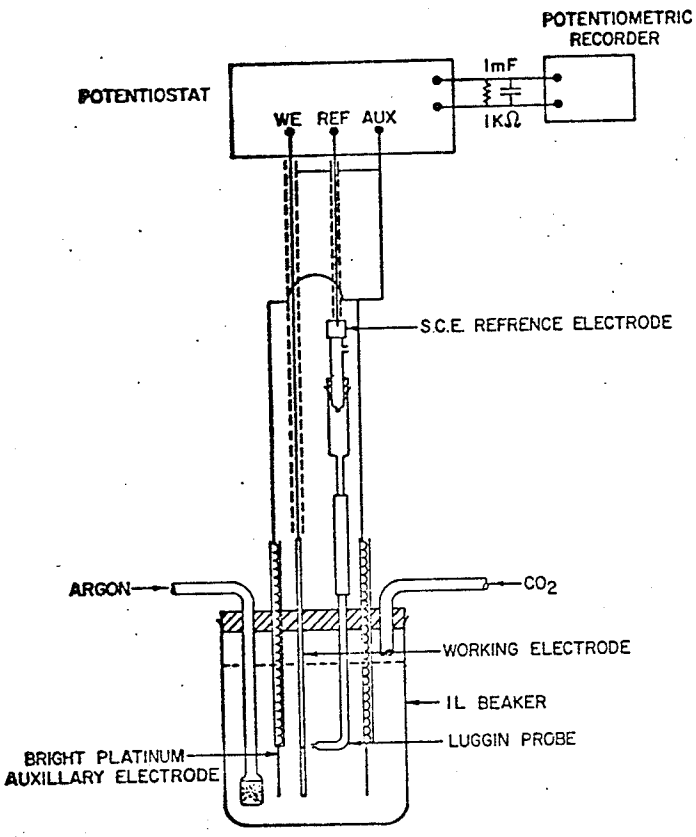

(b)

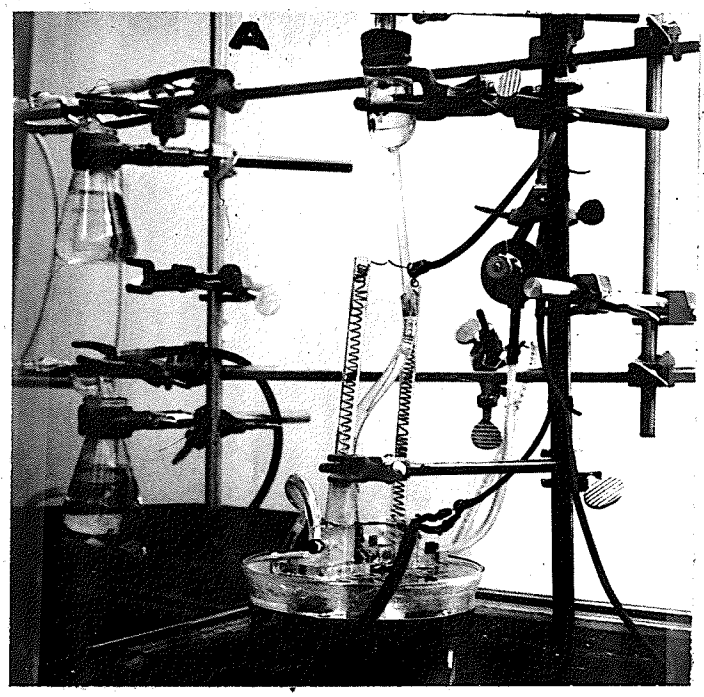

Fig. 40 (a) Schematic for anodic potentiostatic polarization;
(b) Actual experimental set-up

as a stable voltage source and decades of 22 megohm resistors in series to produce constant currents of 0.024, 0.040, 0.059, 0.079 to 0.235 μA. The current values were chosen so that 4 or 5 current increments would be required to cause an overpotential of about 10 mV from the rest potential. The tests were conducted in the anodic (positive) direction from the rest potential, with the positive terminal of the power source connected to the working electrode and the negative terminal to the two auxillary electrodes. The potentiostat was also used in this test functioning simply as a voltmeter in conjunction with the potentiometric recorder allowing measurements of overpotential (ε) within 0.1 mV. The general procedure in conducting the test was to hold the current constant for about 3-5 minutes before a new stable rest (mixed) potential had been reached. The recorder allowed close observation to ascertain that a stable rest potential had been reached before the current was increased by decreasing the external resistance. The circuitry is shown in Fig. 41.

The specimen was allowed to stabilize in the solution for about 24 hours before an anodic linear polarization was attempted. Several polarization runs were carried out with each specimen with usually about 24 hours between runs to allow the specimen to return to a stable rest potential. This technique was also used with specimens which had been potentiostatically polarized beyong the critical potential to determine whether a noticeable change in the passivation characteristics of the stainless steel could be observed.

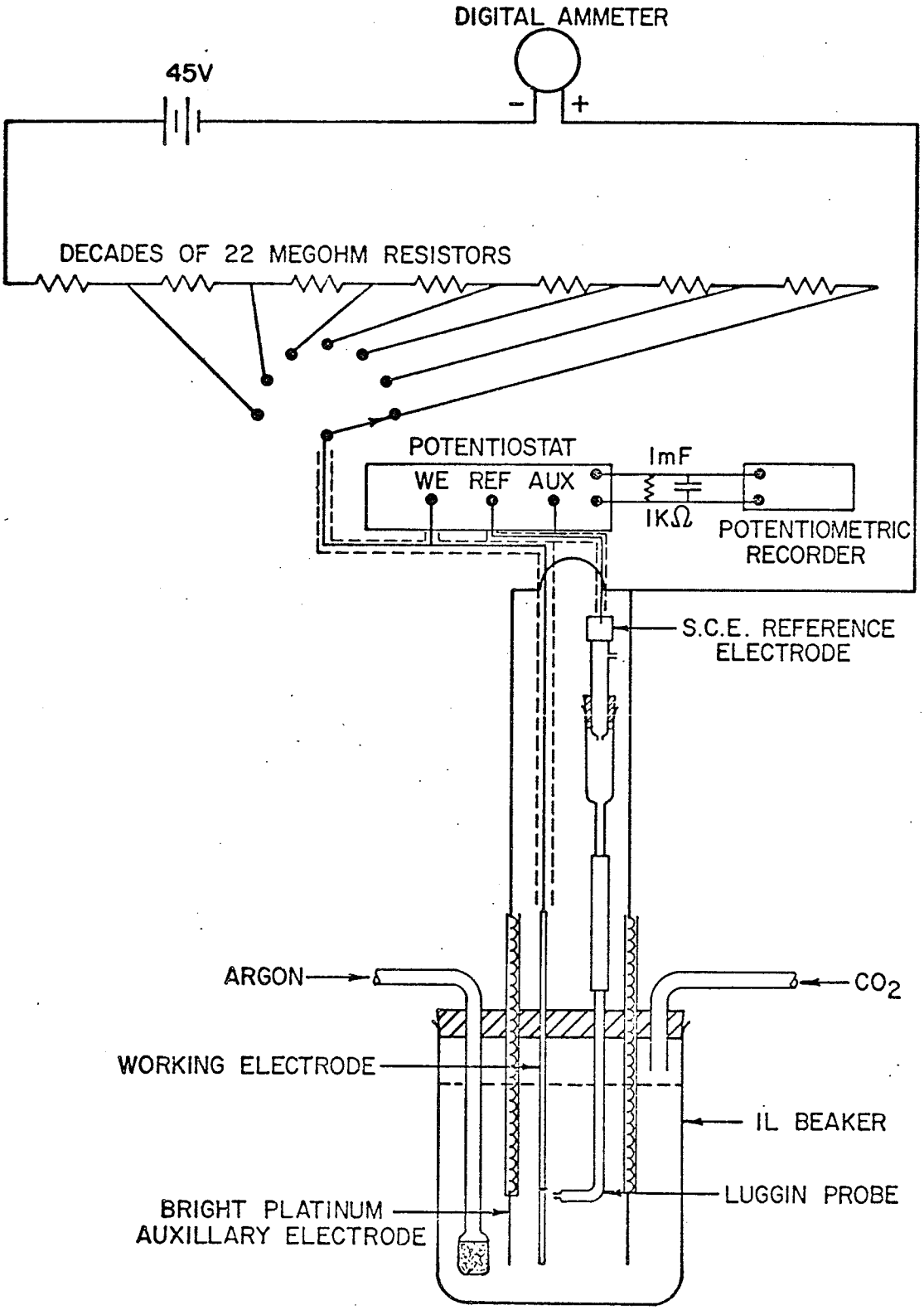

Fig.41 Schematic for galvanostatic linear polarization.

Chapter VI

OBSERVATIONS AND DISCUSSION

6.1 Potential-Time Measurements

(i) Single electrode corrosion potential

The single electrode potentials for both cold worked and annealed stainless steel samples in solutions of various O_2 and CO_2 concentrations are shown in Fig. 42(a-c). In general these curves exhibited a fluctuating nature which is interpreted to be a result of a break-down and then ensuing build-up of a passive layer in an oxidizing environment. A breakdown or dissolution of a surface film means that a progressively larger anodic area is exposed to the corrodant. But as the cathodic process can consume electrons at a limited rate, this increased production of electrons on the surface of the anode leads to gradual fall in the corrosion potential. In the low pCO_2, low pO_2 (Fig. 42 (a)) solution there was a pronounced variation in potential with cold work. After a 23 day exposure the corrosion potential for the 200 DPH specimen from the slowly falling E-t curve of Fig. 42(a) was approximately -220 mV compared to -400 mV for the 400 DPH one. The larger fluctuations, from -300 to -400 mV for the cold worked specimen would indicate an instability of the passive state.

In the high pCO_2, low and high pO_2 solutions, the corrosion potentials of the annealed and cold-worked stainless tended to drift towards a common value. This was probably due to an ionic derivative of carbon dioxide precipitating and forming a relatively non-protective compound on the surface of the metal. This compound sometimes as a

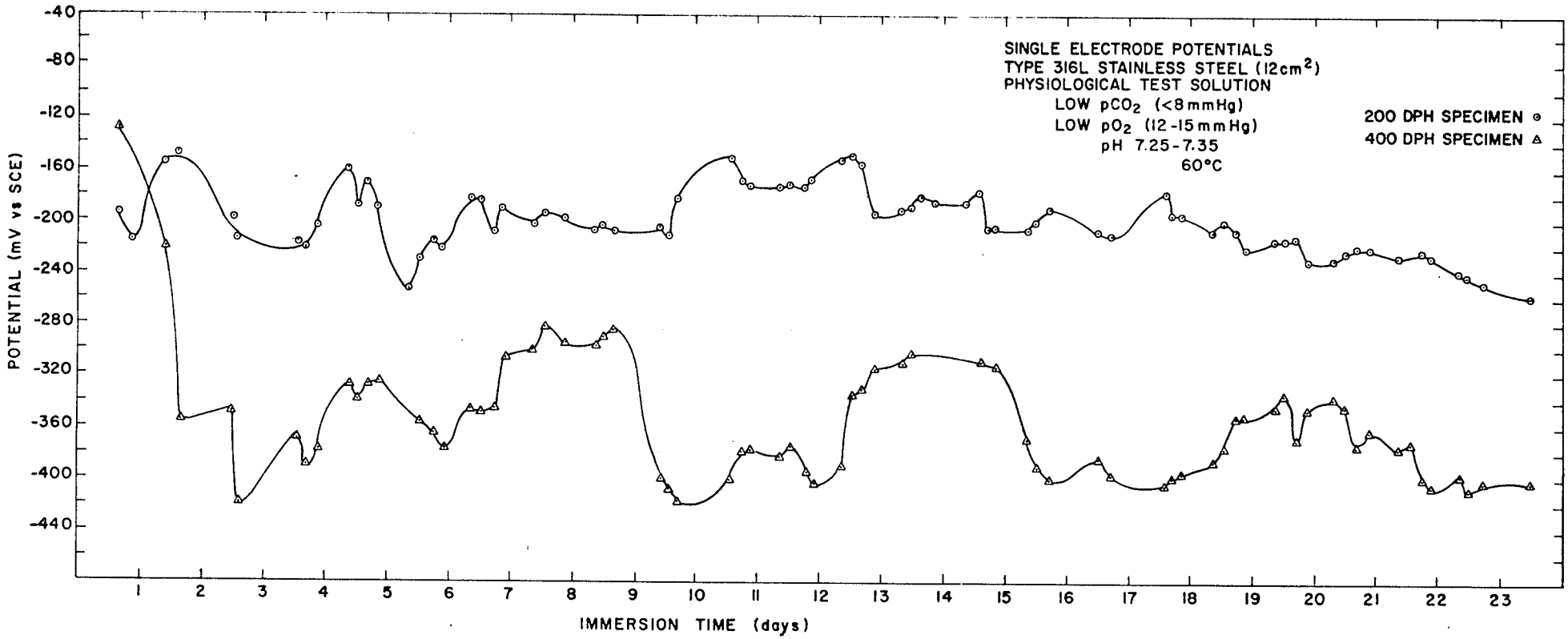

Fig.42(a) Single electrode corrosion potential-time measurements for 200 and 400 DPH Type 316L SS in solutions with varying blood gas concentrations (a) low pCO_2, low pO_2; (cont'D)

corrosion product in an impervious layer, is not as stable as the chromium oxide compound felt responsible for the passivity of stainless steel. Such a general coverage of the metal surface rather than just the de-activation of anodic sites is typical of a cathodic inhibitor. In such a situation bicarbonate HCO_3^- is precipitated as a carbonate film under the alkaline conditions generated at the cathode,

$$O_2 + 2H_2O + 4e \longrightarrow OH^-$$

$$HCO_3^- + OH^- \rightleftharpoons CO_3^= + H_2O \qquad (1b)$$

This situation is analagous to the Fe - H_2O system at 25°C (Pourbaix diagram), where a high concentration of dissolved CO_2 (as HCO_3^- and $CO_3^=$) leads to a relatively unprotective layer of $FeCO_3$ corrosion product which displaces and extends over most of the stability range of the passive film $Fe(OH)_2$ resulting in the corrosion of iron (by so-called "aggressive CO_2") [38]. This CO_2 in excess of that required to equilibrate HCO_3^-, called "aggressive carbonic acid" by Evans [70], is said to be a form of undissociated H_2CO_3 (free CO_2) by Pourbaix [71] which in the physiological system would be a portion of the extracellular [CO_2(d) + H_2CO_3]. The carbonate layer is formed from bicarbonate (through the cathodic reduction reaction of Eq. (1b) rather than a chemical precipitation by an excess of carbonate) only when the CO_2 content is limited to that amount required to stabilize the bicarbonate. An excess of carbon dioxide as aggressive carbon dioxide will cause the electrolyte to dissolve any carbonate film present and interfere with the formation of protective carbonate films on bare metal. The rest potentials reached for essentially - annealed and cold-worked specimens in the high pCO_2 environment were: -240 mV

with a low pO_2, Fig. 42(b); and +50 mV with high pO_2, Fig. 42(c). Thus this carbonate film would mask the different characteristics of the passive films formed on annealed and cold-worked metal surfaces and would lead to potential measurements essentially independent of the quality of the chromium oxide passive film.

Increasing the concentration of the reducible component, dissolved oxygen, yields a greater maximum current density of reduction. The consequent passivation effect by this oxidizing agent was to displace the potential of the metal in the noble direction from -240 to +50 mV. The rest potential in the high pCO_2, high pO_2 was almost identical to that of 18 Cr - 10Ni - 3Mo - 0.07C (chemically polished) in aerated Hank's physiological solution which was 60 mV vs S.C.E. after 20 days as measured by Hoar and Mears [44].

(ii) Corrosion Potential - Time Measurements in a Model Crevice

Results are shown in Fig. 43 (a-c) Before interpretation of these results it should be kept in mind that current theories on the topic of localized corrosion in crevices are varied and in several instances quite contradictory. This unsettled state of affairs will become evident as this section of the discussion proceeds.

The potentials measured in a crevice did not show a natural tendency to decrease relative to those for a single electrode in similar solutions. Therefore the mechanism of crevice corrosion via a mechanism involving an active crevice and passive outer surface as suggested by some workers [72,73], was not operative. Basically this concept regards the rate of corrosion to be dependent upon the potential in the crevice which becomes active (more negative) for one of several reasons, one of which is the depletion of oxidizers during chemical exposure. An optimum situation for this to occur was in the low pO_2

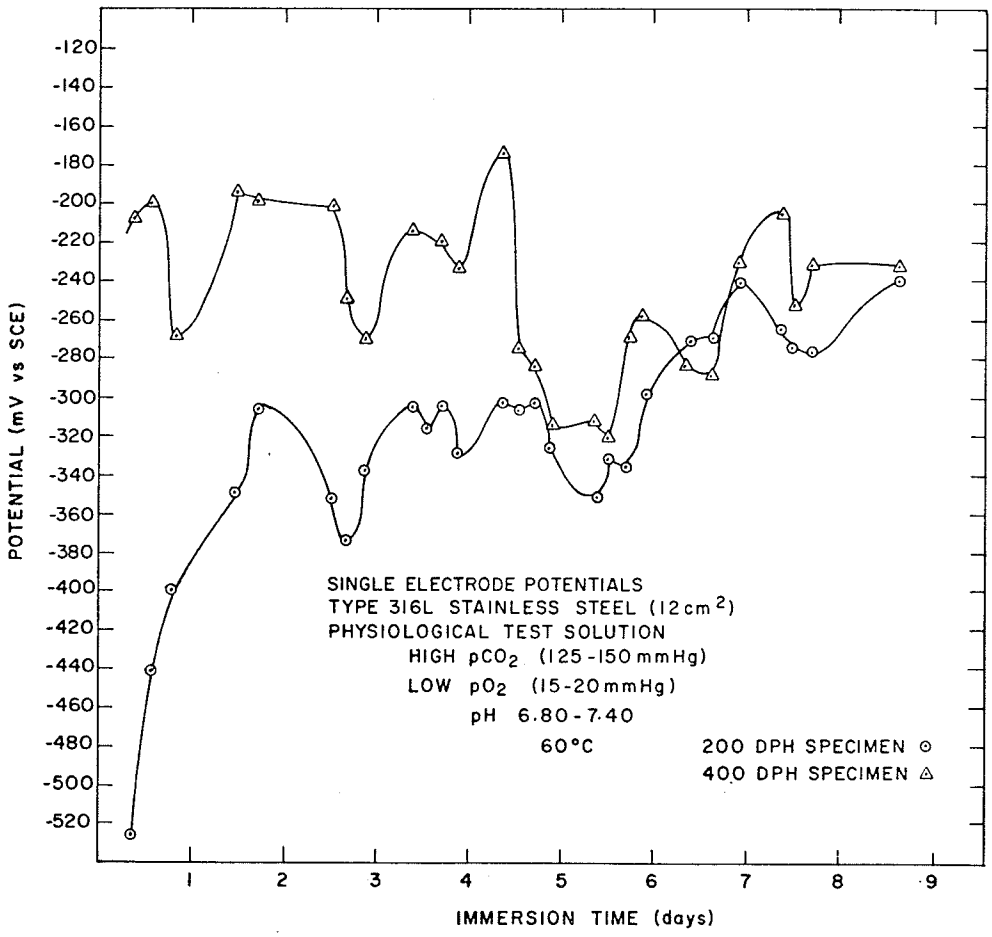

Fig.42(b) High pCO_2, low pO_2; (con^{t}d)

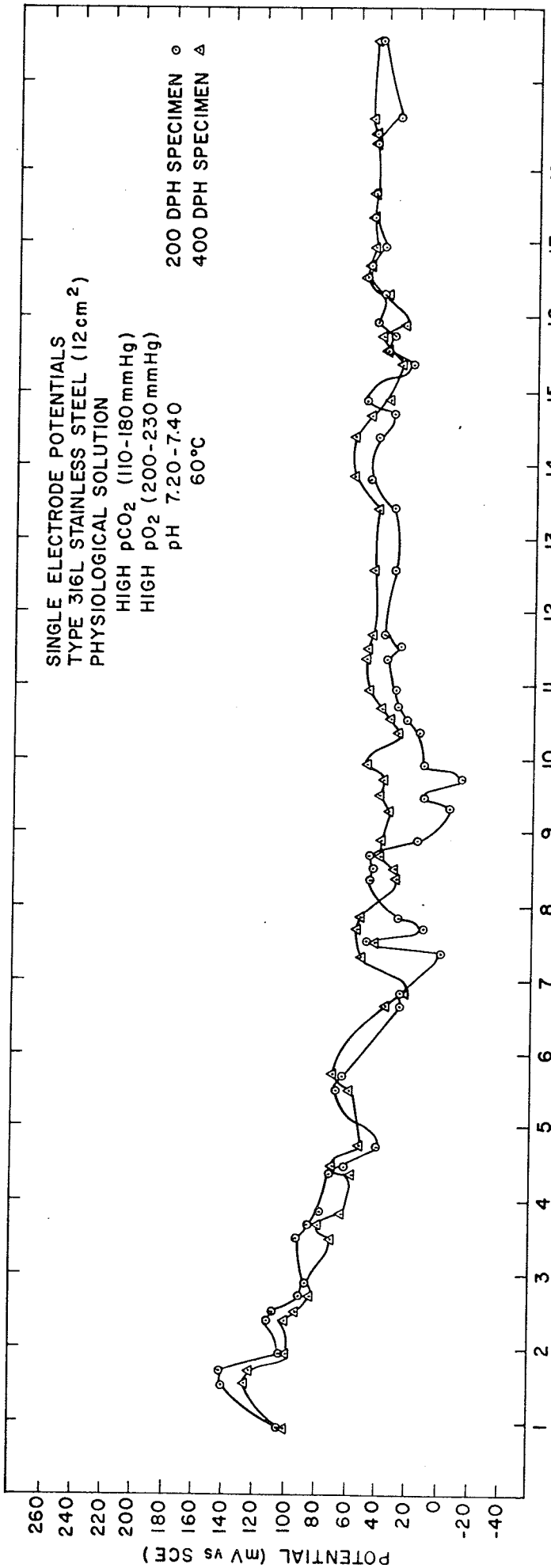

Fig.42(c) High pCO_2, high pO_2.

solutions where it should have been possible for oxygen concentrations to reach even lower concentrations than in the bulk solution. The anticipated lowering of potential in the crevice did not occur. Rather the actual occurence was quite the opposite. In all crevice couples the potential in the crevice became anodic by at least 100 mV (see Fig. 43 (a-c)). Further evidence ruling out differential oxygen concentration as a factor was reported by Rosenfeld and Marshakov [74] where crevice corrosion has been observed in electrolytes free of oxygen.

The presence of the deformed steel in a crevice in which there was actual metallic contact with annealed metal did not appear to cathodically polarize the annealed material to more active potentials. The potential in the crevice of the self-polarizing couple seemed to be controlled, to the greatest extent, by the passivation characteristics of the annealed material. In the low pCO_2, low pO_2 solutions of Fig. 43(a), the steady state corrosion potential for 200/200 and 200/400 DPH couples was essentially the same being -100 mV, and -80 mV for a 400/200 DPH couple (Fig. 43(b)). For a couple composed completely of cold-worked material (Fig. 43(b)), the corrosion potential as would be expected was more negative, being quite steady at -200 mV but still 200 mV anodic to a comparable single electrode specimen. (Fig. 42(a)).

The basic concept that a large potential difference must exist between the crevice and the outer surface for the initiation of corrosion does not seem to be true; (France Jr, [72], Karlberg and Wranglen [73], and Rosenfeld and Marshakov [74]). It would appear that quite insignificant differences in potential between the crevice and open surface initiate corrosion. These authors advance the concept

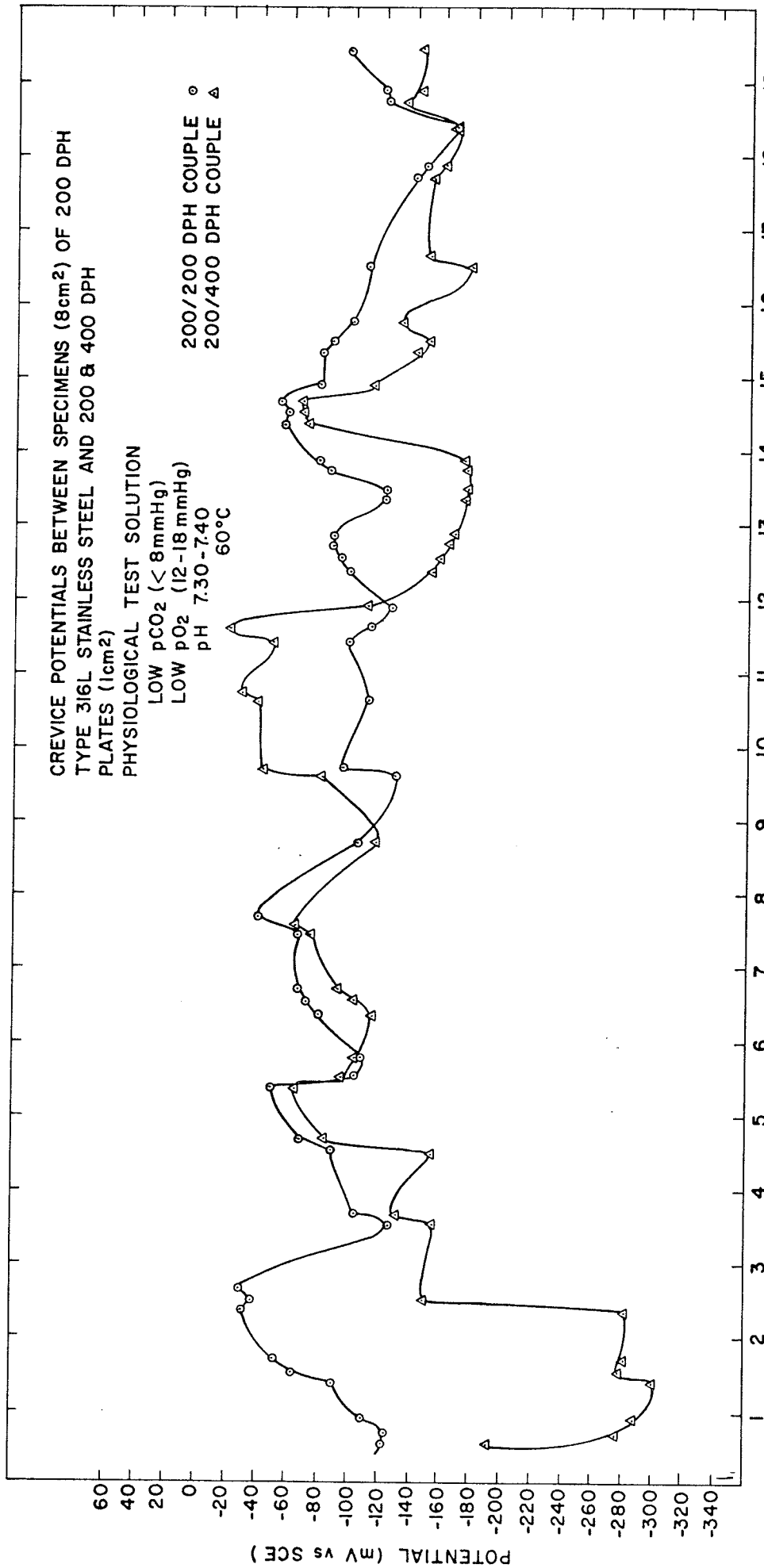

Fig.43 (a) Corrosion potential-time measurements in crevices of Type 316L SS hardness couples:(a) 200/200 and 200/400 DPH couples in low pCO_2,low pO_2physiological solution;

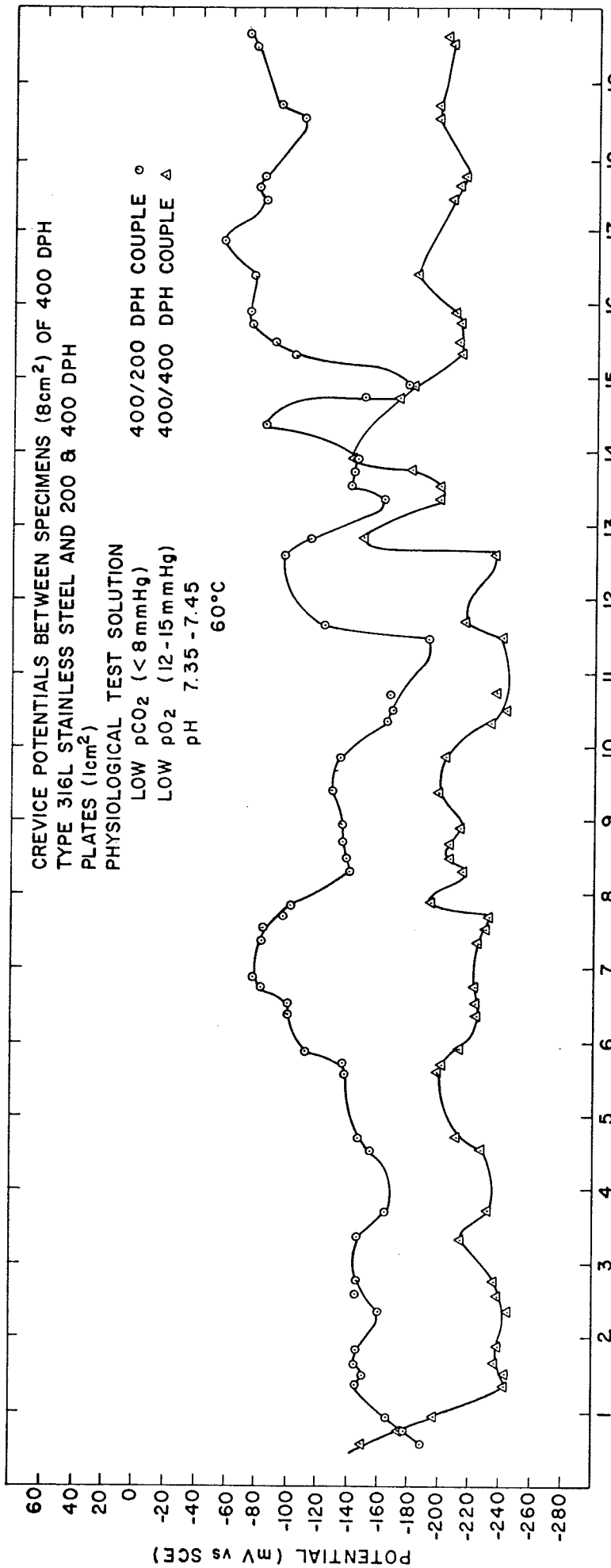

Fig. 43(b) 400/400 and 400/200 DPH couples in low pCO_2, low pO_2 physiological solution; (con'd)

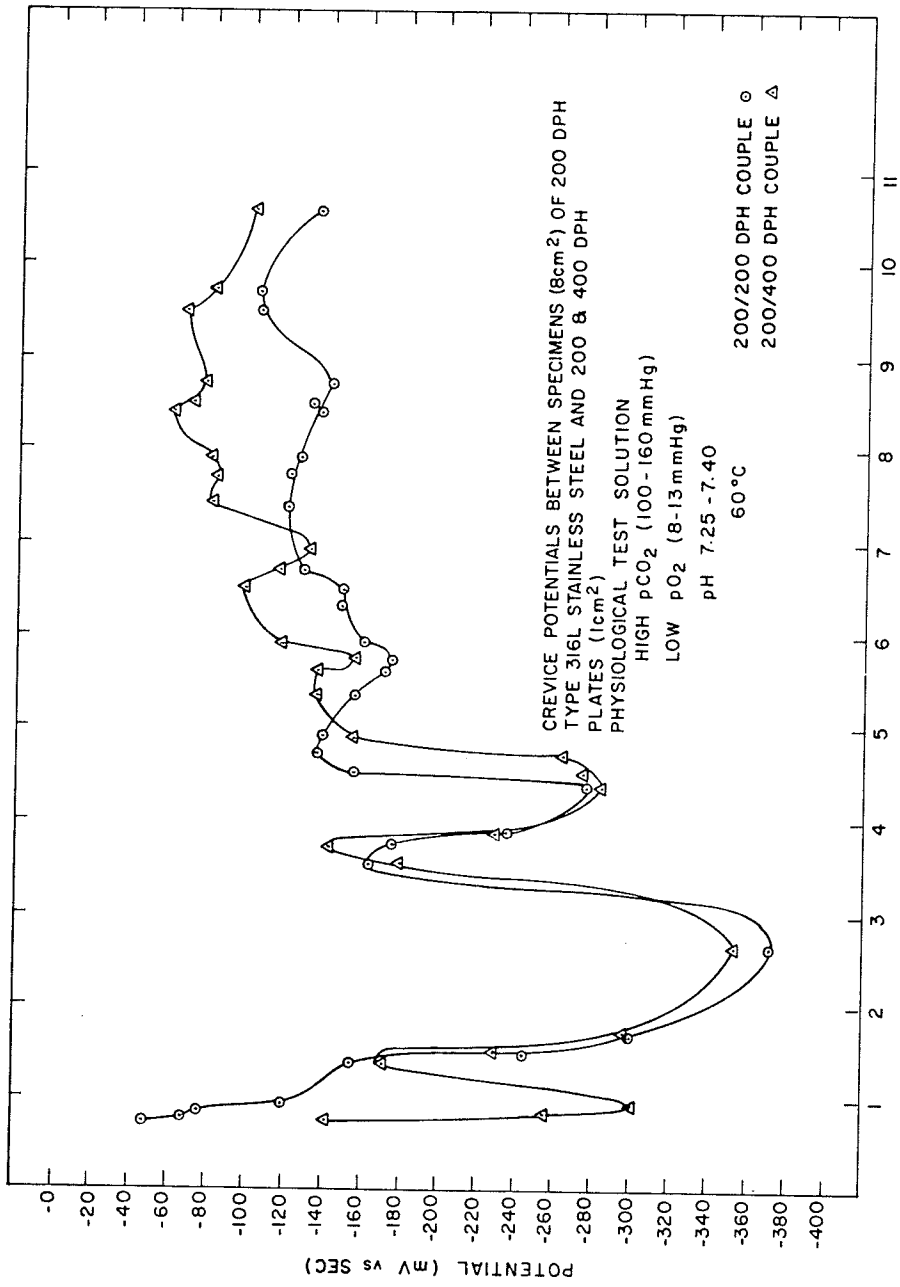

Fig.43(c) 200/200 and 200/400 DPh couples in high pCO_2, low pO_2 physiological solution.

that once initiated, a actively corroding crevice is active to the surface which is at passive potentials. Rosenfeld and Marshakov [74] succeeded in measuring potential differences of several hundred millivolts between a corroding crevice and passive free surface of 13% and 17% Cr stainless steels in 0.5N NaCl only in quite exceptional circumstances. Here the crevice and free surface were not in metallic contact (just simple electrical contact) with one another, whereas in actual working crevices there is a galvanic contact with the outer surface. If the two electrodes were in very close contact, then each would be mutually polarized whereby the potential difference in the working crevice corrosion cell would be expected to be smaller. Karlberg and Wranglen [73] only measured small potential differences of 150 mV for 13% Cr and 50 mV for 17% Cr steels in neutral 3% NaCl, the crevice being negative with respect to the surface. The potential difference decreases with % Cr and should be quite low for a 18% Cr, 14% Ni, 3% Mo steel (type 316). Their experimental crevice was between a metallic specimen and polymethyl methacrylate instead of 2 metals, with the crevice and surface potentials being measured on the same specimen. They found it very difficult to provoke crevice attack if a specimen was kept too long in a dessicator between grinding and immersion. Therefore, this time was limited to 2 hours. Also the test electrolyte had to have a low buffer capacity to allow a substantial lowering of pH within the crevice for the activation of the steel. Perhaps this is one reason why the corrosion in the present work was limited to randoming pitting, as the test solution was quite strongly buffered by HCO_3^-/H_2CO_3 and to a lesser extent by $HPO_4^=/H_2PO_4^-$. The greatest amount of pitting corrosion occurred in the high pCO_2, low pO_2 solution for all three 200 DPH specimens of a 200/400 DPH couple. The pitting

was continuous along the edge of the masked off area and randomly distributed in the central area. The three corresponding 400 DPH specimens suffered no corrosion. In the other two test solutions smaller amounts of pitting corrosion occurred along the edges of a small number of the 200 DPH specimens and none at all in the 400 DPH specimens of 200/400 DPH couples. There was no noticeable corrosion in 200/200 DPH couples.

The specimens in this work were electro-polished and stored for several days. It is well known that an electro-polished surface is the most corrosion resistant. This surface in the buffer environment would more closely resemble the actual usage of a medical implant.

From this data it would appear that the potential in the crevice would not reach an active value during corrosion. It is more likely that the crevice must be polarized in the anodic direction to above the critical potential before crevice attack takes place. This theory, in complete opposition to the activated crevice theory, is supported by recent work done by Pourbaix [75] who found that the rupture potential (or critical potential above which the passivating film became non-protective) for AISI type 316 stainless steel in Cl^- 0.10 molar was roughly 260 mV vs S.C.E. The cathodic protective potential below which pits will not form was quite "active" being in the range -440 to -640 mV vs S.C.E.

6.2 Anodic Polarization Experiments

(i) Potentiostatic

The anodic potentiostatic polarization runs served to illustrate more clearly the nature of the protective passive film and the parameters of film breakdown for annealed and deformed type 316L stainless

steel in electrochemical in-vitro environments which could be extrapolated to surgical applications. These experiments will supply increasing evidence that the localized corrosion in confined areas of medical implants is probably a result of anodic polarization in the crevice by the significantly differing passive currents possessed by stainless steels containing varying degrees of cold work.

Polarization curves for 200 and 400 DPH type 316L stainless steel in three solutions of differing pCO_2 and pO_2 at pH 7.33-7.38 and 60°C, are shown in Fig. 44. Five of the curves approach the schematic situation in Fig. 29 showing the oxidation effects of the surrounding environment to cause passivation of the stainless alloy whereby the cathodic partial reaction curve intersects the real anodic polarization curve in the passive region. Only the curve for 200 DPH material in the high pCO_2, high pO_2 solution shows the cathodic partial reaction curve intersecting roughly in a very small active region. The most interesting feature of the polarization was the anodic current density in the passive range for the annealed metal being one order of magnitude smaller than for metal deformed to 400 DPH. The passive current densities ranged from 10^{-2} to 10^{-1} $\mu A/cm^2$ for annealed metal with the larger values of 10^{-1} to $1 \mu A/cm^2$ for cold-worked metal indicating a larger rate of metal dissolution at a constant rate through the passive oxide film for the cold worked specimens. The annealed steel showed very constant current densities in the passive range with only one exception; the 200 DPH specimen in low pCO_2, low pO_2 which like all the 400 DPH steel had a passive current increasing with anodic potential.

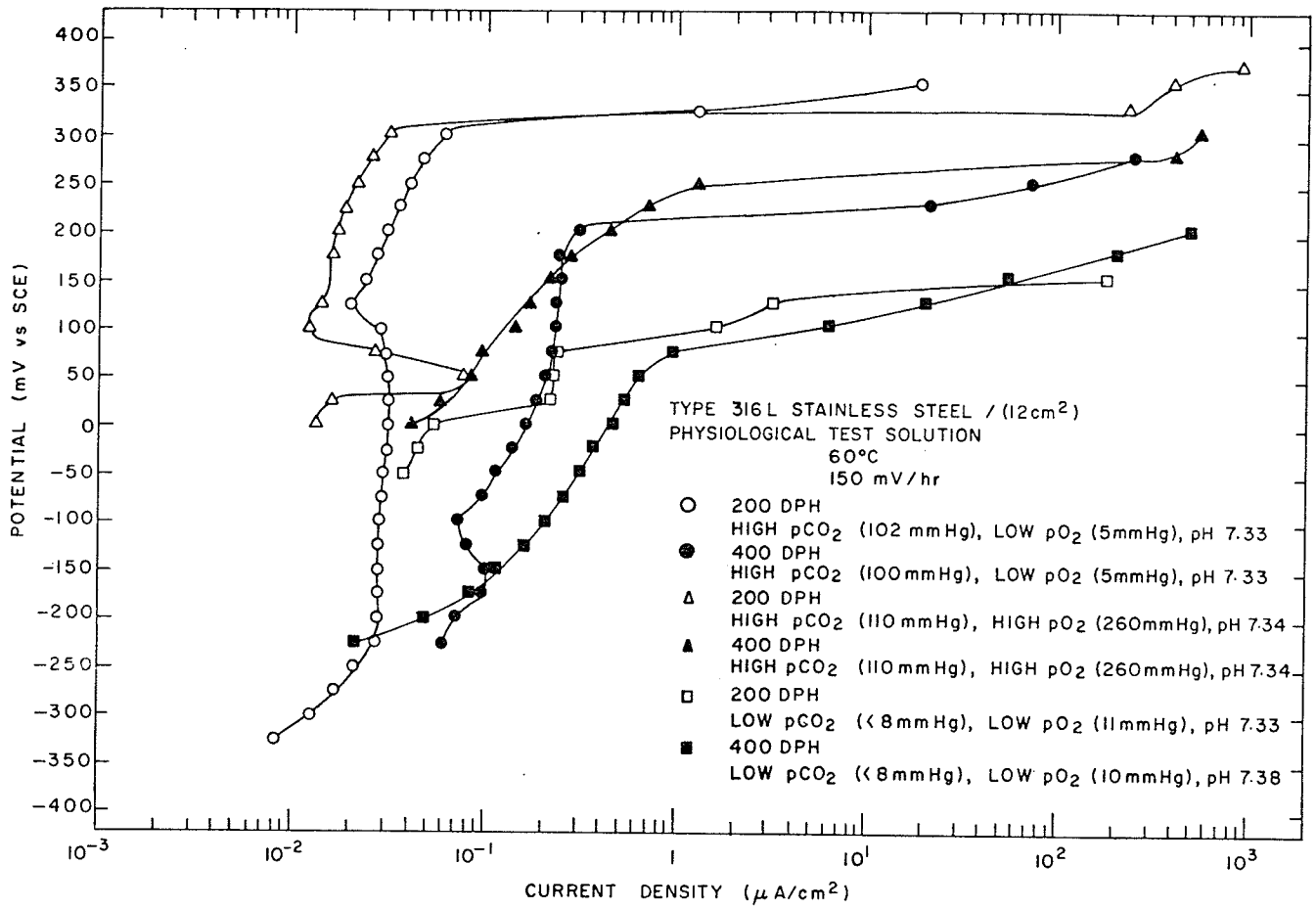

Fig. 44 The effect of pCO_2 and pO_2 on the potentiostatic anodic polarization of 200 and 400 DPH Type 316L stainless steel specimen.

Annealed type 316L in a low pCO_2, low pO_2 solution showed a gradually increasing passive current as a function of anodic potential. The effect of these two dissolved gases on the formation of protective films would be minimal in this test electrolyte. The increasing passive current would indicate the presence of a weakly protective film (perhaps very thin and susceptible to breakdown or a film containing pores which do not readily repassivate in this particular environment). A much lower passive current was observed, (reduced one order of magnitude to 3×10^{-2} $\mu A/cm^2$) on increasing the pCO_2 from <8 mm Hg to 102mm Hg, while maintaining a low pO_2 of 11mm Hg. The passive range was also enlarged. In the case of 400 DPH steel similar reductions in the passive current were noted with the alterations in blood gas concentrations just described. On the other hand the effect of increasing the oxygen concentration to 260mm Hg in combination with an already high pCO_2 was to reduce the passive current slightly from 3×10^{-2} to 1.5×10^{-2} $\mu A/cm^2$ for 200 DPH type 316L. The passive current was similarly reduced for the cold-worked material. Thus carbon dioxide concentration can be seen to be just as important as oxygen concentration in the formation and maintenance of protective layers on stainless steel in surgical usage.

Logically, the oxygen formed passive layer and protective carbonate layer (in the presence of high pCO_2) have a direct effect on the anodic potential at which pitting, considered and accepted as a specific case of crevice corrosion [47,77] commences.

The amount of cold-work introduced into the stainless steel had a direct effect on the lowering of E_{crit}, viz. the 400 DPH specimens being 50-100 mV more active than for a hardness of 200 DPH as compared in Table VII. This would place the breakdown potentials for the cold-

Table VII Comparison of Breakdown Potentials with Corrosion Potentials of Single Electrode and Crevice Hardness Couples for Annealed and Cold-Worked Type 316L Stainless Steel

SPECIMEN	Low pCO_2 (8mm Hg) Low pO_2 (12-18mm Hg) pH 7.25 - 7.40		High pCO_2 (110-180mm Hg) Low pO_2 (15-20mm Hg) pH 6.80 - 7.40		High pCO_2 (110 - 180mm Hg) High pO_2 (200-230mm Hg) pH 7.20 - 7.40	
	Corrosion Potential (after 20 days)	Breakdown Potential	Corrosion Potential (after 20 days) (mV vs SCE)	Breakdown Potential	Corrosion Potential (after 20 days)	Breakdown Potential
Single Electrode						
200 DPH	-200	125	-240*	300	50	300
400 DPH	-400	75	-240*	200	50	250
Crevice Hardness Couples						
200/200 DPH	-100		-100**			
200/400 DPH	-100		-100**			
400/200 DPH	- 80					
400/400 DPH	-200					

* Immersion time of 9 days

** Immersion time of 10.5 days

worked stainless 50-100 mV closer to the highest single electrode (or crevice potentials) encountered during the long term exposure tests. Consequently cold-worked material would be conceivably more susceptible to film breakdown electrochemically. As expected the effect of varying hardness was to yield two different modes of pitting once the transpassive region was entered. The 400 DPH material had a propensity for a large number of very small pits while the softer specimens experienced a continuous line type of pitting attack along the masking agent. The lowering of the passive breakdown potential with the addition of cold-work has been found in other materials: AISI type 1008 steel (0.6 M NH_4NO_3) lowered 30 -100 mV [72] and 250 mV less noble with AISI type 316 (Ringers solution exposed to air) [66].

The critical potential for pitting of 200 DPH steel in low pCO_2 (<8mm Hg), low pO_2 (11mm Hg) solution was 125 mV vs S.C.E. and increased to 300 mV with a pCO_2 of 102mm Hg. Increasing the pO_2 to 260mm Hg with a high pCO_2 did not further enoble E_{crit}. Carbon dioxide concentration affected the film breakdown potentials for 400 DPH specimens in a similar way seemingly independent of O_2 concentration. Therefore it would appear that the physiological parameter pCO_2 (as a protective carbonate layer) significantly affects the pitting resistance of type 316L stainless steel. The $[O_2]$ (in concentrations relevant to the medical situation as given in Fig. 3 previously) does not influence the passive films already existing on the surface. In opposition, Mueller and Greener [66] found that the passive breakdown potential of type 316 in physiological saline solution was dependent upon $[O_2]$ using deaerated, exposed to air, and aerated

solutions. No reference was made to actual measured concentrations of oxygen or how vigorously oxygen was removed or added, in which case the potential could be increased further with pO_2 or similarly lowered.

(ii) Galvonostatic

Knowledge of the magnitude of the anodic current at the corrosion potential during repairing of the passive and/or carbonate layers after the occurence of film breakdown furthers the fundamental understanding of crevice corrosion in the circumstances of fixation devices. Breakdown of the protective layer was electrochemically induced by potentiostatic anodic polarization. Corrosion currents were then determined from measured values of polarization resistance $(\Delta\varepsilon/i_x)$ as shown in Fig. 45-46. In the passive state where there is a limiting anodic current and β_a is consequently infinite the corrosion current density can be calculated by taking the limit of Eq. (16) as $\beta_a \to \infty$

$$\text{i.e.} \qquad i_{corr} = \frac{\beta_c}{2.30\ (\Delta\varepsilon/\Delta i_x)}$$

A value of β_c = 119 mV/decade was chosen from the literature [61] and used in the calculation of the corrosion current. This equation produced corrosion current values which were in good agreement with the range of passive currents determined potentiostatically. However, this method also allowed the observation of the corrosion currents and the state of the protective layer on the surface as a function of time.

A comparison of corrosion rates before and after film breakdown is given in Table VIII. For annealed and cold-worked specimens in low pCO_2, low pO_2 solution there is steady decrease in corrosion current for

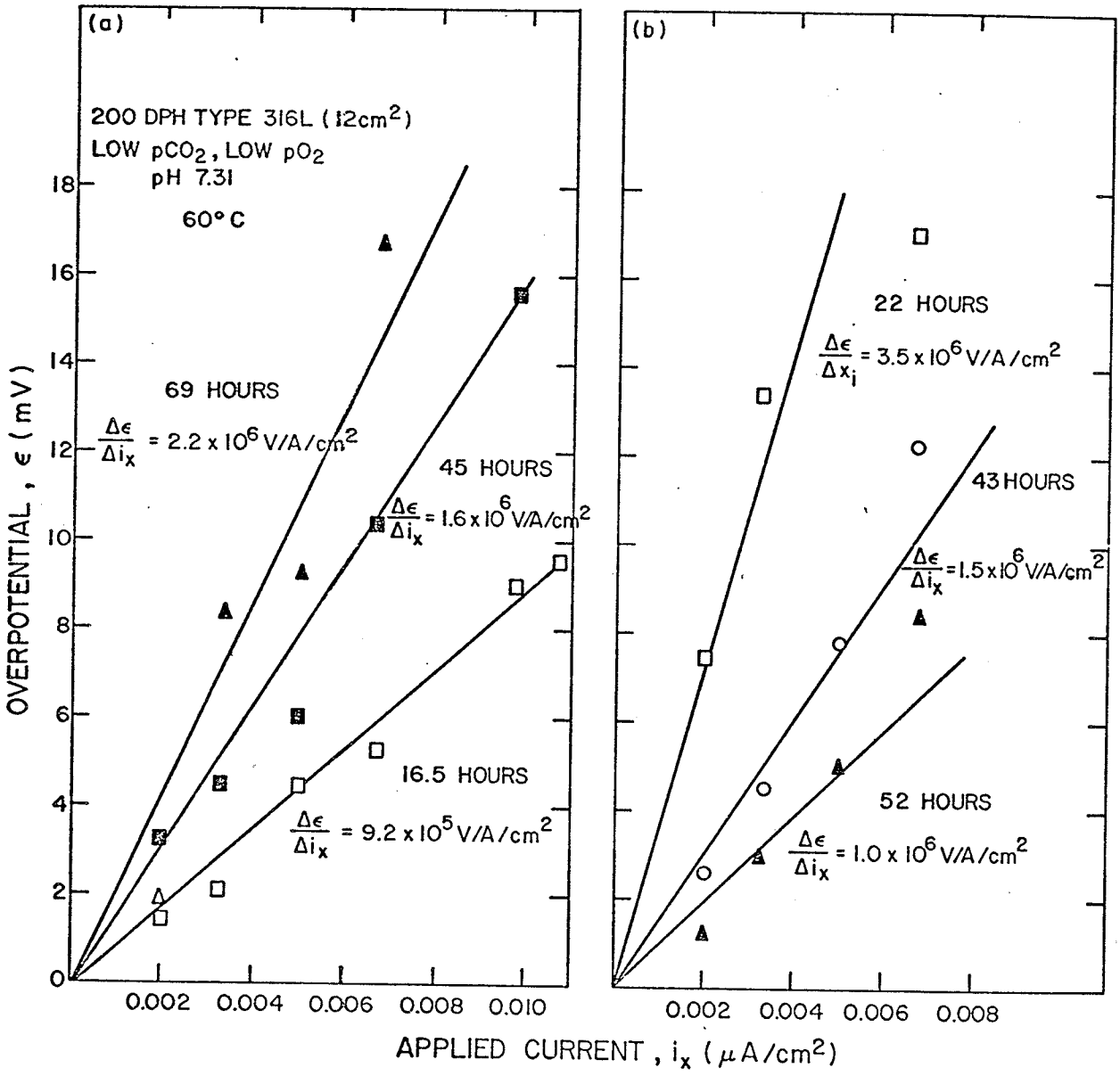

Fig. 45 Variation of polarization resistance of 200 DPH Type 316L stainless steel with time: (a) As electropolished conditions (b) Material where film breakdown had occurred.

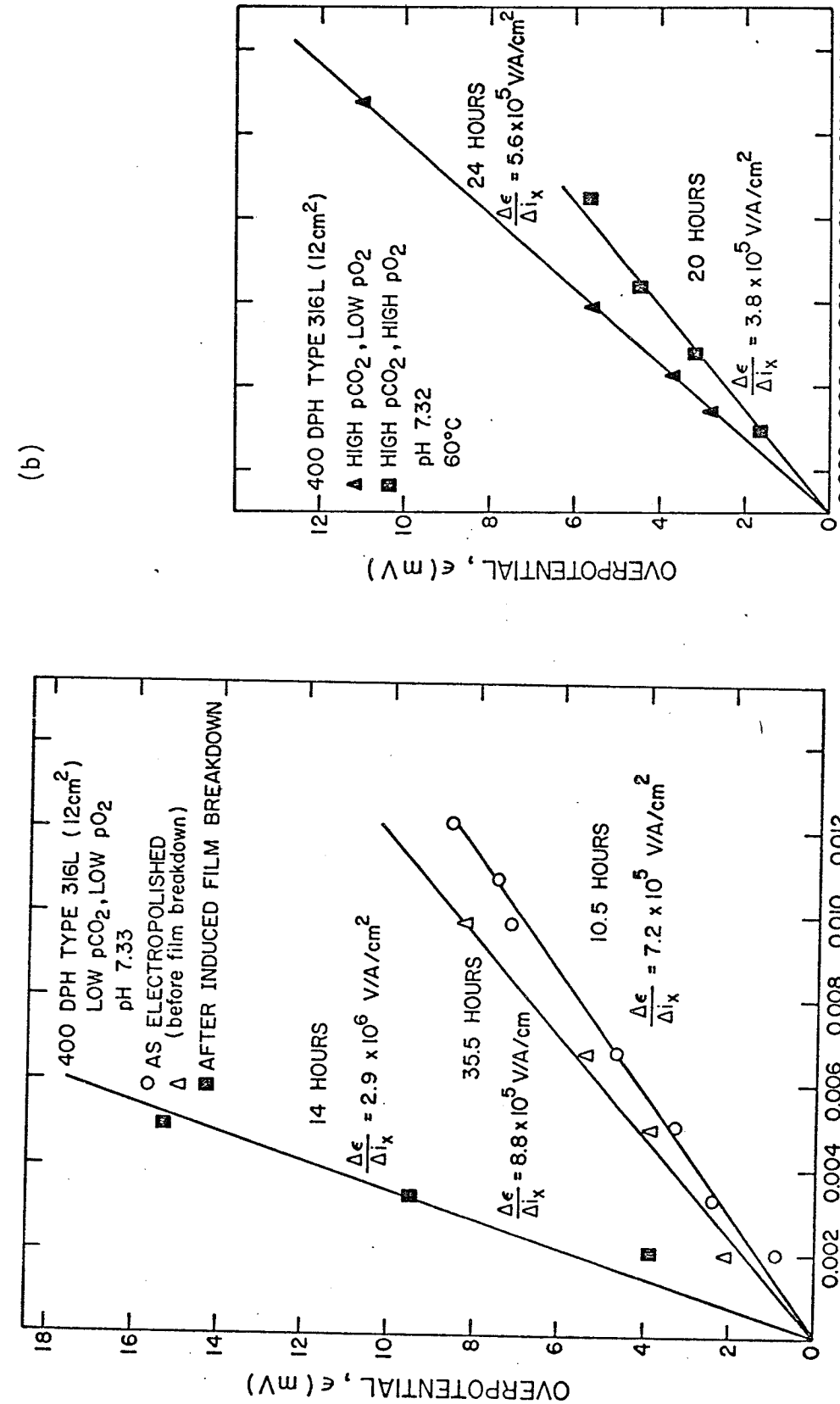

Fig. 46 Time dependence of polarization resistance for 400 DPH Type 316L stainless steel: (a) In the as electropolished condition and after film breakdown had been induced in low pCO_2, low pO_2 solution, (b) After film breakdown had been induced in solutions of high pCO_2, low and high pO_2.

Table VIII Comparison of Corrosion Rates Before and After Film Breakdown.

Low pCO_2 (8mm Hg) Low pO_2 (12-18mm Hg) pH 7.31-7.33	High pCO_2 (102mm Hg) Low pO_2 (5mm Hg) pH 7.32	High pCO_2 (110mm Hg) High pO_2 (260mm Hg) pH 7.32
Corrosion Rate (Immersion Time) ($\mu A/cm^2$)* (hrs.)		
200 DPH	400 DPH	400 DPH
5.68×10^{-2} (16.5)	7.25×10^{-2} (10.5)	
3.26×10^{-2} (45)	5.92×10^{-2} (35.5)	
2.38×10^{-2} (69)		
Corrosion Rate After Breakdown		
1.49×10^{-2} (22)	1.80×10^{-2} (14)	9.32×10^{-2} (24)
3.48×10^{-2} (43)		
5.22×10^{-2} (52)		

400 DPH
1.37×10^{-1} (20)

* $1 \mu A/cm^2$ is equivalent to a corrosion rate of 1 mil/year.

the periods monitored; 2.38×10^{-2} $\mu A/cm^2$ after 64 hours for the 200 DPH specimen and 5.92×10^{-2} $\mu A/cm^2$ after 35.5 hours for the 400 DPH specimen. The cold-worked stainless showed corrosion currents 50-100% higher compared to annealed metal. Following induced pitting the corrosion currents for both specimens after 14-22 hours were approximately the same at 1.5 to 1.8×10^{-2} $\mu A/cm^2$. Further measurements with the 200 DPH specimen showed that there was a continual increase in corrosion current up to 52 hours when the test was halted with the current 5.22×10^{-2} $\mu A/cm^2$. This would indicate that the instaneous repassivation immediately following film breakdown was relatively unstable with a tendency to dissolve. Following film breakdown in high pCO_2 solutions of high and low pO_2 the 400 DPH material displayed corrosion currents one order of magnitude higher than in the low pCO_2 solution. These values showed there was no drastic reduction in corrosion currents after repassivation and that the high anodic current densities typical of passive cold-worked material were maintained.

6.3 Proposed Theory of Crevice Corrosion Between Orthopedic Devices and Screws

The role of the mechanical damaging of protective films formed on the surface of medical implants appears to be an important factor in localized corrosion between bone plates and screws where there is great likelyhood of movement. This was concluded from the very minor nature of the corrosion observed in simple immersion tests after extended periods. It if further postulated that the crevice corrosion observed in actual practice has taken place above the break-

down potential in the transpassive region rather than by lowering of potential below the Flade potential into the active region. Evidence for this was indicated by the tendency of corrosion potentials in crevices to become more noble with time rising to within 200-300 mV of the film breakdown potential. It is quite conceivable that the extracellular fluid could provide an environment sufficiently oxidizing to cause the steel to reach high positive potentials. It is agreed that annealed stainless steel being most stable in the passive range is preferrable to the cold-worked condition. But in an application where it is in physical contact with cold-worked material where rupture of the passive/protective film has taken place the annealed material appears to undergo crevice corrosion whilst repassivation of the cold-worked material is taking place. An explanation of this type of corrosion would go as follows.

It has been shown in Table III that there is a marked variation in hardness between components of orthopedic devices particularly between plates and screws. The screws generally being much harder show the least corrosion damage. When mechanical breakdown or weakening of the protective films on both screw and plate occurs simultaneously the action of the oxidizing environment is to cause repassivation by cathodic reduction currents (concentration of oxidizing agent must be large enough to provide such a current) to maintain the material in the passive region. For repassivation of the cold-worked material, the same current must pass through the annealed material of the plate as well. However, the in vitro potentiostatic curves showed that the passive currents were about one order of magnitude larger than for annealed

material. The passage of such a current would raise the corrosion potential of annealed material above the critical value for film breakdown into the transpassive region (as shown in Fig. 47) where dissolution of the film would occur and subsequent transformation into metallic ions passing into the tissues. Simultaneously, film repair would be occurring in the cold-worked stainless steel and steady corrosion of the annealed metal in contact with it. This mechanism of corrosion would explain severe crevice corrosion in high pCO_2 solutions where a protective carbonate layer is also present and is very easily ruptured or weakened.

CONCLUSIONS

Implications for Surgical Implants

The analyses of a number of excised stainless steel implants in which the type of corrosion was intergranular due to the precipitation of carbides or an intermetallic phase did emphasize an important point. Implants should be manufactured from the low carbon form of AISI type 316 stainless steel or even more preferrably of type 316L VM (which by vacuum melting allows close control of composition limits and freedom from contamination). Thus this type of corrosion problem which is well known and documented in the engineering literature could be easily eliminated with today's technology.

The experimental studies considering the mixed usage of annealed and cold-worked conditions of AISI type 316L stainless steel resulted in the following observations regarding the ever present problem of crevice corrosion:

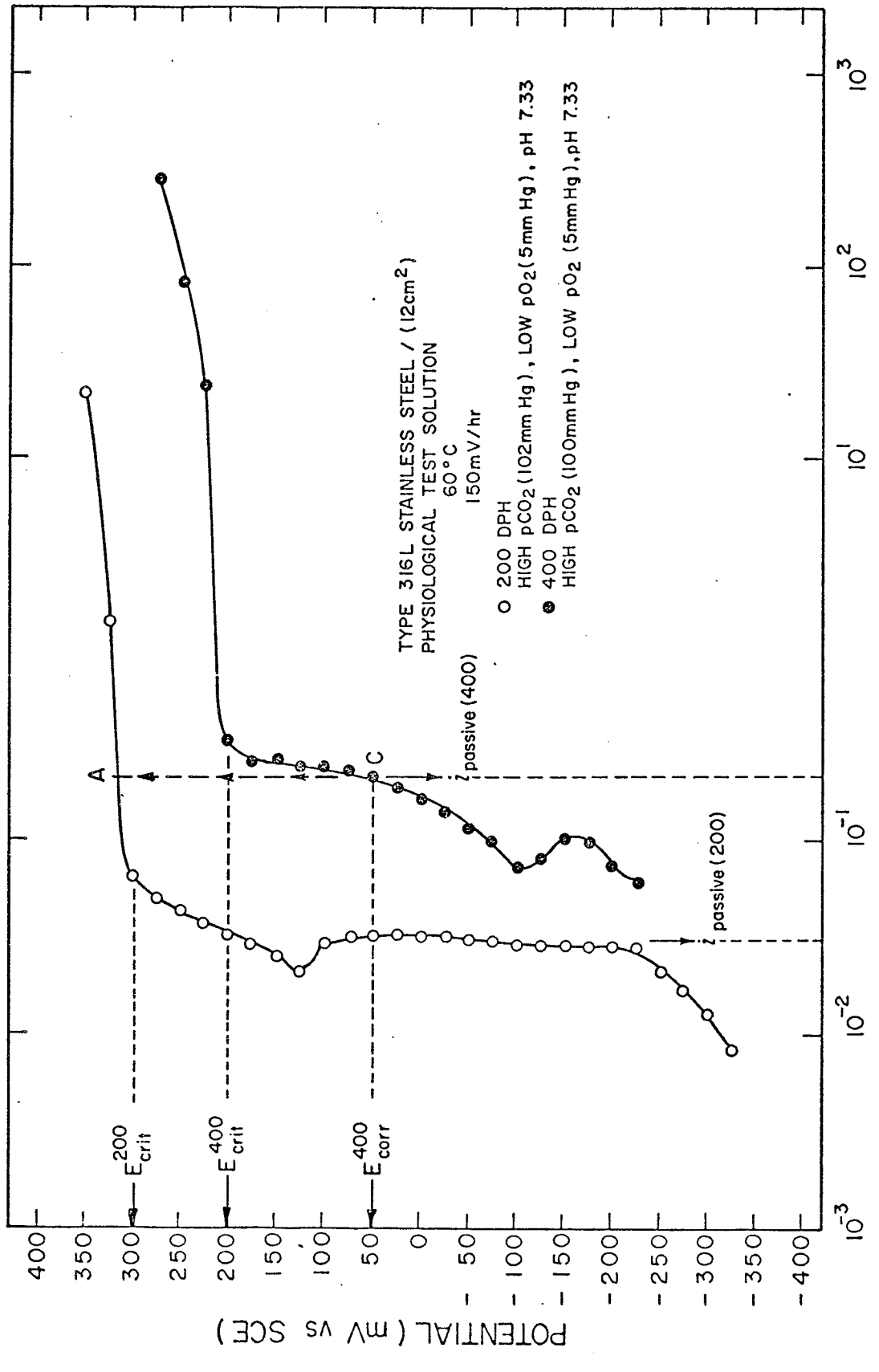

Fig. 47 Schematic representation of crevice corrosion mechanism showing polarizing effect, of passive current for cold-worked metal on the annealed stainless steel.

1. In vitro testing of implant materials should focus attention on the effect of pCO_2 on the formation of protective layers. Dissolved carbon dioxide appears to have a greater influence on protective layers than pO_2 with which investigators have usually limited their studies. Furthermore, quantitative rather than qualitative measurements should be made of these blood gases to clarify their effects.

2. The long term corrosion potentials in low pO_2 environment, of both high and low pCO_2 were between -200 and -400 mV with the cold-worked material having a more active potential only in the low pCO_2 solution. The general effect of a high pCO_2 was to prevent a significant difference in potential between the annealed and cold-worked state. Increasing the pO_2 did enable the corrosion potentials in a high pCO_2 solution to a value of 50 mV for both the 200 and 400 DPH condition from -240 mV for a low pO_2. In the crevice configuration the potentials were about 100 mV more positive.

3. Breakdown potentials were 50-100 mV higher for annealed type 316L stainless steel than for similar cold-worked material in the three representative electrolytes. The pCO_2 seemed to have a more marked effect on increasing the breakdown potential than pO_2.

4. Anodic current densities in the passive region were approximately one order of magnitude smaller for a hardness of 200 DPH than for the harder 400 DPH steel. By itself this smaller passive current would be proportional to a much

smaller corrosion rate in the passive state and would mean a more stable passive state even during a temporary shortage of the passivating agent because of the slow rate of destruction of the film. Again pCO_2 had a pronounced influence in reducing passive current densities for annealed and cold-worked conditions. A crevice corrosion mechanism is advanced where the passage of this greater anodic current during film repair of cold-worked material results in pitting of contacting annealed metal. It would appear that the surgical use in human tissues of stainless steel of varying hardness favours the occurence of crevice corrosion in contacting, confined areas. The most inert surgical device would be one fabricated completely of annealed material. If it is absolutely necessary to have the mixed use of metals, then perhaps separating the metals by a hard inert insulator like the ceramic Lucalux (high purity aluminum oxide) would beneficial.

This work could be extended to determine what variation in hardness for components of an implant could be tolerated before differences in passive currents become unacceptable. In this way passive currents would be limited to a common value in the event of mechanical rupture or thinning of the protective films if hardness was one of the properties rigidly controlled in the manufacture of surgical implants. Further efforts in seeking superior implant materials should be conducted with recently introduced industrial stainless steels. An excellent candidate as an implant material could be Armco 22-13-5* stainless steel which is accredited with having a

* Composition of Armco "22-13-5" stainless steel; 22% Cr, 12.5% Ni, 5% Mn, 2.25% Mo, 0.4% Si, 0.3% N_2, 0.18% Cb, 0.18% V, 0.05% C, balance Fe.

corrosion resistance equal or superior to types 316 or 316L, plus approximately twice the yield strength at room temperature. Perhaps the present stainless steel could be modified by a technique developed by the General Electric Co. in which a layer of tantalum is diffused on stainless steel to vastly increase corrosion resistance in harsh environments. Also to be considered is E-Brite 26-1**, a high purity ferritic stainless steel. It is produced via the electron-beam continuous hearth refining process which provides carbon and nitrogen levels significantly lower than those obtained with conventional melting techniques. For example, 26-1 contains 0.002% C and 0.008% N_2 compared to 0.020% C and 0.060% N_2 for type 316L making it very much less susceptible to preferential attack.

With increasing interest and effort in this specialized medical-engineering field, today's modern metal technology should provide the surgical profession with physiologically compatible metals in the truest sense of the word.

** Composition of E-Brite 26-1: 26% Cr, 0.002% C, 0.008% N_2, 1% Mo, balance Fe (from [78]).

BIBLIOGRAPHY

1. Weisman, S., "The Skeletal Structure of Metal Implants", Biomedical and Human Factors Conference, Washington, D.C. ASME (1967).

2. Hicks, J.H., "Pathological Effects from Surgical Metal", Modern Trends in Surgical Materials, Butterworth & Co. (Publishers) Ltd., p. 29 (1958).

3. Hochman, R.F. and Taussig, L.M., "Improved Properties of Type 316L Stainless Steel Implants by Low-Temperature Stress Relief", Journal of Metals, 1, 425 (1966).

4. Venable, C.S., Stuck, W.G., and Beach, W., Annals of Surgery, 105, 917 (1937).

5. Hudack, S.S., Archives of Surgery, 40, 867 (1940).

6. Key, J.A., Archives of Surgery, 43, 615 (1941).

7. Murray, C.R., and Fink, C.G., Report to the National Research Council and the Army and Navy (1943).

8. Fink, C.G., and Smatko, J.S., "Bone Fixation and the Corrosion Resistance of Stainless Steels to the Fluids of the Human Body", J. of the Electrochemical Society, 94, 271 (1948).

9. Blunt, J.W., Hudack, S.S., and Murray, C.R., Clinical Congress Am. College of Surgeons, New York, September (1952).

10. Schmeisser, G., "Progress in Metallic Surgical Implants", 2, 951 (1968).

11. Statland, H., Fluid and Electrolytes in Practice, J.B. Lippincott Co., (Philadelphia & Montreal, 3rd ed. 1954).

12. Bland, J.H., Clinical Metabolism of Body Water and Electrolytes, W.B. Saunders Co. (Philadelphia & London). (1963).

13. Crimmins, D.S., "The Selection and Use of Implants for Surgical Materials", Journal of Metals, 21, 38 (1969).

14. Pitts, R.F., Physiology of the Kidneys and Body Fluids, Year Book Medical Publishers Inc., Chicago (1963).

15. Moore, W.J., Physical Chemistry, 3rd edition, Prentice-Hall Inc., Englewood Calf., N.J., (1962).

16. Christensen, H.N., Body Fluids and Their Neutrality, Oxford University Press, New York (1963).

17. Ludbrook, J., "Estimation of pCO_2 By Means of the Henderson-Hasselbach Equation", Symposium on pH and Blood Gas Measurement, Chapter 5, J. & A. Churchill Ltd., (London (1959)).

18. Ganong, W.F., Review of Medical Physiology, Lange Medical Publications (1969).

19. Altman, P.L., Blood and Other Body Fluids, Federation of American Societies for Experimental Biology, Washington (1961).

20. Bourne, G.H., The Biochemistry and Physiology of Bone, Academic Press, New York (1956).

21. Murray, C.R., "The Healing of Fractures", Archives of Surgery, 29, 446 (1934).

22. Murray, C.R., "The Timing of the Healing Process", J. Bone and Joint Surgery, 23, 598 (1941).

23. Laing, P.G., "The Use of Metal in Surgery", Modern Trends in Surgical Materials, Butterworth & Co. (Publishers) Ltd., Chapter 2 (1958).

24. Lauren, E.L. and Kelly, P.J., "Blood Flow, Oxygen Consumption, Carbon Dioxide Production and Blook Calcium and pH Change in Tibial Fractures in Dog", J. of Bone and Joint Surgery, 51-A, 298 (1969).

25. Siggord-Anderson, The Acid-Base Status of Blood, Williams and Wilkins, Baltimore, 3rd edition.

26. Wray, J.B., "A Study of the Biochemistry of Human Fracture Hematoma", Proceedings of the American Orthopedic Association, J. of Bone and Joint Surgery, 49-A, 1473, October (1967).

27. ASTM Standards, 1969, Part 3, ASTM Designation F55-66, p. 938.

28. ASTM Powder Diffraction File for Inorganic Compounds, #17-536 (1967).

29. Ibid, #17-156.

30. Gilman, J.J., Koh, P.K., and Zmeskal, O., Transactions of the American Society for Metals, 41, 1371 (1949).

31. Ellis, R.G., and Pollard, G., Technical Note: The Observation of Sigma Phase After Short Aging Times In a Duplex Steel, J. of the Iron and Steel Institute, August (1970).

32. Bowden, F.P., Williamson, J.B., and Laing, P.G., "The Significance of Metallic Transfer in Orthopedic Surgery", J. of Bone and Joint Surgery, 37-B, 678 (1955).

33. Scales, J.T., "Biological and Mechanical Factors in Prosthetic Surgery", Modern Trends in Surgical Materials, Butterworth & Co. (Publishers) Ltd., London, Chapter 5 (1958).

34. Colongelo, V.J., and Greene, N.D., "Corrosion and Fracture of Type 316 SMO Orthopedic Implants", J. of Biomedical Materials Research, 3, 247 (1969).

35. Scales, J.T., Winter, G.D., and Shirley, H.T., Brit. Med. J., 2, 478 (1961).

36. Bechtol, C.O., Ferguson, Jr., A.B., and Laing, P.G., Metals and Engineering in Bone and Joint Surgery, The Williams and Wilkins Company, Baltimore (1959).

37. Schmeisser, Jr. G., "Fasteners in Orthopedic Surgery", Fasteners, 24, 3 (1969).

38. West, J.M., Electrodepisition and Corrosion Processes, D. Van Nostrand Company Limited,(London (1965)).

39. Winters, W.R., Knud, E., and Dell, R.B., Acid Base Physiology in Medicine, The London Company, Cleveland (1969).

40. Segel,I.H. , Biochemical Calculations, John Wiley & Sons Canada, Ltd., Rexdale, Ontario (1968).

41. Bockris, J. O'M., and Reddy, A.K.N., Modern Electrochemistry: Volume 2, Plenum Press, New York (1970).

42. Lyons, Jr. E.H., Introduction to Electrochemistry, D.C. Heath and Company, Boston (1967).

43. Phelps, E.H., "Electrochemical Techniques for Measurement and Interpretation of Corrosion", Corrosion, 18, 239t (1962).

44. Hoar, T.P., and Mears, D.C., "Corrosion-Resistant Alloys in Chloride Solutions: Materials for Surgical Implants", Royal Society Proceedings, Series A 294, 486 (1966).

45. Clarke, E.G.C., and Hickman, J., "An Investigation into the Correlation Between the Electrical Potentials of Metals and Their Behavior in Biological Fluids", J. of Bone and Joint Surgery, 35B, 467 (1953).

46. Greene, N.D., "Predicting Behavior of Corrosion Resistant Alloys by Potentiostatic Polarization Methods", Corrosio, 18, 136t, (1962).

47. Leckie, H.P., and Uhlig, H.H., "Environmental Factors Affecting the Critical Potential for Pitting in 18-8 Stainless Steel", J. of the Electrochemical Society, 113, 1262 (1966).

48. Rocha, H., Werstoffe u. Korrosion, 11, 352 (1960).

49. Uhlig, H., and Merril, M., Ind. Eng Chem. 33, 675 (1941).

50. Wilde, B.E., and Williams, E., "On the Breakdown of Passivity on Stainless Steel in Halide Media", J. of the Electrochemical Society, 116, 1539 (1969).

51. Trabanelli, G., and Zucchi, F., "Measuring the Corrosion Resistance of 4 Alloys in Chloride Solutions", Materials Protection and Performance, 9, 16 (1970).

52. Stern, M., "A Method for Determining Corrosion Rates From Linear Polarization Data", Corrosion, 14, 60 (1958).

53. Skold, R.V., and Larson, T.E., "Measurement of the Instaneous Corrosion Rate by Means of Polarization Data", Corrosion, 13, 69 (1957).

54. Stern, M., and Geary, A.L., "Electrochemical Polarization - I. A Theoretical Analysis of the Shape of Polarization Curves", J. Electrochem. Soc., 104, 56 (1957).

55. Steigerwald, R.F., "Electrochemistry of Corrosion", Corrosion, 24, 1 (1968).

56. Makrides, A.C., "Dissolution of Iron in Sulfuric Acid and Ferric Sulfate Solutions", J. Electrochem. Soc., 107, 869 (1960).

57. Sherwin, M.P., Taylor, D.E., and Waterhouse, R.B., "An Electrochemical Investigation of Fretting Corrosion in Stainless Steel", Corrosion Science, 11, 419 (1971).

58. Evans, S. and Koehler, E.L., "Use of Polarization Methods in the Determination of the Rate of Corrosion of Aluminum Alloys in Anaerobic Media," J. Electrochem. Soc. 108, 509 (1961).

59. Stern, M. and Weisert, E.D., "Experimental Observations on the Relation Between Polarization Resistance and Corrosion Rate", Amer. Soc. for Testing of Materials Proceedings, 59, 1280 (1959).

60. Jones, D.A. and Greene, N.D., "Electrochemical Detection of Localized Corrosion", Corrosion, 25, 367 (1969).

61. Revie, R.W. and Greene, N.D., "Comparison of the in Vivo and in Vitro Corrosion of 18-8 Stainless Steel and Titanium", J. Biomed. Mater. Res., 3, 465 (1969).

62. Popiel, W.J., Labratory Manual of Physical Chemistry.

63. Park, W.G., Experimental Physical Chemistry, 2nd Edition.

64. Eisman, G., Bates, R., et al, The Glass Electrode, pp. 63, John Wiley & Sons, New York (1965).

65. Metals Handbook, 8th Ed., p. 544, The American Society for Metals, Metals Park, Ohio (1969).

66. Mueller, H.J. and Greener, E.H., "Polarization Studies of Surgical Materials in Ringer's Solution", J. Biomed. Mater. Res., 4, 29 (1970).

67. Revie, R.W. and Greene, N.D., "Corrosion Behavior of Surgical Implant Materials: I. Effects of Sterilization", Corrosion Science, 9, 755 (1969).

68. Mahan, B.H., University Chemistry, Addison-Wesley, Publishing Company Inc. (1969).

69. Szklarska-Smialowska, Z., "Review of Literature on Pitting Corrosion Published Since 1960", Corrosion, 27, 223 (1971).

70. Evans, U.R., The Corrosion and Oxidation of Metals: Scientific Principles and Practical Applications, Edward Arnold (Publishers) Ltd. (1961).

71. Pourbaix, M., Lectures on Electrochemical Corrosion, Plenum Press (1967).

72. France, Jr., W.D., "Effects of Stress and Plastic Deformation on the Corrosion of Steel", Corrosion, 26, 189 (1970).

73. Karlberg, G. and Wranglen, G., "On the Mechanism of Crevice Corrosion of Stainless Cr Steels", Corrosion Science, 11, 499 (1971).

74. Rosenfeld, I.L., and Marshakov, I.K., "Mechanism of Crevice Corrosion", Corrosion, 20, 115t, (1964).

75. Pourbaix, M., "Significance of Protection Potential in Pitting and Intergranular Corrosion", Corrosion, 26, 10 (1970).

76. Prazak, M., "Evaluation of Corrosion-Resistant Steels Using Potentiostatic Polarization Curves", Corrosion, 19, 75t (1963).

77. Uhlig, H.H., Corrosion Handbook, p. 172, John Wiley, New York (1940).

78. Knoth, R.J., Lasko, G.E., and Matejka, W.A., "New Ni-Free Stainless Bids to Oust Austenitic", Chemical Engineering, 77, 170 (1970).